DOI: 10.51975/23380101.som
Journal of the Nigerian Society of Chemical Engineers, 38(1), 2023

LIQUID-LIQUID EQUILIBRIA OF TERNARY MIXTURE CONTAINING CASTOR OIL BIODIESEL, METHANOL AND GLYCEROL AT DIFFERENT TEMPERATURES AND ATMOSPHERIC PRESSURE

***Adama, K. K. and Aluyor, E. O.**
Department of Chemical Engineering, Faculty of Engineering,
Edo State University Uzairue, Edo State, Nigeria
*adama.kenneth@edouniversity.edu.ng, adamakenneth@gmail.com

ABSTRACT

In this work, ternary liquid-liquid equilibrium (LLE) data (binodal solubility curves and tie-lines) for castor oil biodiesel + methanol + glycerol at six different temperatures (25, 35, 40, 50, 55 and 60) °C and atmospheric pressure were determined using modified cloud point titration and gas chromatographic analysis. Temperature and time interval influences on the phase diagrams were studied. Spectrometric analysis of the biodiesel and oil were also investigated. The distribution coefficients and solvent selectivities were calculated. The results showed high values of methanol distribution and selectivities at the investigated conditions. Methanol solubilized preferentially in the glycerol heavy phase. The distribution coefficients and solvent selectivity values showed methanol as a good solvent for the separation of castor oil biodiesel from glycerol. The analysis of the biodiesel and oil using Fourier transform infra-red (FTIR) spectrometry showed that the most prominent functional group was methyl ricinoleate which impacted on the character of the biodiesel. The knowledge of the phase equilibrium behaviour of the system is important in the design of efficient separation process, optimization of biodiesel purification and development of appropriate models to elucidate on the purification process.

Keywords: *Liquid-liquid equilibria; Castor oil biodiesel-methanol-glycerol system; Ternary phase diagrams; Spectrometric analysis; Distribution coefficient; Solvent selectivity*

1.0 INTRODUCTION:

The use and application of biodiesel for industrial and domestic processes is gradually gaining wide-spread attention partly due to price fluctuation in the energy market occasioned by the unstable nature of fossil fuel economy but more importantly, due to environmental concerns (Borugadda and Goud, 2012; Atabani et al., 2013; D'Amato et al., 2017). Biodiesel production most often is associated with the presence of impurities such as non-reacted alcohol, glycerol and catalyst. Product requirement constraints are imposed by the relevant standards (ASTM D-6751, ASTM D-9751 and EN 14214) and as such, these impurities must be removed which is mostly achieved by washing with water. The direct product of the biodiesel production can be assumed to be a ternary mixture of the specific biodiesel, alcohol and glycerol systems. Biodiesel has excellent fuel properties which include renewability, biodegradability, and environmentally benign (Vicente et al., 2004; Encinar et al., 2005). The properties of any biodiesel are usually strongly affected by the purity of the end-product. Industrially, biodiesel is produced by alcoholysis of vegetable oils and/or animal fats. However, a major area of concern in the reaction sequence is the immiscibility of the reactants; usually methanol or ethanol and the vegetable oils or animal fats. As a result of this challenge, mass transfer limitations at the beginning of the process are always generated. Consequently, the products of the reaction (biodiesel and glycerol) are not miscible which is an important characteristics used for the initial separation stage in most industrial processes. Phase equilibrium description of any system consisting of biodiesel, alcohol and glycerol is a fundamental requirement for understanding, designing, optimizing and reducing cost of the biodiesel production process.

Castor oil contains about 30% to 55% oil by weight depending on the breed and has the highest viscosity amongst vegetable oils (Adama et al., 2018; Mosquera et al., 2016; Nangbes et al., 2013; Ogunniyi, 2006). It contains naturally occurring triglycerides giving it the appearance of a pure compound. It is used for various purposes including the production of biodiesel. Castor oil biodiesel has many excellent properties that influences its use as combustion fuel. The major character of the biodiesel is the high concentration of the ricinoleate ester that greatly influences the behaviour of both the oil and

biodiesel (Adama et al., 2018; Mosquera et al., 2016; Nangbes et al., 2013; Ogunniyi, 2006)

Liquid-liquid equilibrium data are important prerequisite needed to attain biodiesel final product specification (Knothe and Van Gerpen, 2009) due to the fact that a settling unit operation process is used mostly. Therefore, distribution coefficients as well as selectivity are essential parameters needed to ascertain any solvent's ability to promote and enhance phase separation. Consequently, experimental data of multi-component liquid-liquid equilibrium systems are essential for design, operation and optimization of any extraction process (Seader and Henley, 2006). It can be used to understand the process of purification and separation of the light phase from the heavy phase in biodiesel production. Several studies have been presented that describes the liquid-liquid equilibrium (LLE) data of biodiesel, glycerol, and methanol or ethanol systems (Adama et al., 2021; Noriega et al., 2016; Do-Carmo et al., 2014; Rostami et al., 2013; Ardila et al., 2013; Machado et al., 2012; Franca et al., 2009; Machado et al., 2011; Mesquita et al., 2011; Follegatti-Romero et al., 2010; Ming-Jer Lee et al., 2010). In our previous studies (Adama et al., 2018 and 2021), we investigated the tie lines for the purification of castor oil biodiesel/methanol/glycerol system at 20 °C and 30 °C and the component distribution associated with phase separation and purification of tropical almond biodiesel at different temperatures respectively. Further studies on the production, characterization and application of phase system analysis for purification of biodiesel produced from tropical almond seed oil was also investigated (Adama et al., 2020). However, the investigations were limited to few parameters.

The limited knowledge and information data-base on the liquid-liquid equilibrium behaviour of castor oil biodiesel/methanol/glycerol ternary system important for greater elucidation on actual purification process in terms of components distribution and phase behaviour using ternary phase diagrams necessitated this research. The binodal solubility curve compositions as well as the tie line data were determined. The distribution or partition coefficient and the solvent selectivity were calculated to ascertain the behaviour of the ternary mixture in real-life industrial biodiesel purification processes.

2.0 MATERIALS AND METHODS

2.1 Materials

Castor oil biodiesel was produced, separated and purified according to previous work (Adama et al., 2018). The study also presented the fatty acid profile of the castor oil biodiesel. Other chemicals as reported include glycerol (99 %-100 % JDA, Acros Organics, USA), Methanol (Merck, Germany, 99.5 % purity) and potassium hydroxide pellets (85 % BDH Labtech Chemicals, Poole, England). The equipment used for the liquid-liquid experiments were burette, mechanical agitator - the stirrer, analytical balance, pipette, thermostatic water-bath with a circulation pump for temperature control, conical flasks, stopwatch, beakers and analytical instrument for analysing the composition of the mixture - Gas chromatograph-mass spectroscopy/flame ionization detector (GCMS/FID).

2.2 Methods

The procedures for characterization of the castor oil and castor oil biodiesel, spectroscopic analysis of the oil and biodiesel and the liquid-liquid equilibrium experiments were performed as in our previous works (Adama et al., 2018; 2020 and 2021) in addition to approaches employed by several other researchers (Machado et al., 2012; Mesquita et al., 2012; Ardila et al., 2013; Rostami et al., 2013; Noriega et al., 2016). The binodal solubility curve and tie line data for the castor oil biodiesel ternary system at the investigated temperatures and time intervals were determined by a modified cloud point method using titration procedure under isothermal conditions. The modification involved withdrawing samples from the mixture at 2 min intervals for 32 min under constant agitation. Each sample, at a different time interval, was then analyzed using GC for the component composition from the withdrawn mixture.

3.0 RESULTS AND DISCUSSIONS

Figure 1 shows the Fourier Transform Infra-Red (FTIR) spectrometry of the castor oil biodiesel and castor oil respectively.

DOI: 10.51975/23380101.som
Journal of the Nigerian Society of Chemical Engineers, 38(1), 2023

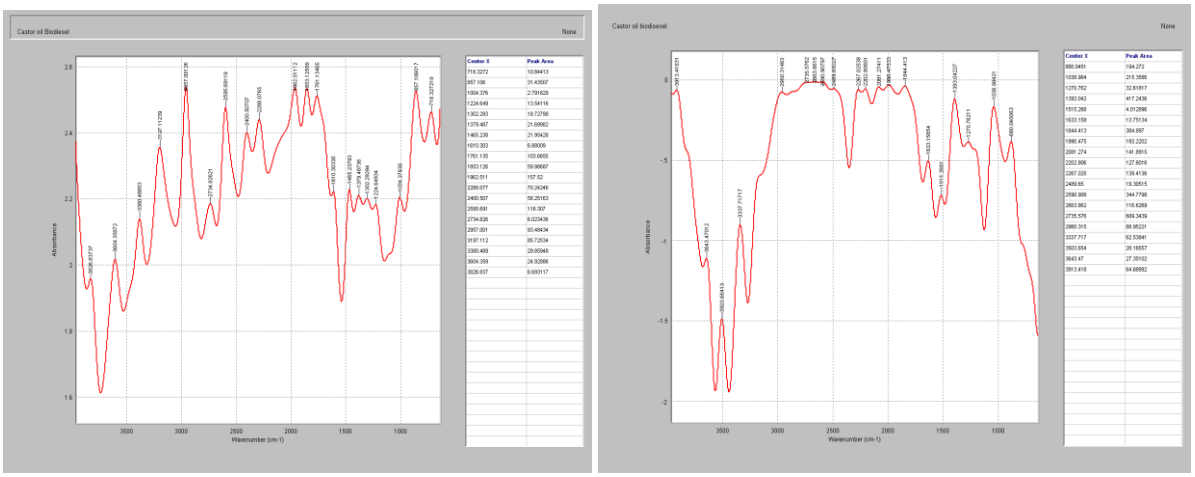

A B

Figure 1: (A) Castor oil biodiesel FTIR Spectrum (B) Castor oil FTIR Spectrum

The Figure 1 indicated the presence of several functional groups. The dominant functional groups of the biodiesel and oil were =C-H, C-O-C, RO-H, R-OH and C=O for the biodiesel and =C-H, CH_2, C=O and O-H groups for oil. However, other functional groups present are CH_2, C≡O, -C≡C-, >C=C<, RC≡N and OH in both the oil and biodiesel which had minimal influence on the oil and biodiesel to absorb infrared radiation at the investigated absorbance range (cm^{-1}). The use of infrared spectroscopy in the analysis of the oil and biodiesel was based on the principle that almost all molecules absorb infrared light at those frequencies where the infrared light affected the dipolar moment of the molecule. In the castor oil and biodiesel molecules, the differences of charges in the electronic fields of their atoms produce the dipolar moment of the molecules. The molecules with dipolar moments allowed infrared photons to interact with other molecules causing excitations to higher vibrational states. The results of the analysis of the tie line data for the castor oil biodiesel mixture composition (castor oil biodiesel/glycerol/methanol) at the investigated temperatures (25, 35, 40, 50, 55, and 60) °C and time of 2 mins to 32 mins, at 2 mins interval for the overall phase mixture composition before phase separation are presented in Figure 2.

From Figure 2, it could be observed that the tie line data predicted and showed how castor oil biodiesel, methanol and glycerol components distributed in the phase mixture composition (feed composition) before separation at the various temperatures and time intervals. The components were observed to be evenly distributed and concentrated at each temperature in the feed composition to appreciable extent at the various time intervals during investigation.

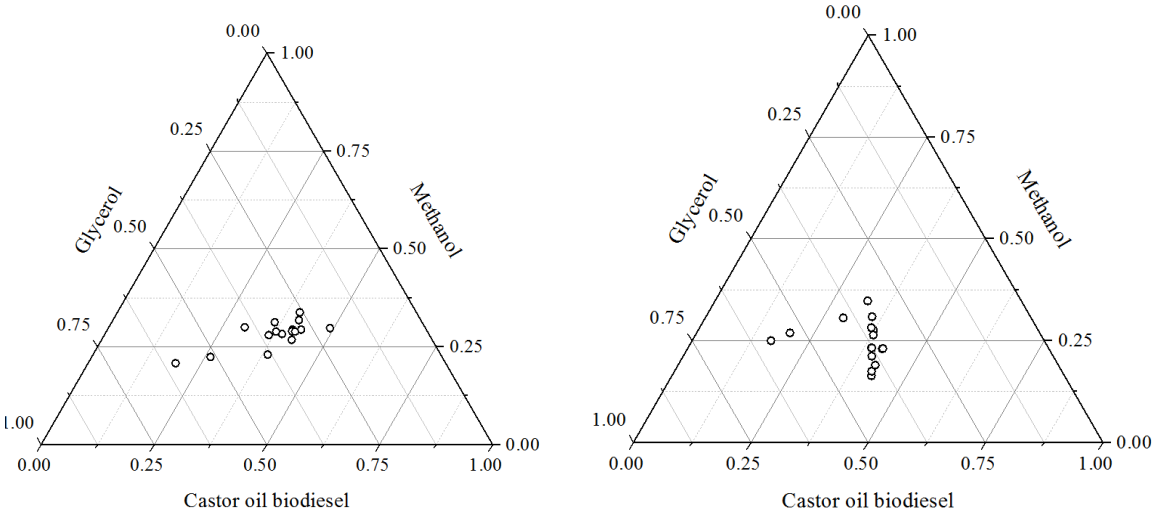

(A) (B)

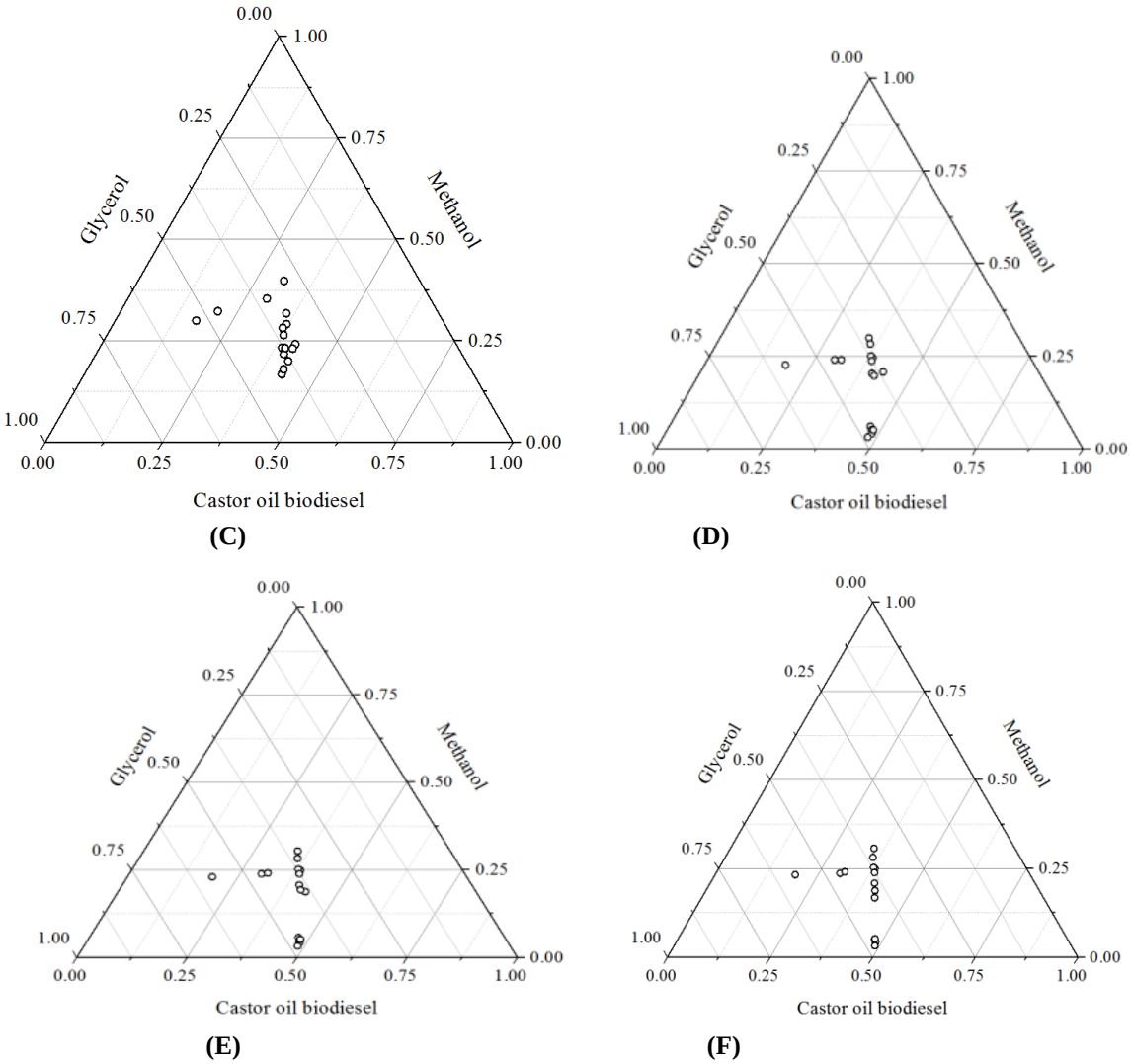

Figure 2: Tie-line plot for overall mixture composition before phase separation at (A) 25 °C (B) 35 °C (C) 40 °C (D) 50 °C (E) 55 °C (F) 60 °C

The results of the analysis of the tie line data and plots for castor oil biodiesel light phase and glycerol heavy phase mixture composition after phase separation at the investigated temperatures and time intervals are presented in Figure 3.

Figure 3 shows the tie line plots for castor oil biodiesel light phase and glycerol heavy phase after phase separation at the investigated temperatures and time of 2 mins to 32 mins at 2 mins intervals. From the ternary phase diagram plot, it can be observed that the compositions between the equilibrium light phase and the heavy phase were represented by the tie lines data. This also represented the conjugate phases in equilibrium which were the extract and the raffinate phases of the ternary mixture. The figures showed non-horizontal tie lines at the investigated compositions. It was observed that the solubility of methanol in the heavy glycerol phase was greater and higher than in the light biodiesel phase as seen by the size of the phase region bordering methanol and glycerol and the gradient of the tie lines. Methanol readily solubilizes in the heavy glycerol phase due to its strong affinity for glycerol; hence increase in the size of the two phase region bordering the glycerol and methanol.

DOI: 10.51975/23380101.som
Journal of the Nigerian Society of Chemical Engineers, 38(1), 2023

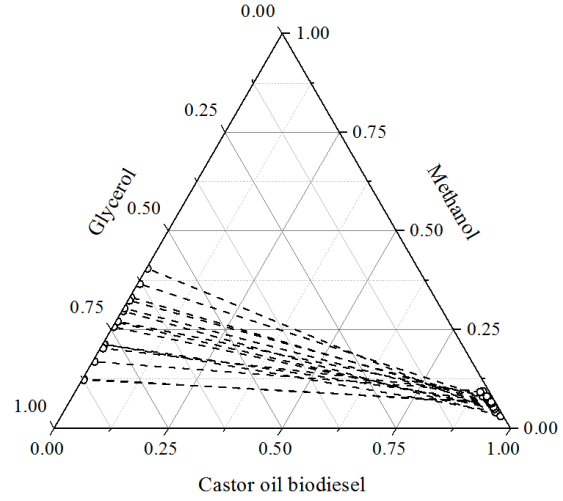

(A)

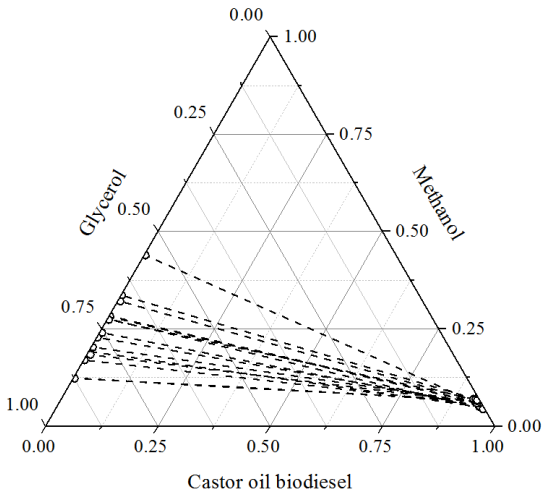

(B)

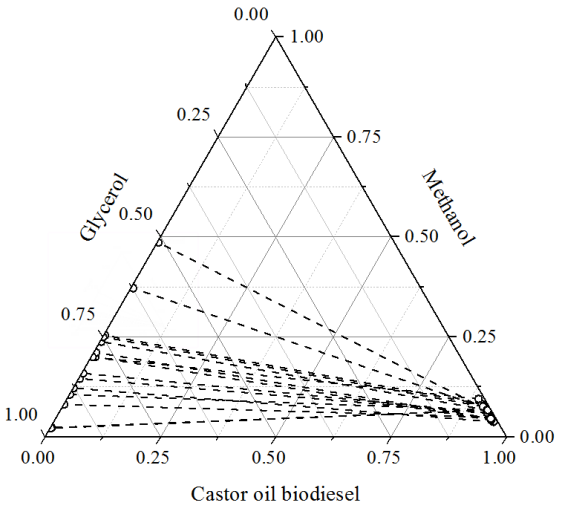

(C)

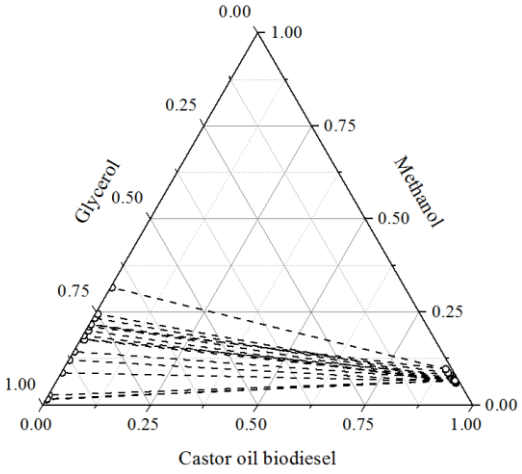

(D)

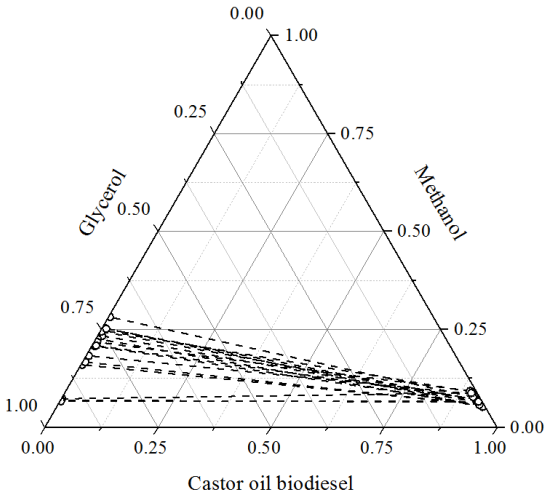

(E)

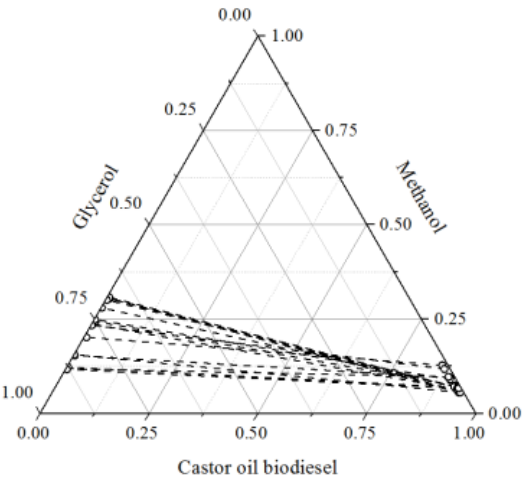

(F)

Figure 3: Tie-line plot for castor oil biodiesel/glycerol/methanol system after phase separation at (A) 25 °C (B) 35° C (C) 40 °C (D) 50 °C (E) 55 °C (F) 60 °C

The binodal solubility curve composition plots at the investigated temperatures and time intervals for castor oil biodiesel phase mixture composition are presented in Figure 4.

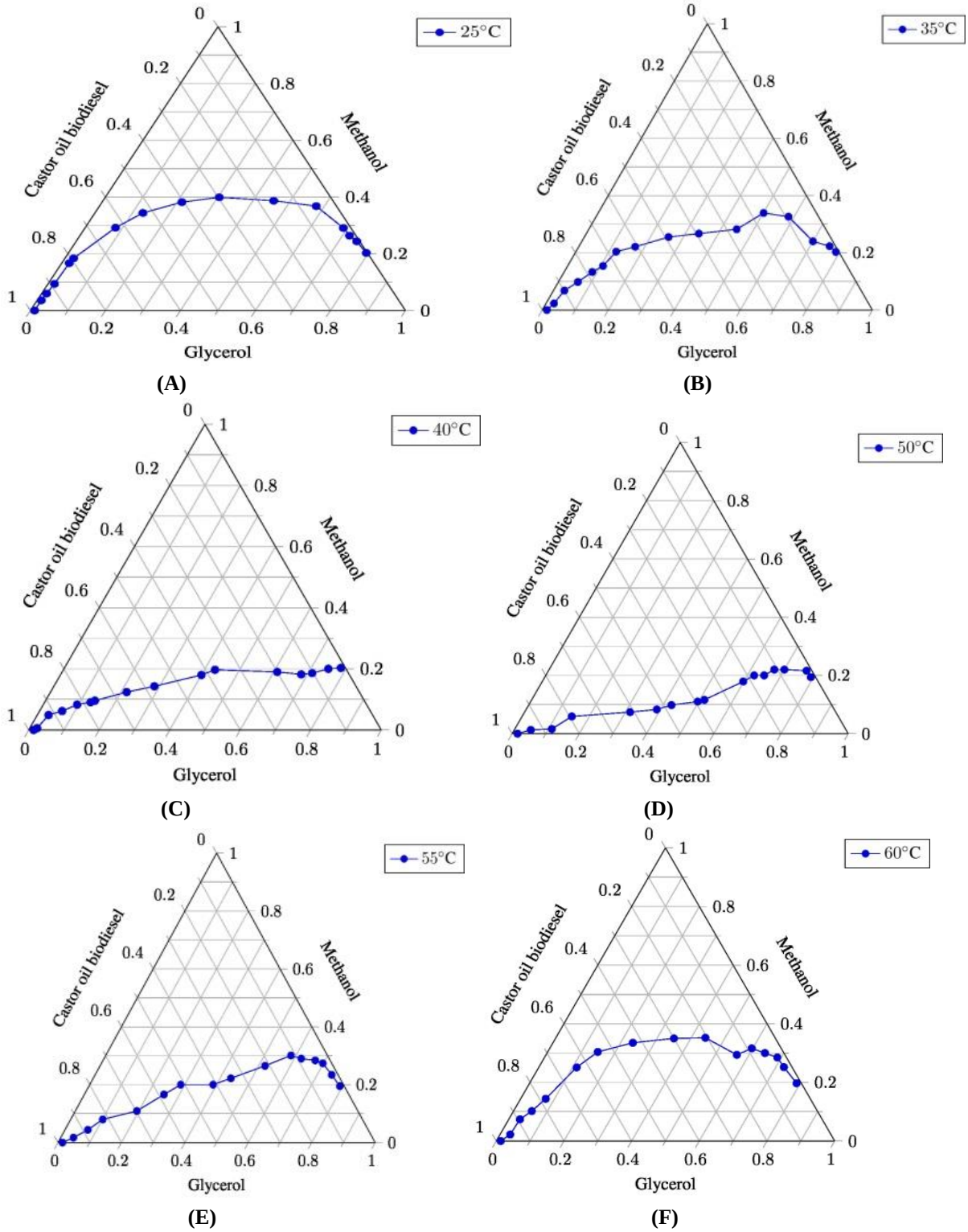

Figure 4: Binodal solubility composition plots for castor oil biodiesel/glycerol/methanol system at (A) 25 °C (B) 35 °C (C) 40 °C (D) 50 °C (E) 55 °C (F) 60 °C

DOI: 10.51975/23380101.som
Journal of the Nigerian Society of Chemical Engineers, 38(1), 2023

Figure 4 shows the binodal solubility curve composition plots for castor oil biodiesel/glycerol/methanol system, at the different withdrawal time intervals and

temperatures. Several measurements of different pairs of the conjugate solutions of the light phase and the heavy phase at each temperature and time interval were obtained at the different temperatures and time intervals. From experimental analysis, it was observed that castor oil biodiesel and glycerol were partially miscible and soluble in methanol. However, castor oil biodiesel and glycerol were totally immiscible in each other. This behaviour was observed to be in agreement with other studies (Mesquita et al., 2011; Rostami et al., 2013). It could be seen from the binodal solubility curve composition diagrams of the different figures that the castor oil biodiesel had higher solubility in the heavy phase at the studied temperatures and time intervals investigated.

The results of the ternary equilibrium data for distribution coefficient of glycerol ($K_{glycerol}$), methanol ($K_{methanol}$) and selectivity (S) at the different temperatures and withdrawal times for castor oil biodiesel/methanol/glycerol phase compositions are presented in Figure 5.

In Figure 5, it can be verified that the distribution coefficient of methanol ($K_{methanol}$) in the biodiesel light phase was higher causing the biodiesel to drag the greatest amount of methanol present in the biodiesel light phase. This gives an appreciable purification of the biodiesel phase of the biodiesel with minimal fraction of glycerol in the biodiesel which was in agreement with studies conducted on different biodiesel ternary systems (Machado et al., 2011; Ardila et al., 2013, Adama et al., 2021). Thus, the drying process of the biodiesel was greatly favoured. At other temperatures, the distribution coefficient of methanol with regards to temperature and time intervals was observed to exhibit consistent values of relatively less than one. This behaviour of the distribution coefficient may be explained in terms of the polarity of the hydroxyl group of the methyl ricinoleate molecule making the distribution of the more polar components (methanol) to increase in the biodiesel light phase which can be readily separated.

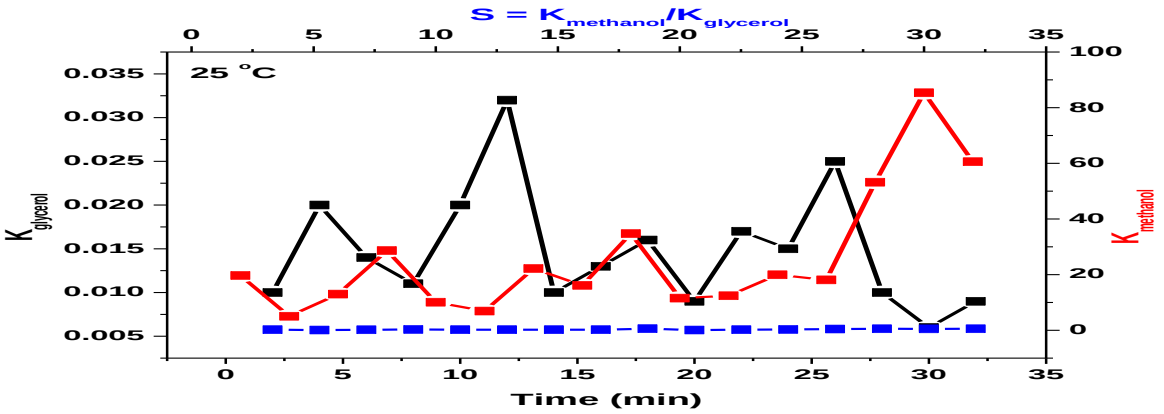

(A)

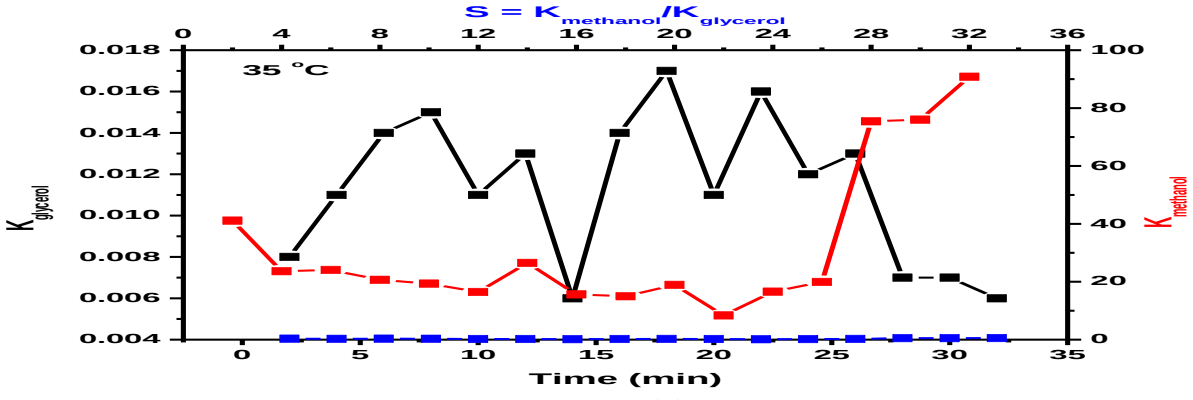

(B)

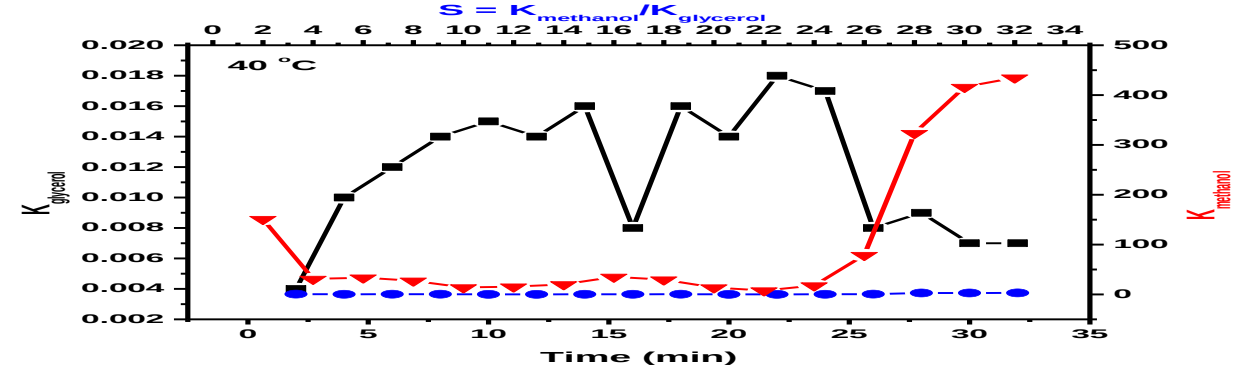

(C)

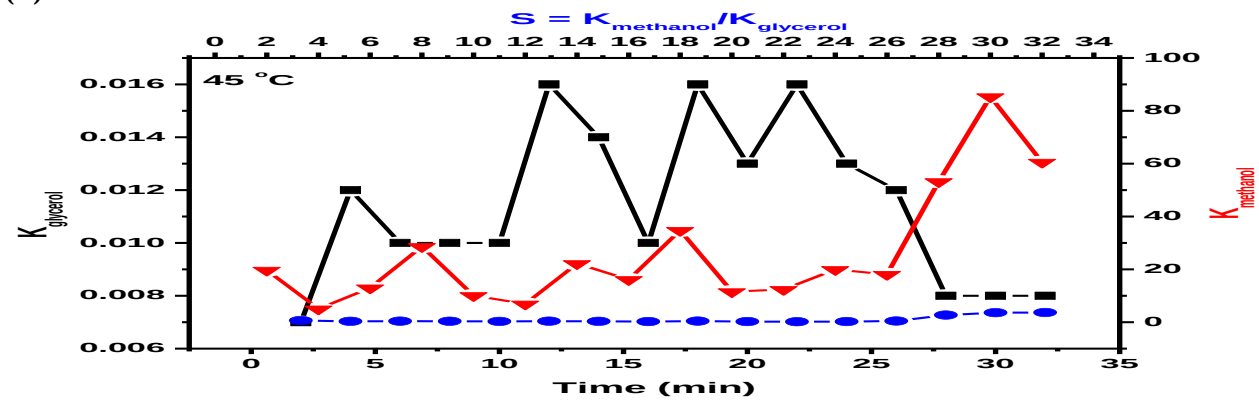

(D)

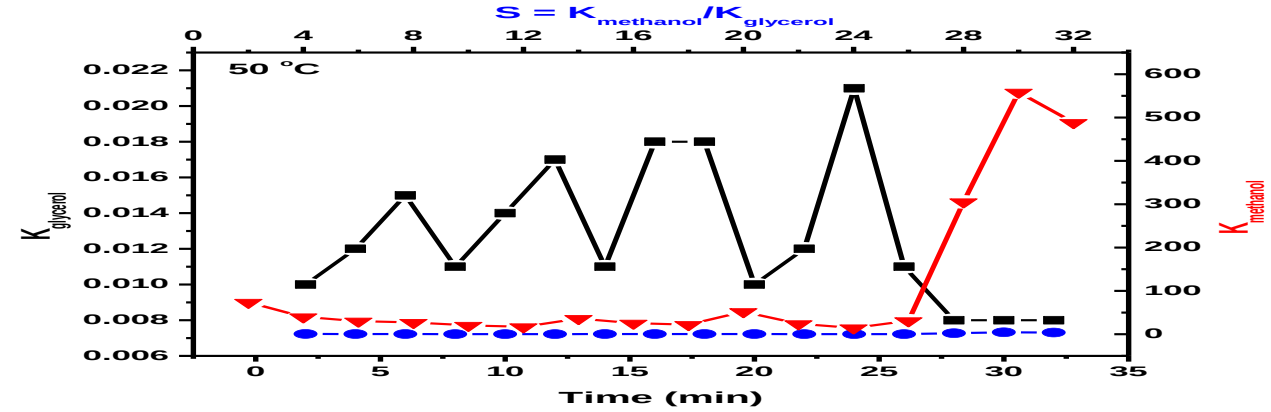

(E)

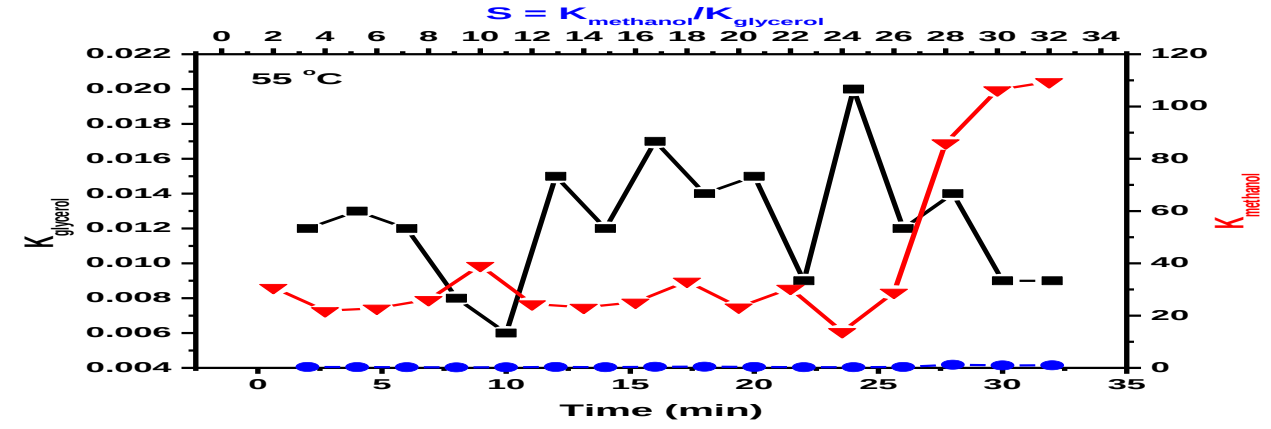

(F)

Figure 5: Distribution coefficients of glycerol ($K_{glycerol}$), methanol ($K_{methanol}$) and selectivity (S) at (A) 25 ℃ (B) 35 ℃ (C) 40 ℃ (D) 50 ℃ (E) 55 ℃ (F) 60 ℃ and withdrawal times for castor oil biodiesel/methanol/glycerol phase compositions

The selectivity of biodiesel in the biodiesel light phase showed its preference to solubilize methanol; the solute or glycerol; the diluent. At all system temperatures and atmospheric pressure, the solubility values (*S*), were between 2 and 488. Also, it was observed that a decrease in the mass fraction of methanol in the glycerol heavy phase gave an increase in the selectivity of biodiesel for methanol. This was due probably to the presence of methanol in the glycerol heavy phase that solubilizes an amount of glycerol in addition to methanol, thus affecting the selectivity (*S*) values. This observation was also in agreement with studies conducted (Machado et al., 2011 and Ardila et al., 2013). For ternary systems, increasing the temperature gives an increase in selectivity, *S*, as verified by low methanol mass fraction values. At the investigated conditions, similar '*S*' profile were observed. Increasing the methanol mass fraction in the glycerol heavy phase gives a decrease in selectivity of the biodiesel. This could be probably due to the presence of methanol in the glycerol heavy phase which enhances the solubility of the phase in the biodiesel light phase. This then solubilizes an amount of glycerol with methanol; which act as a glycerol carrier; thereby diminishing the solubility '*S*' values. This observation is in agreement with studies conducted (Machado et al., 2012).

Basically, distribution coefficient and selectivity parameters are essential in the comprehension of the solvent's ability to promote phase separation. Essentially, lower values for distribution coefficients implies higher concentrations of glycerol in the glycerol heavy phase and lower amounts of glycerol solubilized in the biodiesel light phase. Selectivity is directly related to the extraction capability of the solvent and it was observed that all values of the selectivity was larger than 1. However, the alcohol concentration is the main factor that affects biodiesel product solubility and selectivity (Franca et al., 2009). The agreement of the tie lines with the feed composition indicated low experimental error by loss of mass or analysis accounted for the quality of the LLE data obtained. The entire work complements the researches conducted by several other researchers (Franca et al., 2009, Machado et al., 2011 and Ardila et al., 2013).

4. CONCLUSION

Liquid-liquid experimental data consisting of binodal solubility curves and tie-lines were obtained for ternary system of castor oil biodiesel, methanol and glycerol at six different temperatures and atmospheric pressure (25, 35, 40, 40, 55 and 60) °C using modified cloud point titration method and gas chromatographic analysis. Distribution coefficient and selectivity analyses were performed. The system presented high values of methanol distribution and selectivity at the investigated conditions. The separation factor was greater than 1 at all investigated conditions. This indicated that methanol solubilized preferentially in the glycerol heavy phase. It also showed that methanol is a good extraction solvent for the separation of castor oil biodiesel and glycerol mixtures. The effect of temperature was observed to be negligible for the system studied. Spectroscopic analysis of the castor oil biodiesel and castor oil indicated the presence of several functional groups with methyl ricinoleate being the most pronounced. The knowledge of the phase equilibrium for the castor oil biodiesel, methanol and glycerol system is important in optimizing biodiesel purification process as well as developing models for simulating and optimizing ternary systems behaviour.

REFERENCES

Adama K.K., Onochie U.P and Gbeinzi E. **(2020):** Production, Characterization and Application of Ternary Phase Diagrams for the Purification of Biodiesel Produced from Tropical Almond Seed Oil, ***Nigerian Journal of Technology***, 39, 4, 1066 – 1075.

Adama, K. K., Aluyor, E O. and Audu, T. O. K. **(2018):** Tie Line Analysis of Ternary Phase Diagrams for Purification of Castor Oil Biodiesel/Methanol/Glycerol System at 20 °C and 30 °C, ***Nigerian Research Journal of Engineering and Environmental Sciences***, 3 (2), 517 – 528

Adama, K. K., Aluyor, E.O. and Audu, T.O.K. **(2021):** Component distribution associated with phase separation and purification of tropical almond biodiesel at different temperatures. ***Renewable Energy***, *165, 67 – 75*

Ardila, Y.C., Machado, A.B., Pinto, G.M.F., Filho, R.M., and Maciel, R.W. **(2013):** Liquid-Liquid Equilibrium in Ternary Systems Present in Biodiesel Purification from Soybean Oil and Castor Oil at 298.2K and 333.2K. ***Journal of Chemical and Engineering Data,*** 58, 605-610.

Atabani, A.E., Silitonya A.S., Irfan A.B., Mahlia T.M.I, Masjuki H.H., and Mekhilef S.A. **(2013):** Comprehensive reviews on biodiesel as an alternative energy resource and its characteristics, ***Renewable and Sustainable Energy Reviews;*** 16, 2070e2093

Borugadda, V.B., and Goud V.V. **(2012):** Biodiesel production from renewable Feedstocks: status and opportunities. ***Renewable and Sustainable Energy Reviews***; 16:4763 – 4784.

D'Amato D., Drose N., Alten B., Kettumen M., Lahtinen K., Korhonen J., Leskinen P., Matthies B.D.,

and Toppinen A. **(2017):** Green, circular bio economy: a comparative analysis of sustainability avenues, ***Journal of Cleaner Production***; 168, 716 – 734.

Do-Carmo, F.R., Evangelista, N.S., Santiago A.R.S., Fernandes, F.A.N., and Sant'Ana, H.B. **(2014):** Evaluation of Optimal Activity Coefficient Models for Modeling and Simulation of Liquid-Liquid Equilibrium of Biodiesel + Glycerol + Alcohol Systems. ***Fuel,*** 125, 57-65.

Encinar, M., Gonzalez, J.F., and Rodriguez-Reinares, A. **(2005):** Biodiesel from used Frying Oil-Variables Affecting the Yields and Characteristics of the Biodiesel. ***Industrial & Engineering Chemistry Research;*** 44, 5491-5499.

Follegatti, R.L.A., Lanza, M., Batista, F.R.M., Batista, E.A.C., Oliveira, M.B., Continho, J.A.P., and Meirelles, A.J.A. **(2010):** Liquid-Liquid Equilibria for Ternary Systems Containing Ethyl Esters, Anhydrous Ethanol and Water at 298.15K, 313.15K and 333.15K. ***Industrial & Engineering Chemistry Research;*** 49, 12613-12619.

Franca, B.B., Pinto, M.F., Pessoa, F.L.P., and Uller, A.M.C. **(2009)**: Liquid-Liquid Equilibria for Castor Oil Biodiesel + Glycerol + Alcohol, ***Journal of Chemical and Engineering Data;*** 54, 9, 2359-2364.

Knothe, G., and Van Gerpen J. H. **(2009):** The Biodiesel Handbook, 2nd Edition, AOCS Publishing, Urbana, II.

Machado, A.B., Ardila, Y.C., Hadlich de Oliveira, L., Aznar, M., and Maciel, R.W. **(2012):** Liquid-Liquid Equilibria in Ternary and Quaternary Systems Present in Biodiesel Production from Soybean Oil at 298.2K and 333.2K, ***Journal of Chemical and Engineering Data;*** 57(5), 1417-1422.

Machado, A.B., Ardila, Y.C., Hadlich de Oliveira, L., Aznar, M., and Maciel, M.R.W. **(2011):** Liquid-Liquid Equilibrium Study in Ternary Castor Oil Biodiesel + Ethanol + Glycerol and Quaternary Castor Oil Biodiesel + Ethanol + Glycerol + NaOH Systems at 298.2K and 333.2K. ***Journal of Chemical and Engineering Data;*** 56, 2196-2201.

Mesquita F.M.R., Feitosa F.X., Sombra N.E., Saraiva de Santiago A.R., and San'Ana H. B. **(2011):** Liquid-Liquid Equilibrium for Ternary Mixtures of Biodiesel (Soybean or Sunflower) + Glycerol + Ethanol at Different Temperatures. ***Journal of Chemical and Engineering Data;*** 56 4061-4067.

Mesquita, F.M.R., Evangelista, N.S., Batista S.A. H., and Saraiva S.A.R. **(2012):** Liquid-Liquid Equilibrium for the Glycerol + Alcohol + Coconut Biodiesel System at different Temperatures and Atmospheric Pressure. ***Journal of Chemical and Engineering Data;*** Dx.doi.org/10.1012/je7300749n.

Ming-Jer L., Yu- Ching K., Pei- Jung L. and Ho- Mu L. **(2010):** Liquid- Liquid Equilibria for Ternary Mixtures Containing Vegetable Oils, Methanol and Co-solvents. ***The Open Thermodynamics Journal,*** 4, 122-128.

Mosquera A.J.D., Vasco-Leal, J.F., Acosta-Osorio, A.A., Hernandez-Rios, I., Ventura-Ramos, E., Gutierrez-Cortex, E., and Rodriguez-Garcia, M.E. **(2016):** Optimization of Castor Seed Oil Extraction Process using Response Surface Methodology. ***Ingenieria e Investigacion.*** 36(3), 82-88.

Nangbes, J.G., Nvau, J.B., Buba, W.M., and Zukdiamma, A.N. **(2013):** Extraction and Characterization of Castor (Ricinis communis) Seed Oil. ***The International Journal of Engineering and Sciences (IJES)*** 2(9), 105-109.

Noriega, M.A., Narvazez, P.C., Imabachi, A.D., Cadavid, J. G., and Habert, A.C. **(2016):** Liquid-Liquid Equilibrium for Biodiesel-Glycerol-Methanol or Ethanol Systems using UNIFAC Correlated Parameters. ***Energy,*** 111, 841-849.

Ogunniyi, D.S. **(2006):** Castor Oil: A Vital Industrial Raw Material. ***Bioresource Technology*** 97, 1086-1091.

Rostami, M., Raeissi, S., Mahmodi, M., and Nowroozi, M. **(2013):** Liquid-Liquid Equilibria in Biodiesel Production. ***Journal of the American Oil Chemists' Society (JAOCS),*** 90: 147-154, Springer.

Seader J.D., and Henley E.J. **(2006):** Separation Process Principles, 2nd ed.: ***John Wiley and Sons: Hoboken, NJ.***

Vicente G., Martinez M. and Aracil J. **(2004):** Integrated Biodiesel Production: Comparism of Different Homogeneous Catalyst System, ***Bioresoure Technology*** 92, 297-305.

DOI: 10.51975/23380102.som
Journal of the Nigerian Society of Chemical Engineers, 38(1), 2023

EXTRACTION OF BIOEMULSIFIER FROM *CANDIDA TROPICALIS* ISOLATED FROM BANANA (*MUSA* X *PARADISIACA* L.)

Adetoyese, A. O.[1], *Aransiola, E. F.[1], and **Adeniran, H. A.[2]**
[1] *Department of Chemical Engineering, Obafemi Awolowo University, Ile-Ife, Nigeria*
[2]*Department of Food Science and Technology, Obafemi Awolowo University, Ile-Ife, Nigeria.*
[1] abylarry2@gmail.com, [1*]aransiolaef@gmail.com, [2] hexadeniran@gmail.com
*Corresponding author

ABSTRACT

Given the high expense of producing chemical-based emulsifying agents, the risk to human health, and the rising demand for natural products, biotechnologically-based compounds are gradually replacing these chemically synthesized emulsifiers. This work aimed to extract bioemulsifier from yeast strains isolated from available local fruits. Different fruit samples were collected randomly and allowed to grow on Potato Dextrose Agar (PDA) medium supplemented with 0.1 mg mL^{-1} chloramphenicol. The expected yeast isolates were then screened by using the same medium. This resulted in 18 isolates. These isolates were identified and characterized based on morphological and biochemical tests. Isolate E3 from ripe bananas showed the best result and this was used for molecular characterization. The Blast results from the molecular test revealed 98.78% similarity with Candida tropicalis MN450877.1 in the NCBI database. Based on this, the strain was identified as Candida tropicalis. The bioemulsifier was extracted from the Candida tropicalis using the autoclaving method. The yield of the bioemulsifier was 0.34 g/3 g dry yeast and emulsion activity after 24 h was 66.67%. This study has provided information on the potential, technological properties and suitability of Candida tropicalis isolated from ripe bananas as a bioemulsifier.

Keywords: *Banana; Bioemulsifiers; Candida tropicalis; Yeast isolates*.

1. INTRODUCTION

Biotechnologically-based compounds are gradually replacing chemically produced surface-active compounds through either microbiological or enzymatic syntheses (Ahamed and Prasad, 2021). It should be obvious that water and oil do not mix. Owing to their distinct advantages over chemical surfactants, such as biodegradability, biocompatibility, non-toxicity, efficiency at low concentrations, foaming, and good selectivity at various temperatures, pH and salinities. Bioemulsifiers are known as surface-active biopolymers compounds that are capable of stabilizing oil-in-water emulsions and are critical in a variety of industrial applications (Thraeib et al, 2022). Bioemulsifiers are produced by bacteria, moulds, and yeast and may be found in a variety of natural resources. Bioemulsifier has a greater molecular weight than biosurfactants (Ribeiro et al, 2020). In general, high-molecular-mass biosurfactants outperform low-molecular-mass biosurfactants as emulsifiers.

Due to the wide application of yeasts and it is Generally Regarded as Safe (GRAS) status, it is more easily accepted than other microorganisms in bioemulsifier production. Although yeast is present everywhere, it is most typically isolated from samples that are high in sugar. Fruits, berries, and plant exudates are a few excellent examples. Some yeast varieties are connected to soil and insects. It is necessary to consider certain physiological characteristics while evaluating a yeast strain for industrial usage. Numerous insoluble substrates have been fermented using Candida species, and they produce surface-active compounds (Alizadeh-Sani et al, 2018). A rich source of mannoproteins, -glucans and glucomannan with anti-neoplastic, anti-genotoxic, and antioxidative effects is the biomass of Candida yeasts. The generation of extracellular metabolites such as ethanol, erythritol, citric acid, biosurfactants, xylitol and exopolysaccharides are one of the numerous uses of Candida yeasts in biotechnology. These ingredients are employed in the cosmetic, food processing and pharmaceutical industries (Kieliszek et al, 2017). One of the most significant Candida species is *Candida tropicalis*. As an osmotolerant microorganism with the capacity to endure high salt concentrations, *C. tropicalis* may be crucial for the persistence of fungi in saline settings. This species is appropriate for use in biotechnology procedures because of its physiological trait. This study aims at extracting bioemulsifier from

yeast strains isolated from available local fruits and vegetables such as Banana, Orange, Plantain, Apple, Grapes and Tomatoes.

2. MATERIALS AND METHODS

2.1 Isolation of Yeast Strains from various Fruit Sources

Yeast strains are frequently connected to an environment where there is a lot of sugar**.** Fruit samples of Bananas, Oranges, Plantain, Apples, Grapes and Tomatoes were collected randomly from the new market of Obafemi Awolowo University. The fruits' seeds were removed after being peeled. The samples were aseptically pressed or mashed as necessary, and the fruit pulp was sieved using a clean, sterile muslin cloth. They were then put into containers and kept in the refrigerator for future use. Yeast isolates were obtained using the pour plate technique (Bakare et al, 2019). The serial dilution was prepared using sterile distilled water as diluents and about 1ml of each fruit pulp was used as a yeast source. This was further serially diluted in a test tube using 9 ml of sterile distilled water until a concentration of 10^{-6} is reached. About 1 ml of each of the odd-number serial dilutions was spread on top of 39 g/l PDA (potato dextrose agar) with chloramphenicol added at 0.1 mg/ml. Then, the composition was further incubated for 24-48 h at 30 ℃. According to the procedures outlined by Nasir et al (2017), the selected isolates' cell morphology and how it appears on the PDA medium were studied. After being cultivated for 18 to 24 h, yeast isolates were aseptically selected, streaked on a PDA medium, and then incubated for 48 h at 30 ℃. All of the isolates produced were tested as yeast cultures and then evaluated further for their capacity to break down glucose, lactose, and sucrose mixed with the substrate without aeration at 30 ℃

2.2 Yeast Identification

The characteristics of the yeast isolates were determined macroscopically by observing and taking note of the surface, shape, elevation, color, and morphology of the yeast isolates. The yeast isolates were also viewed under a microscope using the wet mount techniques cited by Nasir et al (2017).

2.3 Biochemical Characterization of the Yeast Isolate

The yeast isolates can be identified by the changes in the indicator color when the yeast culture assimilates carbohydrates or fermentation tests, ethanol tolerance and thermo-tolerance.

2.3.1 Sugar fermentation tests

The isolated yeasts were subjected to a sugar fermentation test which involves the use of 1% each of glucose, sucrose and lactose using 0.1% of Bromocresol purple indicator. The bromocresol was added to 8 g L^{-1} of yeast extract and the sugars were added too. Ten millilitres (10 ml) of each of the prepared sugars was introduced into the test tubes. Inverted Durham tubes were introduced into the test tubes and autoclaved. A sterile inoculating loop was used to pick colonies of each isolate and aseptically inoculated into the test tubes, then incubated for 48 h at 37 ℃.

2.3.2 Ethanol tolerance

The yeast isolates were screened for their efficiency in ethanol; by enabling yeast to grow in 5%, 10%, and 20% ethanol broth, the tolerance of each isolate was investigated. The ethanol broth composes of 8 g/l of yeast extract, 0.1% bromocresol and absolute ethanol (5%, 10%, 20%). Each test tube received 10 ml of the prepared medium, which was then sterilized in an autoclave at 121 °C for 15 mins. After allowing it to cool, the medium in the flasks was inoculated with a loop full of yeast isolates aseptically, and then incubated at 37 for 48 h (Bakare *et al.*, 2019). After incubation, the color change was indicative of a positive reaction.

2.3.3 Detection of thermotolerance

Thermotolerance of the selected yeast isolates was detected using the PDA liquid medium. Test tubes containing ten millilitres of the medium were autoclaved and cooled. A 48-hour-old selection of yeast isolates was then inoculated into a half loop. Every 24 h, the optical density of each tube was measured against a blank medium using a spectrophotometer set to 600 nm. All cultures were incubated at 30, 37, and 43.5 °C for three days.

2.3.4 Detection of Growth with Time

To detect the growth of the isolates with time, the isolates were inoculated into a 5% sterile glucose solution. The samples were withdrawn every 24 h for 72 h, and absorbance was taken with a spectrophotometer.

2.4 Molecular Characterization of Yeast Strains

Based on the biochemical tests, the yeast isolates with the appropriate technological properties for bioemulsifier production were selected and identified using molecular techniques. The molecular identification was carried out at Africa's Genomics Company, Inqaba Biotec West Africa Ltd, Opposite IITA Bus-Stop Moniya, Ibadan, Nigeria.

By analyzing the nuclear DNA (rDNA) through the Internal Transcribed Spacer (ITS) region, yeast isolates may be identified. DNA of the 48 h old test organism was

first extracted with a test kit. The Quick-DNA™ Fungal/Bacterial Miniprep Kit (Zymo Research, Catalogue No. D6005) was used to extract genomic DNA from the cultures.

The 16S target area was amplified using the universal primer 27F and 1492R (White *et al.*, 1990). The respective sequence of these primers is ITS-1: 5'-TCCGTAGGTGAACCTGCGG-3' and ITS-4: 5' TCCTCCGCTTATTGATATGC-3'. Using the primers highlighted above and One Taq® Quick-Load® 2X Master Mix (NEB, Catalogue No. M0486), the ITS target area was amplified. The PCR results were run on a gel, and the extracted fragments were then purified using Zymo Research's ZR-96 DNA Sequencing Clean-up Kit™ (Catalogue No. D4050) and forward and reverse sequenced using Nimagen's Brilliant Dye™ Terminator Cycle Sequencing Kit V3.1, BRD3-100/1000. For each reaction and each sample, the purified fragments were examined using the ABI 3500xl Genetic Analyzer (Applied Biosystems, ThermoFisher Scientific). Sequences were subsequently employed for taxonomic identification using a BLAST search and compared to the Gen Bank database (http://www.ncbi.nlm.nih.gov/BLAST/).

2.5 Extraction of Bioemulsifier

The technique of Torabizadeh *et al*. was modified to extract the bioemulsifier from Candida tropicalis cells. The technique was used to purify the bioemulsifier (Dikit et al, 2010). The supernatant was mixed with three volumes of acidic ethanol (ethanol that contains 95% alcohol and 10 ml/l acetic acids) and incubated for the duration of the precipitation at 3–4 °C. Once the precipitate has been centrifuged for 10 mins at 10,000 rpm, it will then be freeze-dried.

2.6 Analysis of Bioemulsifier

The bioemulsifier's molecular weight was estimated using the (SDS-PAGE) sodium dodecyl sulphate gel electrophoresis method with 100 g/l resolving gel (Dikit et al, 2010). BSA was used as the standard to quantify protein using the Folin-Ciocalteau reagent as outlined by (Lowry et al, 1951) (Spectrophotometer Perkin, Elmer). The technique of Dubois et al (1956) was used to colorimetrically measure total carbohydrates.

3. RESULTS AND DISCUSSIONS

3.1 Isolation of Yeasts

By using a PDA medium, 12 microbial isolates were recovered from each substrate (tomatoes, oranges, apples, bananas, plantains and grapes), and each of the isolates was further screened by subculturing using a selective medium to obtain pure yeast colonies. Previous research has revealed that samples high in sugar, such as flowers, leaves, tree exudates, sweet fruits, roots, grain, dung, and soil, and insects are commonly associated with yeast (Tikka et al, 2013). Further screening in the PDA medium supplemented with chloramphenicol resulted in 18 isolates, being able to show the yeast's morphological character. The eighteen isolates (A1, and A9 from overripe oranges, B1, B6 and B10 from overripe plantain, C2, C8 and C10 from overripe apples, D4, D6 and D11 from rotten tomatoes, E3, E4, E7 and E12 from overripe banana, F4, F8 and F11 from fermented grape juice) were selected after being cultivated on PDA agar at 30 ℃. Therefore, those 18 isolates were continuously assayed for their capability to use.

3.2 Growth of Isolates

After 3 days of incubation at 30 ℃, colonies were cream, smooth, and yeast-like on the surface of the PDA media. The summary of the results is shown in Table 1.

3.3 Microscopic Observation

The cell morphology of the selected isolates observed under the microscope shows the presence of round yeasts with single, pairs, or triple budding, and the germination consists of small, medium, and large types of budding. After 48 h of incubation at 30 °C, the isolates were found to be at the budding stage with a cream color and the elevation raised. The microscopic morphology of isolates in the form of blastopores that are round, cylindrical, or ovoid short and long affected by its strain and confirmed to be yeast.

3.4 Biochemical Characterization

3.4.1 Sugar fermentation test

The isolated yeast varied in terms of three distinct sugars (Table 1). The strain used glucose (dextrose), and sucrose, but fail to grow on lactose indicating they are diverse in sugar utilization. The fermentation was verified by the change in the media color from wine to yellow. Observations were made following a 48 h inoculation.

3.4.2 Ethanol tolerance

The isolate was chosen because it passed the ethanol tolerance test for yeast. It was shown that B3 and E3 can grow faster in 5%, slightly in 10% and weakly in 20% containing liquid media of yeast extract and bromocresol (Table 2).

Table 1: Sugar fermentation

Code	A1	A2	A3	B1	B2	B3	C1	C2	C3	D1	D2	D3	E1	E2	E3	F1	F2	F3
Glucose	++	++	+	+	-	++	+	+	+++	-	++	++	++++	++	+++	-	+++	+++
Gas production	Yes	Yes	Yes	Yes	Yes	Yes	Yes	Yes	Yes	Yes	Yes	Yes	Yes	Yes	Yes	Yes	Yes	Yes
Lactose	-	-	-	-	-	-	-	-	-	-	-	-	-	-	-	-	-	-
Gas production	No	No	No	No	No	No	No	No	No	No	No	No	No	No	No	No	No	No
Sucrose	++	++	+	+	+	++	+	+	-	-	+	+	++++	++	+++	-	-	-
Gas production	No	No	No	No	No	No	No	No	No	No	No	No	No	No	No	No	No	No

- No change + weak yellow ++ Dark yellow +++ light yellow ++++ Bright yellow

Table 2: Ethanol tolerance

Ethanol - containing media	A1	A2	A3	B1	B2	B3	C1	C2	C3	D1	D2	D3	E1	E2	E3	F1	F2	F3
5%	++	++	++	++	++	++	+	+	+	++	++	++	++	++	++	++	++	++
10%	+	+	+	+	+	++	+	+	+	++	+	-	+	+	++	+	+	+
20%	+	+	+	+	+	+	+	+	+	+	+	-	+	+	++	-	+	+

- No change + weak yellow ++ Dark yellow

The two isolates' highest growth was observed in 5% ethanol-containing media. The change in color shows the growth after 7 days at 5%, 10%, and 20% of ethanol-containing liquid media. The concentrations of ethanol play a significant role in regulating the fermentation process. It has been proven that fermentation cultures with incredibly high ethanol concentrations can depress or hinder the fermentation process. A similar result with Nasir et al (2017) for E3 isolates that tolerated up to 20% ethanol was seen in the present investigation, which is much more consistent with the other results (Table 2).

3.4.3. Effect of temperature on growth

Eighteen media containing yeast cells were incubated for 48 h at 30 ℃, 37 ℃, and 43 ℃. From Figure 1, all isolates were able to grow at 30 ℃ up to 37 ℃ and some up to 43 ℃. The maximum growth was found to be 37 ℃ with code E3 with the highest growth. The isolates can be classified as mesophilic. The effect of temperature is consistent with earlier research (Sulman and Rehman, 2013). For this reason, the operating temperature in standard yeast fermentation reactors must be kept between 30 and 35 °C. It has been observed from previous studies that yeast cell viability was adversely affected by high temperatures. However, there are few reports on the effective selection and isolation of yeasts capable of growing or fermenting at temperatures of at least 40 °C (Nasir et al, 2017).

3.4.4 Effect of time on growth

The growth pattern was studied by growing the isolates in a 5% sterile glucose solution, and the optical density was observed for each isolate at an interval of 24 h (Figure 2). The growth curve was shown for the best three isolates.

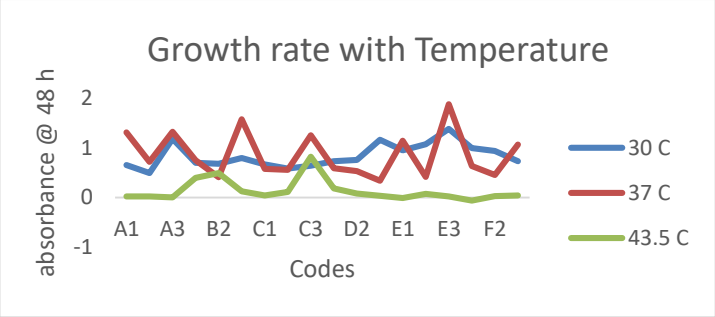

Figure 1: Effect of temperature on Growth rate

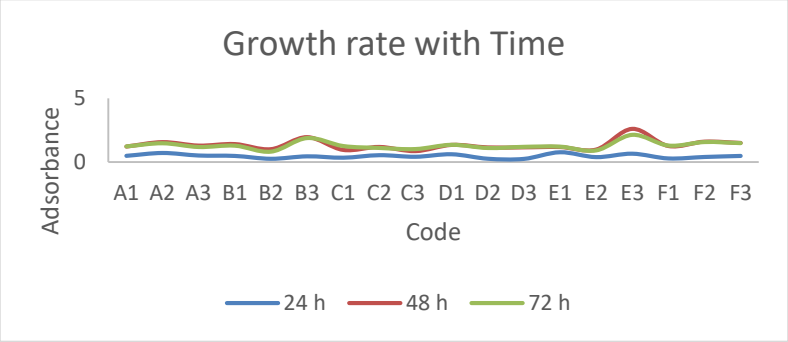

Figure 2: Effect of time on Growth rate

3.5 Molecular Identification of Yeast Strains

Due to the high accuracy of identification by molecular techniques, it was used in parallel with biochemical tests for the identification of species. After the isolates were identified and characterized based on morphological and biochemical tests, Isolate E3 from ripe bananas showed the best result and this was used for molecular identification. The results of the sequencing domain of the universal primer 27F and 1492R are used to amplify the 16S target region. Agarose gel electrophoresis was performed to resolve the amplified products, the photographic image of an agarose gel indicating the amplification of the ITS target region. The Blast results correspond to the similarity between the sequence queried and the biological sequences within the NCBI database. It revealed 98.78% similarity with *C. tropicalis* MN450877.1. Based on the result, the strain was identified *as Candida tropicalis.*

3.6 Extraction of Bioemulsifier

The results of the autoclaving time at 2 h had a not very clear band with a range of molecular weights at 7.5 KDa, 16.90 KDa, and 34.2 KDa in gel electrophoresis (Figures 3 and 4). The yield of the bioemulsifier was 0.34 g/3 g and emulsion activity after 24 h was 66.67%. The protein and carbohydrate content of this bioemulsifier are estimated to be 30.41 mg/g (11.32%) and 238.54 mg/g (88.675%) respectively which is similar to the composition of structural mannoprotein (approximately 10% protein and 90 % carbohydrate) (Barriga et al, 1999).

4. CONCLUSION

This work has revealed that a biotechnologically useful yeast could be isolated from an underutilized, readily available waste product like overripe fruits; where bioemulsifier could be extracted. Different yeast strains were isolated, screened, and characterized biochemically and molecularly. This study has provided information on the potential, technological properties and suitability of *Candida tropicalis* isolated from ripe bananas as bioemulsifier.

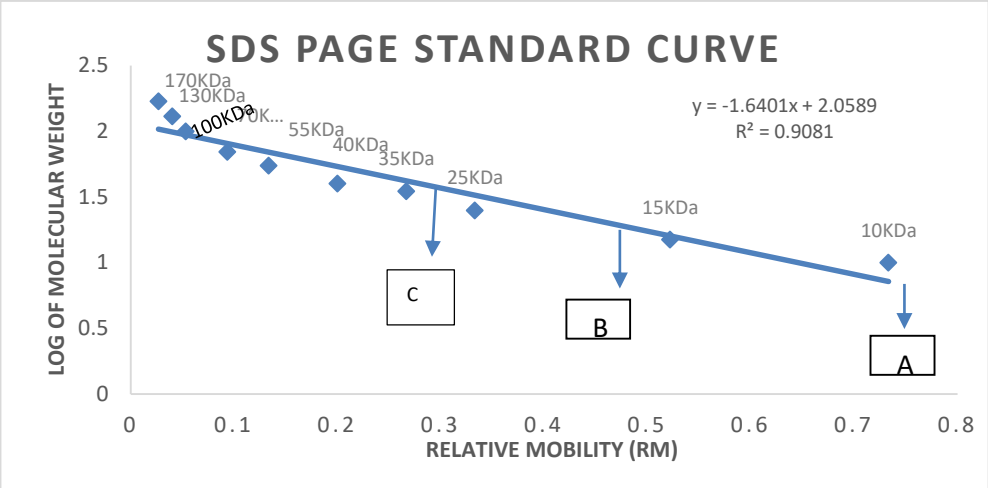

Figure 3: Standard Plots for the Determination of Molecular weight of bioemulfier

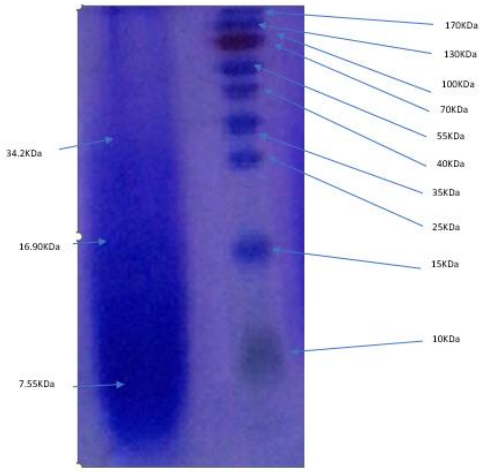

Figure 4: SDS-PAGE with Coomassie brilliant blue staining of bioemulsifiers extracted after 2 h of autoclaving and standard prestaining.

REFERENCES

Ahamed, M. I. and Prasad, R. (2021). *Microbial Biosurfactants: Preparation, Properties and Applications*, Springer Nature.

Alizadeh-Sani, M., Hamishehkar, H., Khezerlou, A., Azizi-Lalabadi, M., Azadi, Y., Nattagh-Eshtivani, E., Fasihi, M., Ghavami, A., Aynehchi, A. and Ehsani, A. (2018). Bioemulsifiers Derived from Microorganisms: Applications in the Drug and Food Industry. *Advanced pharmaceutical bulletin*, 8**:** 191.

Bakare, V., Abdulsalami, M., Onusiriuka, B., Appah, J., Benjamin, B. and Ndibe, T. (2019). Ethanol Production from Lignocellulosic Materials by Fermentation Process Using Yeast. *Journal of Applied Sciences and Environmental Management*, 23**:** 875-882.

Barriga, J. A., Cooper, D. G., Idziak, E. S. and Cameron, D. R. (1999). Components of the Bioemulsifier from S. Cerevisiae. *Enzyme and Microbial Technology*, 25: 96-102.

Dikit, P., Maneerat, S., Musikasang, H. and H-Kittikun, A. (2010). Emulsifier Properties of the Mannoprotein Extract from Yeast Isolated from Sugar Palm Wine. *Science Asia*, 36: 312-318.

Dubois, M., Gilles, K. A., Hamilton, J. K., Rebers, P. T. and Smith, F. (1956). Colorimetric Method for Determination of Sugars and Related Substances. *Analytical chemistry*, 28**:** 350-356.

Kieliszek, M., Kot, A. M., Bzducha-Wróbel, A., Błażejak, S., Gientka, I. and Kurcz, A. (2017).

Biotechnological Use of Candida Yeasts in the Food Industry: A Review. *Fungal Biology Reviews*, 31**:** 185-198.

Lowry, O., Rosebrough, N., Farr, A. and Randall, R. (1951). Protein Measurement with the Phenol Folin Reagent. *Journal of Biological Chemistry*, 193**:** 265-275.

Nasir, A., Rahman, S. S., Hossain, M. M. and Choudhury, N. (2017). Isolation of Saccharomyces Cerevisiae from Pineapple and Orange and Study of Metal's Effectiveness on Ethanol Production. *European Journal of Microbiology and Immunology*, 7**:** 76-91.

Ribeiro, B. G., Guerra, J. M. and Sarubbo, L. A. (2020). Biosurfactants: Production and Application Prospects in the Food Industry. *Biotechnology Progress*, 36**:** e3030.

Sulman, S. and Rehman, A. (2013). Isolation and Characterization of Cellulose Degrading Candida Tropicalis W2 from Environmental Samples. *Pakistan Journal of Zoology*, 45**:** 809-16.

Thraeib, J. Z., Altemimi, A. B., Jabbar Abd Al-Manhel, A., Abedelmaksoud, T. G., El-Maksoud, A. a. A., Madankar, C. S. and Cacciola, F. (2022). Production and Characterization of a Bioemulsifier Derived from Microorganisms with Potential Application in the Food Industry. *Life*, 12**:** 924.

Tikka, C., Osuru, H. P., Atluri, N., Raghavulu, P. C. V., Mannur, I. S., Prasad, U. V., Aluru, S. and Bhaskar, M. (2013). Isolation and Characterization of Ethanol Tolerant Yeast Strains. *Bioinformation*, 9: 421.

Torabizadeh, H., Shojaosadati, S. and Tehrani, H. (1996). Preparation and Characterisation of Bioemulsifier Fromsaccharomyces Cerevisiaeand Its Application in Food Products. *LWT-Food Science and Technology*, 29: 734-737.

DOI: 10.51975/23380103.som
Journal of the Nigerian Society of Chemical Engineers, 38(1), 2023

DESIGN AND DEVELOPMENT OF ARDUINO-BASED TEMPERATURE MONITORING SYSTEM FOR A PORTABLE HAEMODIALYSIS SYSTEM

***Sulayman, A. A.[1], Araromi, D. O.[1] and Ayodele, O. E.[2]**

[1] *Department of Chemical Engineering, Ladoke Akintola University of Technology, Ogbomoso, Oyo State, Nigeria*
[2] *Department of Medicine, Ladoke Akintola University of Technology, Ogbomoso, Oyo State, Nigeria*
[1*]aasulayman@lautech.edu.ng, [1]doararomi@lautech.edu.ng [2]gbengaayox@yahoo.ca
* Corresponding author

ABSTRACT

Haemodialysis (HD) is a life-saving treatment option for end-stage kidney disease patients to remove excess fluid, substances and waste products through a semi-permeable membrane (dialyser, also known as the artificial kidney). This makes HD a perfect illustration of the synergy between chemical engineering principles and medical care. Although commercial haemodialysis machines are available, high cost, large space consumption, and accessibility to poor masses are significant concerns. This work develops an Arduino-based temperature monitoring system for a low-cost portable haemodialysis machine. In vitro HD system design was verified by experiment using porcine blood, and it can monitor blood and dialysate temperature in real-time using Arduino microcontroller. The accuracy of the designed HD system was determined using Urea Reduction Ratio (URR) and Creatinine Reduction Ratio (CRR). Results of the URR and CRR obtained were 71.97% and 65.29%, respectively. The developed HD system can be used to monitor temperature during haemodialysis.
Keywords: *Haemodialysis, Kidney disease, Accuracy, real-time monitoring, dialyser*

1. INTRODUCTION

Kidney failure results in the accumulation of fluid and toxic or metabolic wastes in the body. About 10% of the world's population is affected by chronic kidney disease, and the mortality rate increases yearly due to inaccessible affordable treatment (World Kidney Day, 2015). Kidney replacement therapy is the therapeutic option for patients diagnosed with kidney failure, which can be either dialysis or kidney transplantation.

Dialysis treatment can be done either by haemodialysis or peritoneal dialysis. Haemodialysis is an extracorporeal blood purification process whereby blood is circulated out of the body, cleansed and balanced for its constituents such as electrolytes, fluid concentration and fluid concentration through an external device called a dialyser and thereafter returned to the body (Muhammadu et al, 2020). The intermittent haemodialysis method is a commonly recognized treatment in hospitals. However, complications such as intradialytic hypotension (low blood pressure) usually arise and may be associated with high mortality rates (Panhwar et al, 2018).

Most haemodialysis machines available are expensive and require large water treatment plants. These limitations led to the development of an arduino-based monitoring device for a low-cost, portable haemodialysis system. This improvement can potentially monitor some haemodynamic properties in real-time to improve the patient's quality of life and reduce dialysis costs for patients and healthcare providers.

Real-time monitoring requires the instrumentation of a system using microcontrollers. Arduino is open-source, cross-platform software with a programming circuit board called a microcontroller and a set of development boards known as Arduino Integrated Development Environment (IDE). Arduino developed software can support MATLAB, which allows one to obtain and plot real-time data directly from the command window. This helps to construct a real-time monitoring haemodialysis system (Gao *et al*., 2021; Shin & Jeon, 2017; SNikilla, 2016).

2. MATERIALS AND METHODS

2.1 Process Description

The *in vitro* haemodialysis system constructed has two glass jars of 1L capacity that served as the storage tanks for blood and dialysate storage in the experimental rig.

Two peristaltic pumps with model TA7291P were used to pump blood and dialysate. Pump flow rates can be adjusted between 10 and 250 ml/min. A dialyser of type ELISIO™ – 17L (Low Flux) served as an artificial kidney. Two Arduino DS18B20 temperature sensors simultaneously measured the blood temperature and dialysate during the dialysis session. A heating unit adjusted and stabilised the dialysate temperature at 37 °C. The pumps, probes and sensors were calibrated before the start of dialysis. MATLAB ® 2019 served as the hardware-software interface and coordinated different activities during the experiment.

The instrumentation unit was constructed as an assembly of electronic components, which housed a microcontroller, conductivity readers, temperature readers and developmental boards. This unit was built to synchronise the activities of the two peristaltic pumps and measuring devices used in the experiment. The Process Flow Diagram of the haemodialysis process is shown in Figure 1. MATLAB 2019 simulation software was used for simulation.

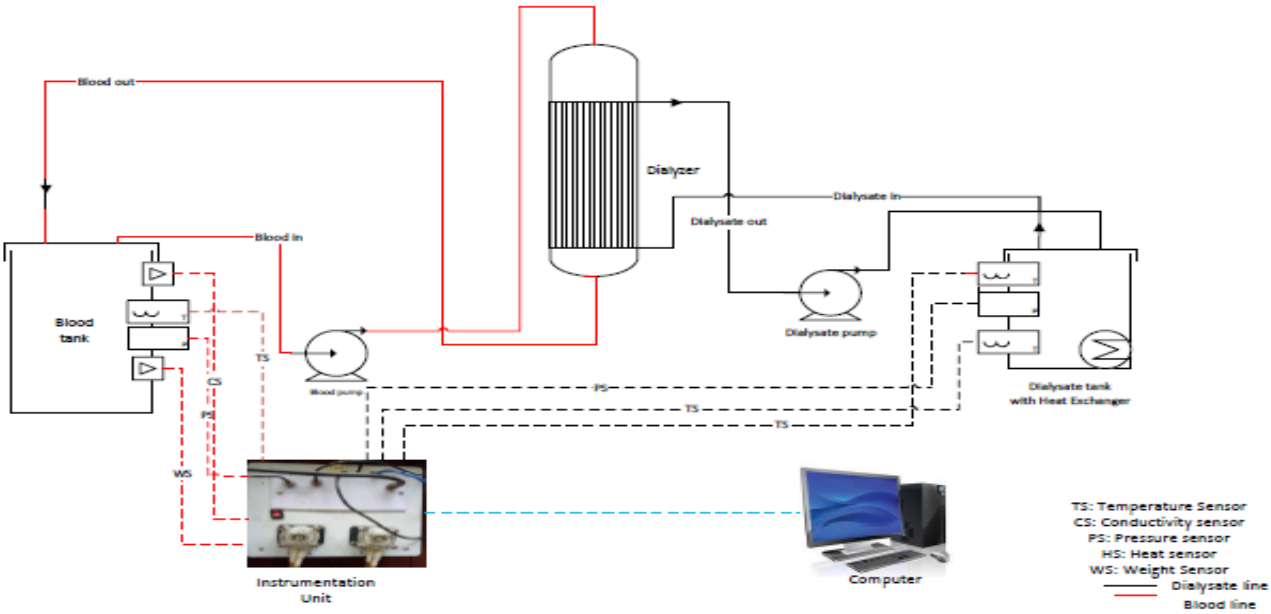

Figure 1: Process flow diagram of haemodialysis process

2.2 Preparation of Solution

The dialysate solution was prepared by mixing acid concentrate for haemodialysis (NIPROSOL 324A) and sodium hydrogen bicarbonate concentrate ($NaHCO_3$) with deionized water at a volumetric ratio of 1:1.72:42.28. Porcine blood was chosen as a substitute for human blood because its haematological constants are close to human blood. The specific gravity of human and porcine blood is 1.05-1.06 and 1.005-1.06, respectively, and both have a relative viscosity of 4 -5 (Panhwar et al, 2018). The blood was obtained from an abattoir. A dose of 3.5–7.0 USP⁄mL heparin was immediately added to the blood to prevent clotting (Olson, 2009). The heparinised porcine blood was then transferred to the laboratory in an insulated vessel. The heparinised porcine blood sample was treated by adding 5.76g of creatinine and 0.9g of urea to 500 mL of heparinised blood since high blood urea nitrogen and creatinine are significantly elevated in patients with uraemia. The treated blood sample is a substitute for human blood samples of patients with uraemia (Panhwar et al, 2018).

2.3 Instrumentation Unit

The main component in the instrumentation unit used for the experimental set-up is the Arduino microcontroller. Arduino was used because it is easy and economical to create a project relating to digital electronics embedded systems (Aqeel, 2018). Arduino contains a programmed circuit board called microcontroller and a set of development boards that contains hardware and software libraries called Arduino Integrated Development Environment (IDE). The microcontrollers deliver information by connecting to a computer with the help of USB cable while Integrated Development Environment was used in programming (C programming language). Arduino board interprets commands in the instrumentation system and then sends appropriate signals to the various units for proper action.

DOI: 10.51975/23380103.som
Journal of the Nigerian Society of Chemical Engineers, 38(1), 2023

2.4 Haemodialysis Experiment

Bloodline was rinsed with normal saline to remove exhaust gas in the bloodline. During the experiment, blood is pumped from the blood tank and sent to a dialyser for purification. In the dialyser, there was a mass transfer of solutes (Blood Urea Nitrogen (BUN) and creatinine) from the sample blood to the dialysate. The mass transfer occurred by diffusion through a semi-permeable membrane inside the dialyser. The dialysate temperature was kept at 37 ^{o}C and passed through the dialysate pump to the dialyser, where the diffusion occurs. The experiment was carried out at blood and dialysate flow rates of 100, 120 ml/min (FL1) and 120, 150 ml/min (FL2) for 60 min. The haemodialysis experimental setup is shown in Figure 2 while its Simulink interface is shown in Figure 3.

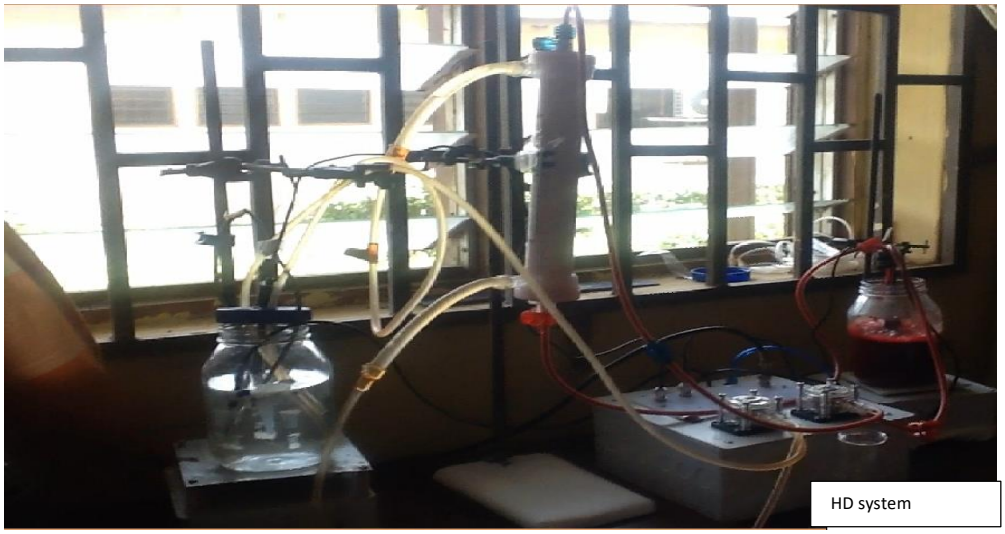

Figure 2: An *In-vitro* haemodialysis system

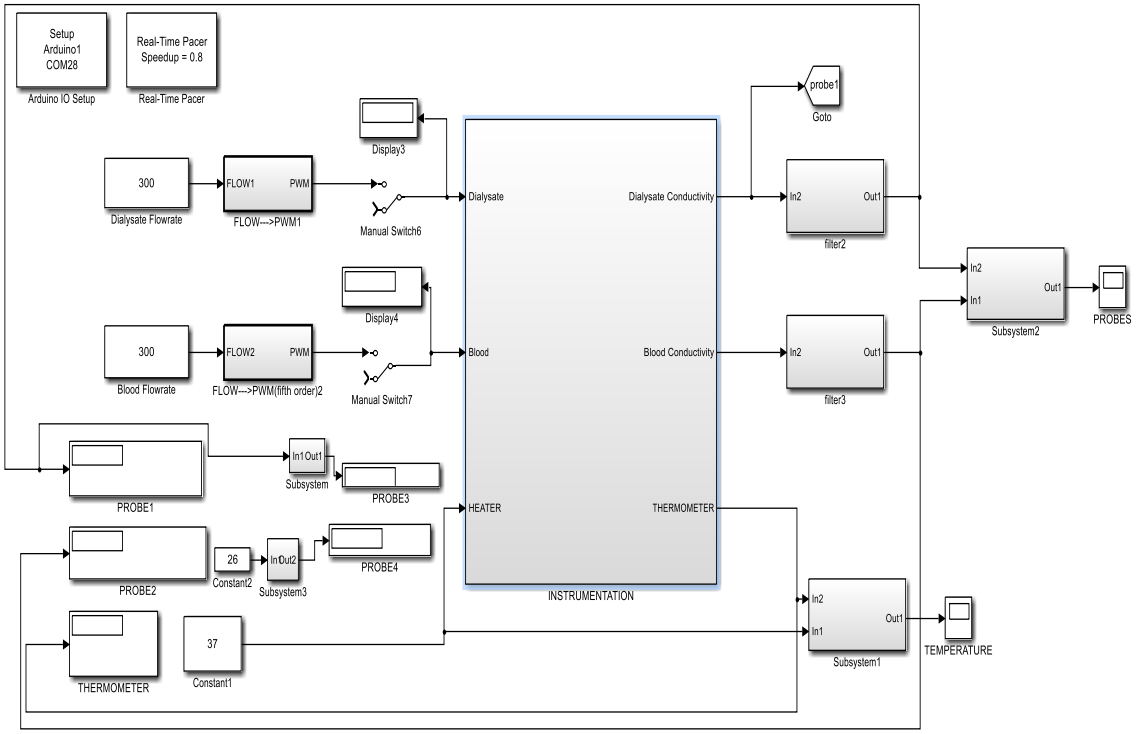

Figure 3: Simulink interface for haemodialysis experimental set-up

2.5 Method of Analysis

Intradialytic blood samples of 1ml at 10 min intervals were taken for BUN and creatinine analysis. BUN and creatinine analyses were carried out using SPM-23A Spectrophotometer using Berthelot and Jeff's method, respectively. Haemodialysis process adequacy was determined using Urea Reduction Ratio (URR) and Creatinine Reduction Ratio (CRR). The National Kidney Foundation Guidelines (DOQI) and the European Renal Association (ERA) have set standards for the adequacy of haemodialysis treatment. The threshold for adequate URR and CRR is 65% (Nafisi et al., 2011; Panhwar *et al*., 2018). The URR and CRR were determined using Equation 1.

$$R = 100(1 - \frac{C_t}{C_o}) \quad (1)$$

Where R= Reduction Ratio (BUN or creatinine), C_t= concentration (BUN or creatinine) at time t, C_o= initial concentration (BUN or creatinine).

3. RESULTS AND DISCUSSION

The results of BUN and creatinine analysis of the *in vitro* haemodialysis system designed are shown in Tables 1 and 2, respectively. Table 1 shows the BUN analysis of FL1 and FL2 before haemodialysis and at 10 mins intervals for 60 mins. Results of BUN analysis of fresh blood collected in FL1 and FL2 were 12.1 mg/dL and 28.0 mg/dL, respectively. BUN of treated blood samples (fresh blood added with BUN and creatinine) for FL1 and FL2 were 70.9 mg/L and 113.1 mg/dL, respectively, before the commencement of haemodialysis. It is observed from the table that a high removal rate of BUN occurred within 10 mins of the dialysis session in both experiments. However, removal rates were low after 10 mins in both experiments.

The result of creatinine analysis shown in Table 2 revealed a high removal rate of creatinine in the 10 mins of dialysis in both FL1 and FL2. However, FL1 had a low creatinine removal rate from 10 minutes to 40 minutes before the oscillatory response. FL2 showed a steady removal rate for 30 mins, and a higher creatinine response was obtained at 40 mins before its decline. The fluctuations in the BUN and creatinine analysis results were due to the analyser used in their analysis. Low removal rates in BUN and Creatinine results were caused by dialysate recirculation. This is because recirculation uses less dialysate, but less mass transfer rate from the blood to dialysate due to a smaller concentration gradient (Olson, 2009).

Table 1: Blood Urea Nitrogen Analysis Result of in vitro Haemodialysis Process

Sampling Time (min)	FL1 (mg/dL)	FL2 (mg/dL)
Pre-dialytic	70.9	113.1
10	41.1	43
20	39.7	38.3
30	38.3	31.3
40	37.3	32.2
50	36.4	31.9
60	36.7	31.7

Table 2: Creatinine Analysis Result of *in vitro* Haemodialysis Process

Sample Time	FL1 (mg/dL)	FL2 (mg/dL)
Pre-dialytic	41.2	36.3
10	18.9	16.7
20	18.3	19.3
30	15.2	11.9
40	15.4	14.8
50	17.1	14.2
60	16.7	12.6

The results obtained in this study were compared with Olson (2009) and Chen *et al.* (2014) results. A 70% removal rate of BUN was achieved by Chen *et al.* (2014) at 29 mins using deionised water for dialysate preparation and 12 mins using plasmon-induced dialysate comprising Au nanoparticles (NPs)-treated (AuNT) water for dialysate preparation. Olson (2009) could not achieve a 70% removal rate at 60 mins using deionised water for dialysate preparation. In this research work, FL2 achieved a 70% removal rate at 25 mins; however, FL1 could not achieve a 70% removal rate at the end of 60 mins. The result showed that micro solutes such as BUN and creatinine were successfully removed through the *in vitro* haemodialysis process experiment and FL2 gave the best removal rate.

The chart of the adequacy of the haemodialysis process evaluated using URR and CRR is shown in Figures 4 and 5, respectively. The trend of the URR chart shown in Figure 4 showed that FL1 attained 65.1% URR at 30 min and was reduced to 62.6% at the end of dialysis. However, FL2 has an adequate haemodialysis process with a final URR of 71.97%. The CRR chart in Figure 5 indicated that the creatinine removal rate was fast at the onset of haemodialysis. However, the removal rate fluctuated during the haemodialysis session, which may be due to the recirculation of dialysate during the dialysis period. The final CRR obtained in FL1 and FL2 at the end of the dialysis session are 59.5% and 65.3%. Since adequate haemodialysis process is obtained at URR or CRR > 65%, it can be concluded that FL2 with a blood pump of 120 ml/min and dialysate pump of 150 ml/min is efficient for the haemodialysis process.

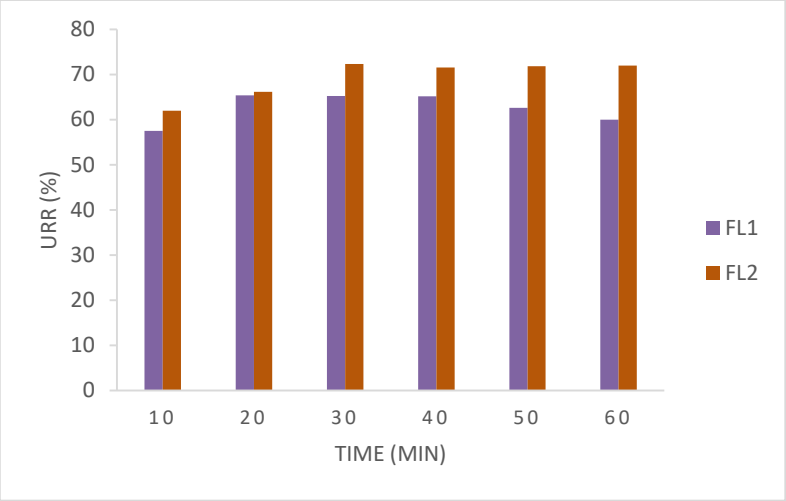

Figure 4: Urea reduction ratio of haemodialysis process

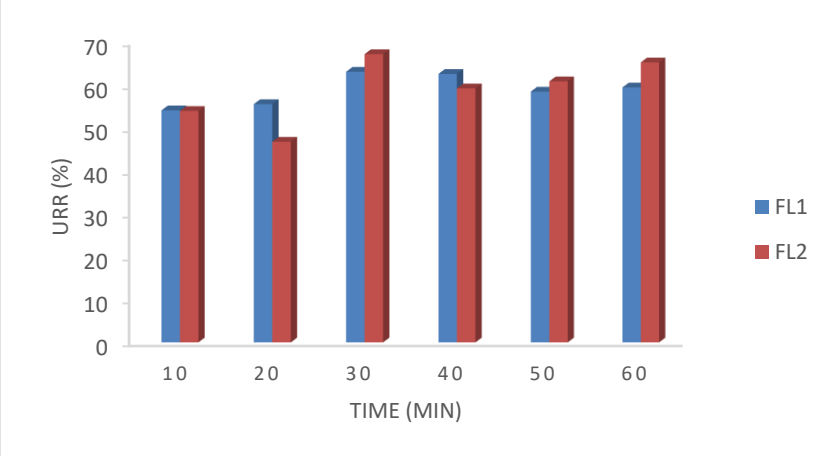

Figure 5: Creatinine reduction ratio of haemodialysis process

Hypotension can occur during a dialysis session. In response to the low blood pressure (hypotension), there is generalised vasoconstriction, which can make the patient complain of coldness and shivering. The blood and dialysate temperatures were monitored in real-time during the haemodialysis process to monitor the patient's

condition. The plot of blood and dialysate temperatures monitored in real-time during *in vitro* haemodialysis session is shown in Figure 5. The dialysate temperature was set at a constant temperature of 37℃ at the start of the haemodialysis session. The heating unit automatically regulated the dialysate temperature as indicated in the dialysate temperature graph. The dialysate temperature was used to regulate the blood temperature. This is because as blood passes through the inner membrane of the dialyser while the dialysate passes countercurrently to the outer layer of the dialyser; thus temperature gradient occurs. There was no increase in the blood temperature from the start of the dialysis session at 32.8 ℃, and this was because the dialysate temperature regulated the dialysate surface line in the dialyser. As the time increases, the blood temperature increases while regulating the dialysate temperature across the 37℃ set temperature. The result showed that the dialysate heating unit could regulate the dialysate temperature across 37 ℃ set temperature. With this observation, it is possible to manipulate the dialysate temperature to control the patient's blood temperature.

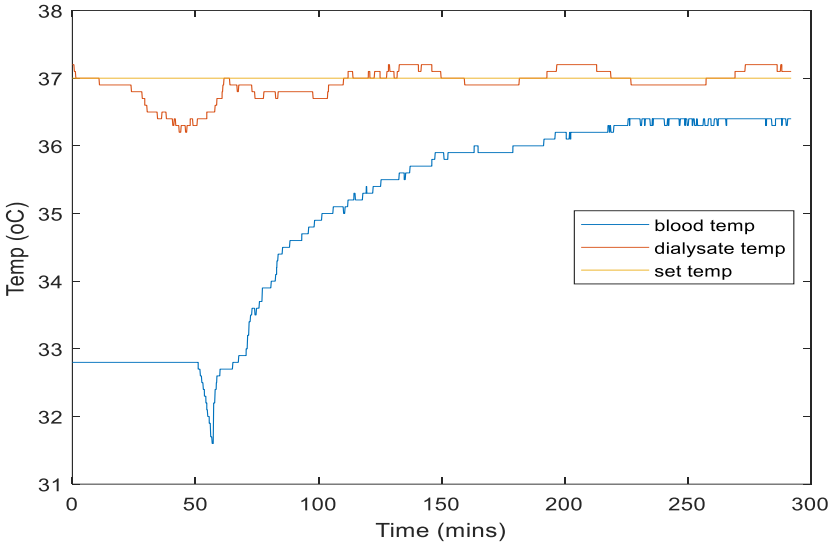

Figure 6: Blood and dialysate temperature curves

4. CONCLUSION

The designed *in vitro* haemodialysis system mimicked the clinical haemodialysis system and removed toxic micro solutes (BUN and creatinine) accumulated in the blood. Experimental results of the designed i*n vitro* haemodialysis system showed that real-time temperature monitoring was successfully achieved at different blood flow rates. Optimum flow rates of blood and dialysate were achieved at 120 ml/min and 150 ml/min, respectively, at URR and CRR at 71.97% and 65.29%.

REFERENCES

Aqeel, A. (2018). Introduction to Arduino Nano. The Engineering Projects, 1-4 [accessed 22nd November, 2021]

Chen, H.C, Lin, H.C, Chen, H.H., Mai, F.D., Liu, Y.C., Lin, C.M., Chang, C.C., Tsai, H.Y., and Yang, C.P, (2014). Innovative Strategy with Potential to Increase Haemodialysis Efficiency and Safety. Scientific Reports, 1 – 4.

Gao, W., Luo, X., Liu, Y., Zhao, Y. and Cui, Y. (2021). Development of an Arduino-based Integrated System for Sensing of Hydrogen Peroxide. *Sensors and Actuators Reports*, 3, p.100045.

Muhammadu, S.K., Revanth, M., Sakthiel, M., Sanjay, K.S. and Thamarai, K. V. (2020). Portable Dialyzer – A Safety Engineering on the Design of Haemodialysis System, *International Journal of Innovative Research in Advanced Engineering*, **7**(3), pp. 39 – 42.

Olson, J. C., (2009). Design and Modelling of a Portable Haemodialysis System. *Unpublished Masters Thesis*, Georgia Institute of Technology.

Panhwar, M. A., Panhwar, F., Zhao, G., and Pirzada, N. (2018). A Low-cost Portable Device for Combined Haemodialysis and Ultrafiltration. *International Journal of Applied Engineering Research*, **13**(7), 5400–5403.

Shin, H.S. and Jeon, J.-C., (2017). Data Acquisition System using Arduino and MATLAB. *Journal of Innovative Research in IT & Computer Science*, 01(01), pp.6–9

SNikilla, R., (2016). Real Time Health Monitoring System using Arduino. *South Asian Journal of Engineering and Technology*, 2(18), pp.52–60.

World Kidney Day (2015). Chronic Kidney Disease. http://www.worldkidneyday.org./fags/kidney-disease [accessed 10th July, 2022].

DOI: 10.51975/23380105.som
Journal of the Nigerian Society of Chemical Engineers, 38(1), 2023

AIR EMISSIONS FROM STEPWISE CO-PYROLYSIS OF PLASTIC MIXTURES

***Oladunni, A. A.[1], Odejobi, O. J.[2] and Sonibare, J. A.[2]**
[1]Department of Chemical Sciences, Ajayi Crowther University, Oyo, Nigeria
[2]Department of Chemical Engineering, Obafemi Awolowo University, Ile-Ife, Nigeria
[1*]aa.oladunni@acu.edu.ng, [2]dareodejobi@oauife.edu.ng, [3]asonibar@yahoo.com
[*]Corresponding author

ABSTRACT

Stepwise air emissions of Hydrocarbon, carbon II oxide (CO), carbon IV oxide (CO_2), nitrogen II oxide (NO), nitrogen IV oxide (NO_2), oxides of nitrogen (NOx), sulphur IV oxide (SO_2), and hydrogen sulphide (H_2S) from co-pyrolysis of Low-density polyethylene (LDPE), Polystyrene (PS) and Polyethylene terephthalate (PET) were studied between 50 ^oC - 450 ^oC using E8500 plus combustion analyzer. The maximum air emissions measured were compared with available Ambient Air Quality Guidelines from World Health Organization and National Environmental Standards and Regulations Enforcement Agency. The result showed that HC, CO, and NO were detected while CO_2, NO_2, SO_2, and H_2S were not. Co-pyrolysis of plastic mixture comprising 50% LDPE, 0%PS and 50% PET gave the highest HC emission of 16,567 mg/m^3 at 400-450 ^oC, while co-pyrolysis of 100% LDPE, 0% PS and 0% PET gave the highest CO emission of 16,239.85 mg/m^3 and NO emission of 138.44 mg/m^3 at 50-100, and 250-300 ^oC respectively. The maximum measured emission of CO far exceeded the maximum allowable standards which implied toxic ambient air within the vicinity of operation.

Keywords: *Co-pyrolysis, Air emission, Ambient air quality, Mixtures, Plastic valorisation.*

1. INTRODUCTION

Thermal degradation of plastics by means of pyrolysis results in depolymerization to yield solid, liquid and gaseous products of high energy value (Miandad *et al.*, 2019). Gaseous emissions from this process oftentimes contain air pollutants which could be hazardous to human health if emitted at high quantity (Kehinde *et al.*, 2020). Although, the acceptance of co-pyrolysis as a thermochemical method of treating plastics has increased across the globe in recent years; rare studies have been conducted to characterize the emissions associated with co-pyrolysis of LDPE, PS and PET. This study seeks to characterize and quantify the emissions associated with the co-pyrolysis of LDPE, PS and PET through experimental simulation of the process in the laboratory at stepwise increase in temperature in comparison with Ambient Air Quality standards.

2. MATERIALS AND METHODS

Low-density polyethylene(LDPE), Polystyrene(PS) and Polyethylene terephthalate(PET) materials were shredded into an approximate uniform size of 10×10 cm and air-dried to minimize energy requirement for drying in the experiment before usage (Yuliansyah *et al.*, 2015).

2.1 Experimental Design

Experimental design showing standard mixture ratios for the co-pyrolysis of LDPE, PS and PET are shown in Table 1. Four experimental points were three-component mixtures, three experimental points were two-component mixtures, and the remaining three experimental points were pure components. The components of the mixtures were calculated in grams and the total weight of each mixture was 60g. The percentage mass fractions of the mixtures are shown in Table 1. The unique mixtures were coded A-J for easy identification. The mixtures were loaded into the reactor according to the mixture fractions and the co-pyrolysis were performed at 50 - 450 ^oC for 90 min at a constant heating rate of 6 $^oCmin^{-1}$ (Demirbas, 2004; Onwudili *et al.*, 2009; Patni *et al.*, 2013).

Table 1: The sample codes and percentage of mass fraction at the experimental design points

Run	Run codes	LDPE (%)	PS(%)
1	A	17.00	17.00
2	B	17.00	66.00
3	C	100.00	0.00
4	D	50.00	0.00
5	E	33.33	33.33
6	F	0.00	0.00
7	G	50.00	50.00
8	H	0.00	100.00
9	I	0.00	50.00
10	J	66.00	16.00

2.2 Experimental Set-up and Procedure

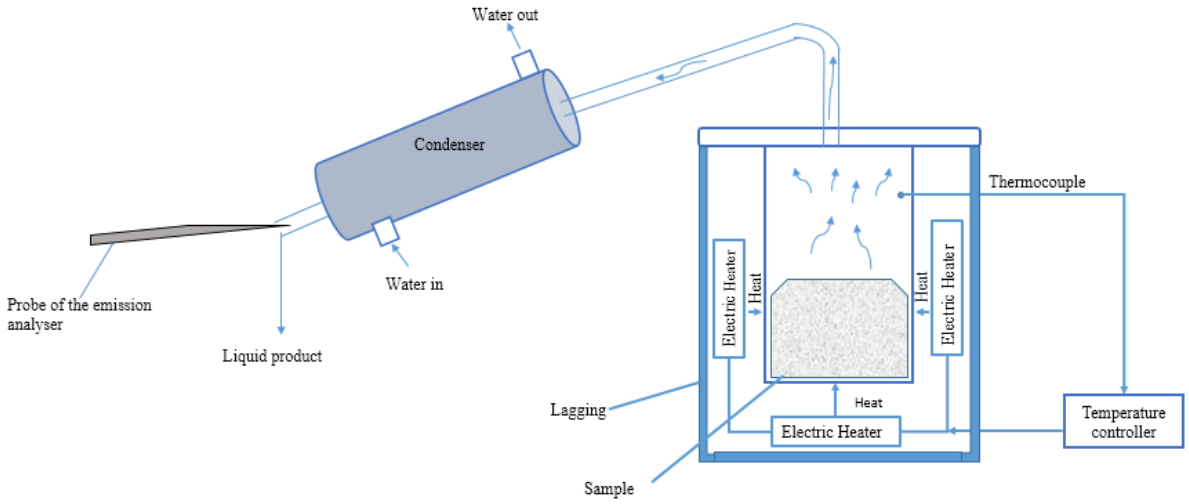

Figure 1: Sketch of experimental set up

The representation of the entire pyrolysis system is shown in Figure 1. The batch reactor was cylindrical and made of stainless-steel material(American Society for Metals, 1980) with a height of 25cm and external diameter of 16cm. Gasket sheet of 0.2 cm thickness was positioned between the cover and the flanges of the reactor to prevent gas leakage. The reactor was loaded and unloaded through a circular opening (12 cm diameter) sealed off by a 13 × 13 cm square plate at the center of the cover. The internal temperature of the reactor was measured by type-K thermocouple controlled by a 1200 ^{o}C range temperature controller. The reactor was placed in a double walled lagged vessel to prevent heat loss. Probe of E8500 plus combustion analyzer was positioned inside the ground end of the Liebig condenser to have a direct contact with the gaseous emissions from the co-pyrolysis process.

The characterized emissions from the co-pyrolysis of the polymeric wastes include, Hydrocarbons (HCs), carbon II oxide (CO), carbon IV oxide (CO_2), nitrogen II oxide (NO), nitrogen IV oxide (NO_2), oxides of nitrogen (NOx), sulphur IV oxide (SO_2), and hydrogen sulphide (H_2S) in accordance with EPA provisional reference methods (EPA-CTM-022, 1995; ICAC, 1999; EPA, 2017). The emissions of the co-pyrolysis of each mixture were measured in milligram per cubic meter(mg/m^3) at a 50 ^{o}C stepwise increase in temperature from 50 - 450 ^{o}C for all the air emissions, and the time taken for each period of measurements were recorded in seconds (s).

2.3 Comparison of Emissions with Air Quality Standards

The emissions from the co-pyrolysis process were compared with various air quality standards by World Health Organization (WHO), National Environmental Standards and Regulations Enforcement Agency (NESREA) and US environmental protection Agency (EPA) to determine compliance with the standard limits.

3.0 RESULTS AND DISCUSSION

3.1 Air Emissions at stepwise 50 ^{o}C increase in temperature in the co-pyrolysis of LDPE, PS and PET

No emissions of CO_2, NO_2, SO_2 and H_2S were detected in all the mixtures studied between 50-450^{o}C. However, there was detection of HC, CO, and NO. Oxides of nitrogen, NOx measured as summation of NO and NO_2 have the same value as NO since NO_2 was not detected. The graphical presentations of the detected emissions are shown in Figure 2, 3, and 4.

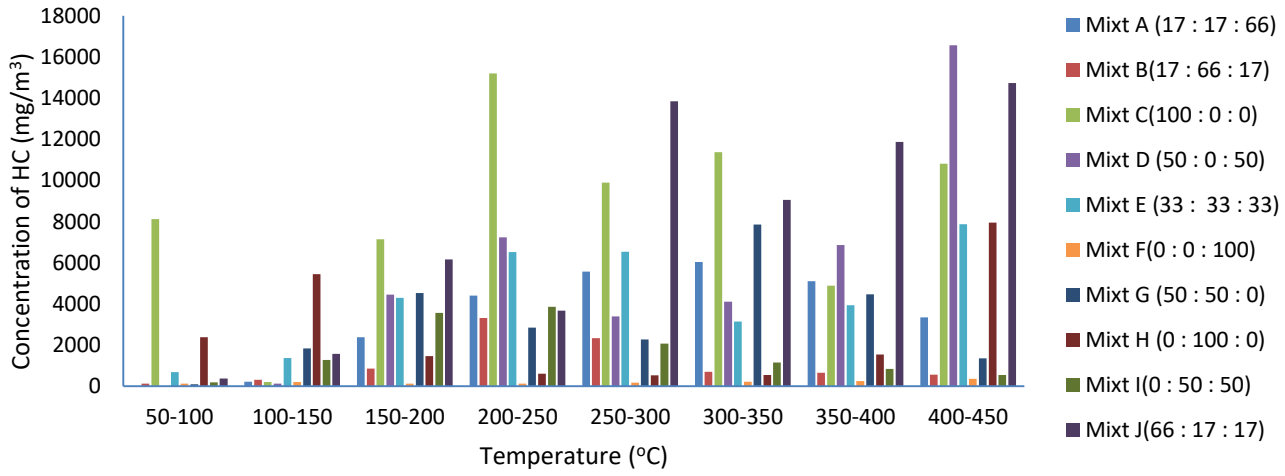

Figure 2: Hydrocarbon emissions at 50 °C stepwise increase in temperature from 50-450 °C for different mixture compositions during co-pyrolysis of LDPE, PS and PET

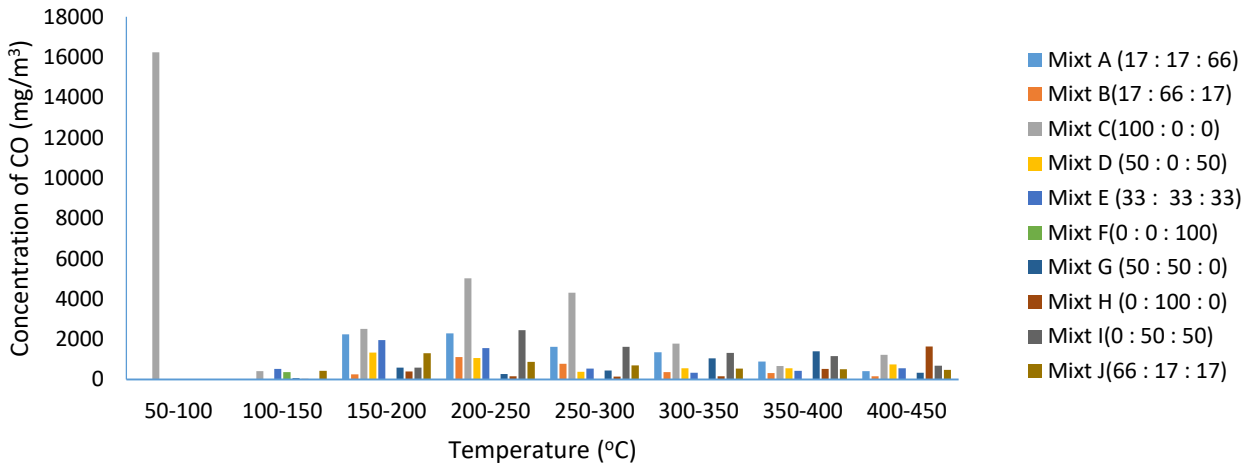

Figure 3: Carbon (II) oxide emissions at 50 °C stepwise increase in temperature from 50-450 °C for different mixture compositions during co-pyrolysis of LDPE, PS and PET

3.1.1 Emissions of HC at 50 °C stepwise increase in temperature in the co-pyrolysis of LDPE, PS and PET

Figure 2 shows the emissions of HC for all the mixture compositions. At 50-100 °C, mixture A and D did not emit any HC. While mixtures B, C, E, F, G, H, I and J gave HC emissions with values ranging from 100 mg/m^3 to 8119.93 mg/m^3. At 100-150 °C, all the mixture emitted HC with emission from mixture H being the highest at 5450 mg/m^3 and that from mixture D being the lowest at 124.92 mg/m^3. At 150-200 °C, all mixture compositions emitted HC with the highest emissions recorded from mixture C as 7144 mg/m^3 and lowest emission from mixture F as 124.92 mg/m^3. At 200-250 °C, all mixtures

emitted HC with mixture C having the highest emission of 15,209 mg/m^3 which also doubled as the highest emission of HC for mixture C throughout the co-pyrolysis, and mixture F still having the lowest emission of HC at 124.92 mg/m^3. At 250-300 ^{o}C, Mixture J has the highest emission of HC at 13,850 mg/m^3 and mixture F the lowest emission of HC at 176.97 mg/m^3. At 300-350 ^{o}C, mixture C emitted the highest HC at 11, 373 mg/m^3 and mixture F the lowest emission of HC at 230.33 mg/m^3. At 350-400 ^{o}C, mixture J gave the highest emission of HC at 11,876 mg/m^3 and mixture F gave the lowest emission of HC at 249.84 mg/m^3. At 350-400 ^{o}C, mixture J gave the highest emission of HC at 11,876 mg/m^3. At 400-450 ^{o}C, mixture D gave the highest HC emission of 16,567 mg/m^3 (the highest observed HC emission in all the experiments) and mixture F gave the lowest HC emission of 367.83 mg/m^3.Throughout the process, it is observed that mixture F which is 100% PET had HC emissions lower than 400 mg/m^3 with its highest emission 368 mg/m^3. This can be attributed to low conversion in pure composition of PET as a result of insufficient thermal energy to completely degrade its molecular structure at 450 °C (Odejobi *et al.*, 2020).

3.1.2 Emissions of CO at 50 ^{o}C stepwise increase in temperature in the co-pyrolysis of LDPE, PS and PET

Figure 3 shows the emissions of CO by the various mixtures. At 50 -100 ^{o}C, only mixtures C, E, H and J emitted CO and mixture C was distinctively higher than others with an emission of 16,239.85 mg/m^3. At 100-150 ^{o}C, all mixtures except B and D emitted CO. However, the CO emissions for all the mixture compositions were less than 100 mg/m^3. At 150-200 ^{o}C, all mixture

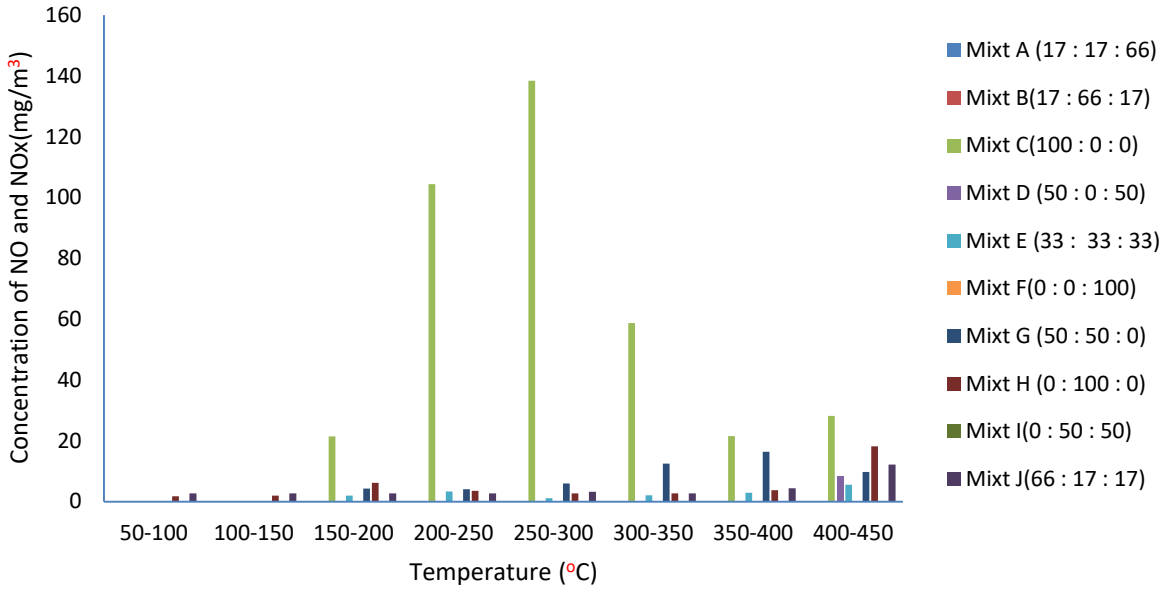

Figure 4: Measured concentrations of Nitrogen II oxide and oxides of Nitrogen at 50 ^{o}C stepwise temperature increase from 50-450 ^{o}C for different mixture compositions in the Co-pyrolysis of LDPE, PS and PET

compositions emitted CO. The highest emission was recorded from mixture C as 2,517.93 mg/m^3 for CO. At 200-250 ^{o}C, all of the mixtures also emitted CO with mixture C having the highest emission of 5,014.21 mg/m^3. At 250-300 ^{o}C, only mixture F did not emit CO. Mixture C still has the highest emissions of CO of 4306.37 mg/m^3. Furthermore, at 300-350 ^{o}C, all mixtures emitted CO with mixture C emitting the highest of 1,779.06 mg/m^3. At 350-400 ^{o}C, mixture G gave the highest CO emission of 1,401.06 mg/m^3. At 400-450 ^{o}C, mixture H gave the highest CO emission of 1,629.70 mg/m^3.

3.1.3 Emissions of NO and NOx at 50 ^{o}C stepwise increase in temperature in the co-pyrolysis of LDPE, PS and PET

In Figure 4, the emissions of NO and NO_x by the various mixtures are displayed. At 50 -100 ^{o}C, only two mixtures H and J emitted NO and NO_x. Similarly, at 100-150 ^{o}C, only mixture compositions H and J emitted NO and NOx. The emissions at both temperature ranges were less than 10mg/m^3 each.

At 150-200 ^{o}C, mixtures C, E, G, H, and J emitted NO and NO_x with C having the highest value of 21.42 mg/m^3. At 200-250 ^{o}C, only mixtures C, E, G, H and J emitted

NO and NO_x. Mixture C had the highest emission of 104.40 mg/m^3. At 250-300 ^oC mixture C gave the highest emission of 138.45 mg/m^3 and lowest emission of 2.68 mg/m^3 at mixture H. Meanwhile there is no emission for mixtures A, B, D, E, F and I. At 300-350 ^oC, mixtures C, E, G, H, and J emitted NO and NOx with C having the highest emissions of 58.8mg/m^3. At 350-400 ^oC, mixture C gave highest emission and NOx emission of 28.2 mg/m^3. At 400-450 ^oC, there was no detection of NO and NOx at mixtures A, B, F and I. However, the remaining mixture compositions C, D,E,G,H and J all emitted NO and NOx with mixture E having lowest value of 5.49 mg/m^3 and mixture C having the highest value of 28.15 mg/m^3.Mixtures A and B did not emit any NO and NO_x throughout the process.

3.2 Comparison of Emissions with Air Quality standards

There are no existing distinct emission standards for pyrolysis processes (Taylor, 2021). The highest measured emissions of the gaseous species investigated(Table 2) were expressed in part per million (ppm) and compared with EPA regulations for small municipal solid waste incinerators(MSWIs) operating at < 250 tons/day (Schwartz *et al.,* 2020) and point source maximum emission limits for facilities and processes set by National Environmental Standards and Regulations Enforcement Agency (NESREA, 2014). There were no standard limits available for air emissions of HCs. Maximum measured CO far exceeded the maximum allowable limits of 50 and 400ppm for EPA and NESREA. Maximum emitted NO on the other hand was lower than EPA and NESREA limits for NOx from small MSWIs and point source emission for facilities and processes respectively. This implies that the point source emission from the co-pyrolysis operation could be regarded as very toxic with respect to emission of CO and not safe for human health.

Table 2: Comparison of highest air emissions measured from the co-pyrolysis of LDPE, PS and PET with WHO and NESREA point source maximum emission limits for facility and processes.

Air emission	Max value recorded mg/m^3	Max value recorded(ppm)	Mixt. Comp. LDPE:PS:PET (%)	Temp. Range(^oC)	EPA OSWI(ppm)	NESREA AQS(ppm)
HC_{Max}	16567.23	25253.7	50:0:50	400-450	-	-
CO_{Max}	16239.85	14175.8	100:0:0	50-100	50	400
NO_{Max}	138.45	112.799	100:0:0	250-300	*500	**244
NO_2	nd	nd	-	-	*500	**244
CO_2,	nd	nd	-	-	-	-
SO_2	nd	nd	-	-	30	
H_2S	nd	nd	-	-	-	5.0

nd-No detection; * NOx from new source; ** emission standard for NOx (NESREA, 2014; Schwartz *et al.*, 2020)

4.0 CONCLUSION

The study established the presence of air pollutants during co-pyrolysis of LDPE, PS and PET. It also showed that during the co-pyrolysis of LDPE, PS and PET; HC, CO, and NO were detected while NO_2, CO_2, SO_2 and H_2S were not at 50 ^oC - 450 ^oC. The study revealed that co-pyrolysis of plastic mixture composition comprising 50% LDPE, 0%PS and 50% PET gave the highest HC emission of 16,567 mg/m^3 at 400-450 ^oC, when compared to all other mixture compositions and temperature range investigated. On the other hand, plastic mixture composition comprising 100% LDPE, 0% PS and 0% PET gave the highest value of 16239.85 mg/m^3 and 138.44 mg/m^3

for CO and NO emissions at temperature range 50-100, and 250-300 ^{o}C respectively. The maximum measured emission of CO far exceeded the maximum allowable limits by EPA and NESREA for small MSWIs and point source emission for facilities and processes respectively. Emitted pollutants observed during the co-pyrolysis process can be addressed by installing air pollution control device to trap HC, CO and NO which can further be separated for various applications.

ACKNOWLEDGEMENT

The authors would like to thank Energy and Simulation as well as Environmental Engineering Laboratories at the Department of Chemical Engineering, Obafemi Awolowo University for making available relevant technical assistance in the course of the research.

REFERENCES

American Society for Metals (1980) *Metals Handbook. 9th Ed. Vol. 3. Properties and Selection Stainless Steels Tool Materials & Special-purpose Metal*, *Neuroscience*. ASM 1980. Available at: http://www.pubmedcentral.nih.gov/articlerender.fcgi?artid=2854659&tool=pmcentrez&rendertype=abstract%0Ahttp://www.pubmedcentral.nih.gov/articlerender.fcgi?artid=3100238&tool=pmcentrez&rendertype=abstract%0Ahttp://www.ncbi.nlm.nih.gov/pubmed/8423474.

Demirbas, A. (2004) 'Pyrolysis of municipal plastic wastes for recovery of gasoline-range hydrocarbons', 72, pp. 97–102. Available at: https://doi.org/10.1016/j.jaap.2004.03.001.

EPA-CTM-022 (1995) 'Epa Ctm-022', pp. 1–16.

EPA (2017) *Method 25B - Determination Of Total Gaseous Organic Concentration Using A Non-dispersive Infrared Analyzer*.

ICAC (1999) *Test Method - Determination of Oxygen, Carbon Monoxide and Oxides of Nitrogen from Stationary Sources*. 1660 L Street, NW, Suite 1100 Washington DC 20036.

Kehinde, O. *et al.* (2020) 'Plastic wastes: environmental hazard and instrument for wealth creation in Nigeria', *Heliyon*, 6(10), p. e05131. Available at: https://doi.org/10.1016/j.heliyon.2020.e05131.

Miandad, R. *et al.* (2019) 'Catalytic pyrolysis of plastic waste: Moving toward pyrolysis based biorefineries', *Frontiers in Energy Research*, 7(MAR), pp. 1–17. Available at: https://doi.org/10.3389/fenrg.2019.00027.

NESREA (2014) *National Environmental (Air Quality Control)Regulations*. 142. Lagos, Nigeria.

Odejobi, O.J. *et al.* (2020) 'Oil yield optimization from co-pyrolysis of low-density polyethylene (LDPE), polystyrene (PS) and polyethylene terephthalate (PET) using simplex lattice mixture design', *Fuel Communications*, 2–5, p. 100006. Available at: https://doi.org/10.1016/j.jfueco.2020.100006.

Onwudili, J.A., Insura, N. and Williams, P.T. (2009) 'Journal of Analytical and Applied Pyrolysis Composition of products from the pyrolysis of polyethylene and polystyrene in a closed batch reactor : Effects of temperature and residence time', 86, pp. 293–303. Available at: https://doi.org/10.1016/j.jaap.2009.07.008.

Patni, N. *et al.* (2013) 'Alternate Strategies for Conversion of Waste Plastic to Fuels', *ISRN Renewable Energy*, 2013, pp. 1–7. Available at: https://doi.org/10.1155/2013/902053.

Schwartz, N.R. *et al.* (2020) 'Analysis of emissions from combusting pyrolysis products', *Fuel*, 274(January), p. 117863. Available at: https://doi.org/10.1016/j.fuel.2020.117863.

Taylor, O.A. (2021) *US EPA Federal Register*.

Yuliansyah, A.T. *et al.* (2015) 'Pyrolysis of plastic waste to produce pyrolytic oil as an alternative fuel', *International Journal of Technology*, 6(7), pp. 1076–1083. Available at: https://doi.org/10.14716/ijtech.v6i7.1241.

DOI: 10.51975/23380105.som
Journal of the Nigerian Society of Chemical Engineers, 38(1), 2023

SEASONAL VARIATION AND HEALTH RISKS OF PARTICULATES AT AND AROUND TRAFFIC HOTSPOTS IN IBADAN -A MODEL AFRICAN METROPOLIS

***Odediran, E. T., Adeniran, J. A. And Yusuf R.O.**
Environmental Engineering Research Laboratory, Department of Chemical Engineering, University of Ilorin, Nigeria
*odedirantolu@yahoo.com

ABSTRACT

Fewer studies have investigated incidents of pollution from vehicular traffic in African cities compared to other parts of the world. This study assessed variation in seasonal concentrations and exposure to health risks of particulates (PM_1, $PM_{2.5}$, PM_{10} & TSP) at and around twenty-five (25) major traffic Intersections (TIs) within Ibadan City, a typical urban environment in Sub-Saharan Africa. The 24h mean concentration of PM_1, $PM_{2.5}$, PM_{10} and TSP sampled at 25 TIs in Ibadan during the dry season were 1.57, 2.29, 4.19 and 4.09 times their corresponding values during the rainy season. The Pearson's correlations of total vehicle on-road with PM_1 and $PM_{2.5}$ were positive while that of PM_{10} and TSP gave negative correlations. Statutory Limit Breach (SLB) values were above the set standards of regulatory agencies at several TIs. Total Respiratory Deposition Doses (TRDD) of PM_1, $PM_{2.5}$& PM_{10} were higher during the dry season by 35.15%, 56.89% and 78.27% than those during the rainy season. SLB and TRDD estimates showed that road users are significantly at risk of exposure to particulates from traffic-related sources.

Keywords: *Particulate, Traffic Intersection, Season, Rush and Non-rush hour, Deposition dose.*

1. INTRODUCTION

The primary sources of urban air pollution are road traffic and industrial activities (Adiang *et al.*, 2017). Globally, over one billion people are exposed to urban air pollution each year (Zhang and Day, 2015). India and China reported more than one million premature deaths per year due to incidences of urban air pollution (Dockery and Evans, 2017). Urban vehicular congestions occur mostly at Traffic Intersections (TIs) resulting in adverse human health effects in cities (Police *et al.*, 2016). Therefore, TIs are foremost traffic hotspots (Adeniran *et al.*, 2017), where vehicular emissions are deposited and dispersed over time (Gunawardena *et al.*, 2013). Exhaust emissions from internal combustion engines of vehicles are significantly gaseous and particulate pollutants which may include: un-burnt fuel, particulate matters (PM), carbon monoxide (CO), carbon dioxide (CO_2), volatile organic compounds (VOCs), polycyclic aromatic hydrocarbons (PAHs), oxides of nitrogen (NO_x), oxides of sulphur (SO_x), lead (Pb), heavy metals and other hydrocarbons (Ugbebor and John, 2018).

The variation in spatial and temporal characteristics and the fate of atmospheric pollutants in a locality are mainly affected by meteorological factors (such as ambient temperature, relative humidity, precipitation, wind speed and direction) and topography. Poor air quality in many African cities caused by urbanization, surge in population, industrialization and increased vehicular emissions impacts poor citizens more negatively (Das *et al.*, 2015; Delkash and Mir, 2016; Singh *et al.*, 2014). Although Africa's urban population is experiencing very rapid growth, studies on urban air pollution in sub-Saharan Africa (especially across West Africa) are very few (Doumbia *et al.*, 2018).

Proportionate urban pollution impacts fluctuate with vehicle type. The large population of vehicles in many African cities predominantly imported automobiles from America and Europe generate high emissions in traffic (Kumar and Barrett, 2008). Emissions from vehicles have adverse effects on visibility, public health and global climate change. Considerable harmful emissions are released by automobiles that are not well-maintained during rush-hour traffic (Essiet and Mmom, 2014).

Prior epidemiological studies have associated traffic-related air pollution with asthma, lung malfunction, and other respiration difficulties in people (Adiang *et al.*, 2017; Gordian *et al.*, 2006; Vallero, 2014). Pollutants generated from fuel combustion activities pose significant health problems, accounting for more than half of the overall traffic emissions of PM in urban areas (Han and Naeher, 2006).

Some researchers have investigated pollutants ambient concentrations in cities across the world (Adeniran *et al.*, 2017; Djossou *et al.*, 2018; Fenech and Aquilina, 2020; Kumar *et al.*, 2021; Morakinyo *et al.*, 2017; Njoku *et al.*, 2016; Olajire *et al.*, 2011; Owoade *et al.*, 2015; Pal *et al.*, 2012; Polednik and Piotrowicz, 2020; Singh *et al.*, 2014; Torkmahalleh *et al.*, 2020; Triantafyllou *et al.*, 2020). However, regardless of the global effort to tackle this key air pollution challenge, little progress has been made in Africa where the problem is prevalent. Pollution from vehicular traffic remains one of the many environmental problems that need consideration in many cities across Africa. The evaluation of the likely exposure risks to air pollutants from road traffic requires data on their ambient concentration levels in the environment. Insufficient statistics on air pollutants related to traffic and their connections with climatic factors in several countries in

Africa (including Nigeria) makes it difficult to develop a reliable emission control strategy. Therefore, this study investigated the seasonal concentration levels and exposure health risks of particulates (PM_1, $PM_{2.5}$, PM_{10}& TSP) in and around major traffic pollution hotspots of Ibadan Metropolis- one of the largest cities in Africa. Monitoring pollutant concentration levels will help relevant government establishments and concerned stakeholders to develop essential mitigation policies to check future deleterious impacts on human health and ensure exposure reduction.

2. MATERIALS AND METHODS

2.1 Study Area Description

Ibadan is positioned between longitudes 7°2'E to 7°40'E and latitudes 3°35'N to 4°10'N (Figure 1). Ibadan is the capital of Oyo State in Nigeria and one of the biggest African cities (Ajayi *et al.*, 2012). The city is located in the south-western part of Nigeria (Ayeni, 1994). Ibadan is heavily populated with more than 3.8 million occupants (NPC, 2006). Ibadan exhibits tropical rainy and dry climate. The rainy period spans between March and October of each year whereas its dry season comes with the cool dry wind (harmattan) covering the months of November to February. Rainfall of about 1420.06mm drops within an average of 109 days. June and September are the two months with the highest rainfall. The city's temperature fluctuates between 20.10°C and 40°C, atmospheric pressure varies from 754.6 to 762.3mmHg and the relative humidity extended from 49.2 to 83.58% (Yusuf *et al.*, 2022). The city has elevations extending from 152 to 213m with a land radius of 12,000m. The lowest and highest wind speed values observed during the dry season vary from 1.1 to 17 km/h. Environmental pollution in Ibadan is triggered by emissions from anthropogenic activities including road traffic in addition to commercial and industrial activities (Liu *et al.*, 2019; Wei *et al.*, 2015).

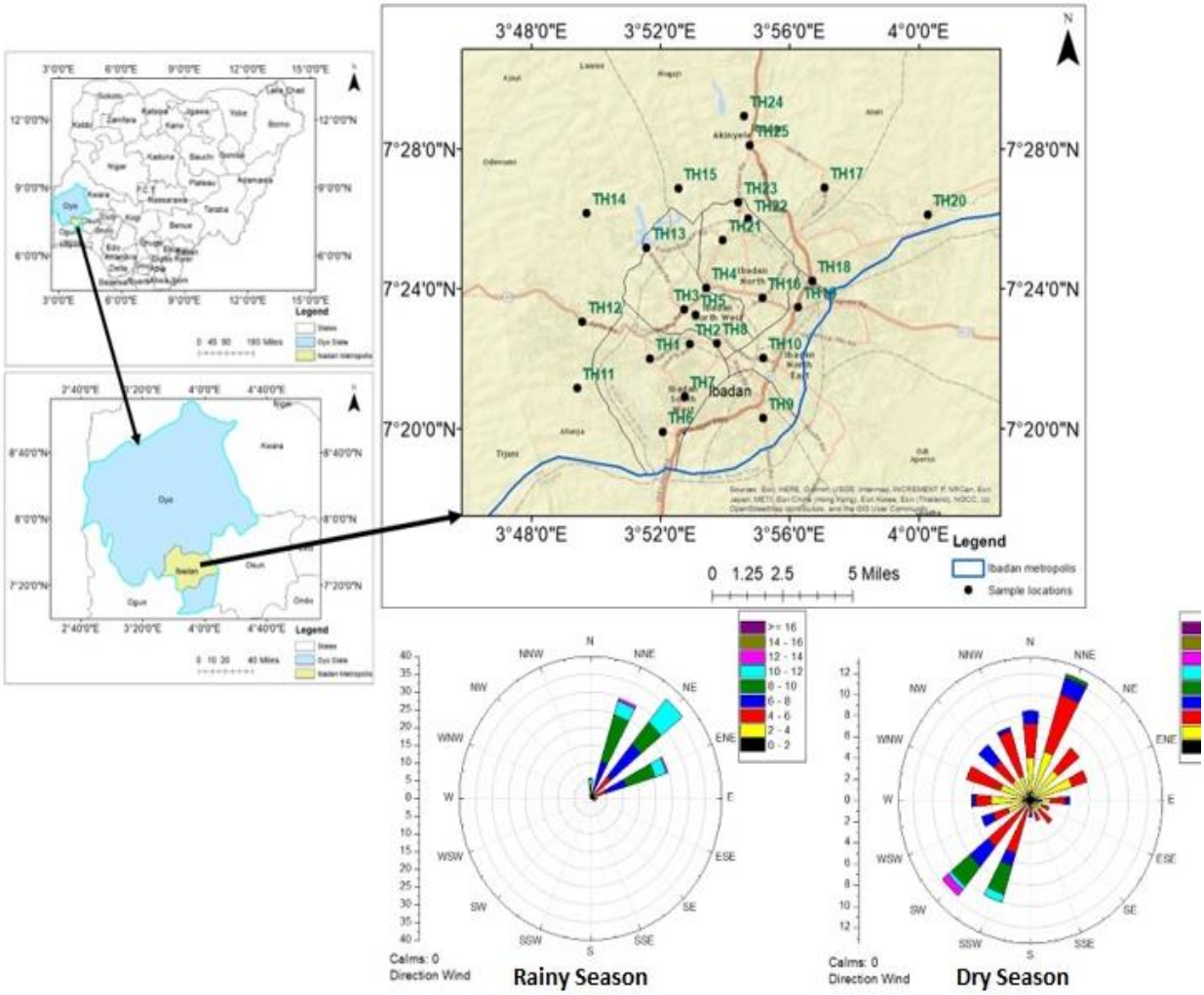

Figure 1: Study location with wind rose of rainy and dry seasons

2.1 Sampling Protocol for PM Pollutants

Particulate matter (PM_1, $PM_{2.5}$, PM_{10}& TSP) was sampled in twenty-five (25) major traffic hotspots during the rainy (wet) and dry seasons in Ibadan. Selected sampling sites were the TIs, evenly and spatially distributed within the Ibadan metropolis, having land use patterns such as industrial, commercial and residential activities (Supplementary Table S1).

This study adopted sampling method used by Adeniran *et al.* (2017). Ambient PM sizes of PM_1, $PM_{2.5}$, PM_{10}& TSP were measured with Aerocet 531S particle counter/mass monitor, placed within the breathing zone of 1-1.5m above the ground level at the selected TIs. This battery-operated, handheld Met One Instruments measured concurrently six mass concentration ranges (PM_1, $PM_{2.5}$, PM_4, PM_7, PM_{10} and TSP) or five particle count sizes (0.3, 0.5, 1.0, 5.0 and 10 μm). Data sample history was displayed on the screen in either mode after capturing of particle. For the rainy and dry seasons data, monitoring of selected PM and gaseous pollutants were carried out simultaneously in all the TIs during heavy traffic (rush hour) and light vehicular traffic (non-rush hour) periods. Atmospheric pressure, ambient temperature and relative humidity were measured for the entire sampling duration using Kestrel 4500 Weather Tracker.

Information on equipment operation and calibration, adjustment of PM values for relative humidity, correction achieved from the correlation of PM data obtained from Hazdust^{TM} sampler and gravimetric analysis with results obtained from Aerocet 531S particle counter have been described in other studies (Adeniran *et al.*, 2017; Adeniran *et al.*, 2018).

2.2 Human Exposure Risk Assessment

Assessments of human exposure risk to airborne pollutants at the TIs were estimated using Statutory Limit Breach (SLB) and the total respiratory deposition dose (TRDD) estimates.

SLB was considered particulate matter ($PM_{2.5}$, PM_{10}& TSP) using Equation 1. SLB is the ratio of concentrations of sampled PM to their corresponding ambient statutory limits. The ambient air quality guidelines or statutory limits taken into consideration include those of the World Health Organization (WHO) (WHO, 2006), the US Environmental Protection Agency (USEPA, 2012) and Nigeria's National Environmental Standards and Regulations Enforcement Agency (NESREA) formerly Federal Ministry of Environment (FMENV) (Gazette FRN, 1991; NESREA, 2020).

$$SLB = \frac{C_{SP}}{P_{SL}} \quad (1)$$

where C_{SP} is the pollutant concentration of sampled PM and P_{SL} is the pollutant concentration of statutory limit of PM. The Equation 1 was used to compute SLB value. The value of SLB greater than 1 is significant and worrisome.

The respiratory deposition dose (RDD) rates for PM_{10}, $PM_{2.5}$ and $PM_{1.0}$ were estimated by using the approach used by Adeniran *et al.* (2017) and Kumar and Goel (2016) as shown in Equation (2):

$$\text{Deposited doses}\left(\begin{array}{c}\text{in thoracic, tracheobronchial,}\\ \text{alveolar regions of PM fractions}\end{array}\right) = (V_T \times f) \times DF_i \times PM_i \quad (2)$$

$$DF = IF \times \left(0.058 + \frac{0.911}{1+\exp(4.77+\text{Ind}_p)} + \frac{0.943}{1+\exp(0.508-2.58\ln d_p)}\right) \quad (3)$$

$$IF = 1 - 0.5\left(1 - \frac{1}{1-0.00076d_p^{2.8}}\right) \quad (4)$$

where V_T is defined as tidal volume, f is known as breathing frequency. DF_i and PM_i are known as the fraction of deposition and mass concentration of particle size *i* in micrometre, respectively. For light exercise conditions, men's values f and V_T were taken as 0.35 and 800 cm^3 per breath, respectively, (Hinds, 1999; Kumar and Goel, 2016). DF_i and IF (inhalable fraction) for PM_1, $PM_{2.5}$ and PM_{10} were evaluated using Equations 3 and 4 suggested by Hinds (1999).

3. RESULTS AND DISCUSSION

3.1 Meteorological Parameters

The seasonal meteorological parameters of the study area obtained during the rush and non-rush hours using the Kestrel 4500 weather tracker (Supplementary Table S2) were consistent with the historical climate data of the Nigeria Meteorological Agency (NIMET, 2019). In the rainy season, the mean temperature ranged between 21.7 and 30.3°C for all the TIs. The relative humidity (RH) ranged from 63 to 98%. Atmospheric pressure was between 757.1 and 762.3mmHg. The highest and lowest recorded wind speeds (WS) were 4.72 and 0.83m/s, respectively. In the dry season, the mean temperature for all TIs ranged between 20.1 and 38°C, RH varied from 12 - 97%, Atmospheric pressure recorded was in the range of 754.6 - 759.8mmHg while wind speed varied from 0.31 to 4.72m/s.

3.2 PM Concentration Variations during Traffic Flow Intensity

The seasonal variation of PM (PM_1, $PM_{2.5}$, PM_{10}& TSP) mass concentrations during the rush and non-rush hours in Ibadan are illustrated in Figure 2. The 24h mean concentrations of PM_1, $PM_{2.5}$, PM_{10}& TSP in Ibadan during rush hours of rainy season were 4.85±1.43, 7.95±2.57, 33.69±13.85 and 60.87±25.51 μg/m^3, respectively while the corresponding values during non-rush hours of the rainy season were 4.37±1.51, 6.66±2.66, 36.17±16.07, 72.83±33.89 μg/m^3, respectively. During the rainy season, 24h concentrations of PM_1 ranged from 1.66μg/m^3 (TH22) to 12.42μg/m^3 (TH6) during rush hours and 5.13μg/m^3 (TH25) to 6.40μg/m^3 (TH7) during

non-rush hour, $PM_{2.5}$ concentration ranged from 2.46µg/m^3 (TH22) to 27.65µg/m^3 (TH6) during rush hour and 3.24µg/m^3(TH25) to 10.67µg/m^3 (TH8) during non-rush hour. PM_{10} ranged from 10.5µg/m^3 (TH21) to 146.28µg/m^3 (TH15) during rush hours and 11.84µg/m^3 (TH22) to 93.43µg/m^3 (TH14) during non-rush hours. TSP 24h concentration varied from 16.17µg/m^3 (TH21) to 345.93µg/m^3 (TH15) during rush hour and 19.87µg/m^3 (TH16) to 234µg/m^3 (TH15) during non-rush hours.

During the dry season, PM_1 24h concentration extended from 4.07µg/m^3 (TH14) to 16.83µg/m^3 (TH2) during rush hours and 4.16µg/m^3 (TH14) to 12.42µg/m^3 (TH6) during non-rush hours, $PM_{2.5}$ ranged from 8.79µg/m^3(TH14) to 45.13µg/m^3 (TH2) during rush hour and 19.2µg/m^3(TH14) to 145.2µg/m^3 (TH12) during non-rush hour. PM_{10} ranged from 34.9µg/m^3 (TH17) to 285.2µg/m^3 (TH19) during rush hours and 34.9µg/m^3 (TH17) to 306.03µg/m^3 (TH9) during non-rush hours and the concentration of TSP ranged from 57.31µg/m^3 (TH17) to 572.79µg/m^3 (TH11) during rush hours and correspondingly 57.31µg/m^3 (TH17) to 670.78µg/m^3 (TH9) during non-rush hours. The 24h mean concentration of PM_1, $PM_{2.5}$, PM_{10}& TSP during rush hour of the dry season were 7.65±1.99, 17.31±4.39, 140±31.50 and 268.27±77.53 µg/m^3 respectively while the corresponding values are 6.82±1.40, 16.07±3.19, 152.40±58.06 and 277.93±95.22 µg/m^3 during non-rush hours.

In the rainy seasons, the highest 24h mean concentrations of PM_1, $PM_{2.5}$, PM_{10}& TSP were found at TH6, TH6, TH15 and TH15 during rush hours and TH7, TH8, TH14 and TH15 during the non-rush hours, respectively. Similarly, the PM_1, $PM_{2.5}$, PM_{10}& TSP highest mean concentrations in the dry season were recorded at TH2, TH2, TH19 and TH11 during rush hours and TH6, TH6, TH9 and TH9 during non-rush hours, respectively.

Elevated concentrations of airborne PM recorded at TIs in Ibadan may be from vehicular exhausts, road dust suspension by pedestrians and moving vehicles, vehicular body wears, wears of tyre, brake and engine parts, waste and bush burning near roads, back-up generators used in roadside shops and commercial buildings and mobile telecommunication base transceiver stations (Adeniran *et al.*, 2017). Heavy vehicular traffic in the city has been identified as a major source of atmospheric air pollutants. (Etim, 2016).

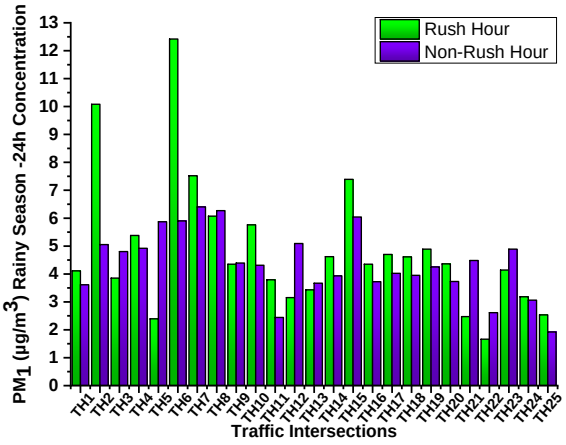

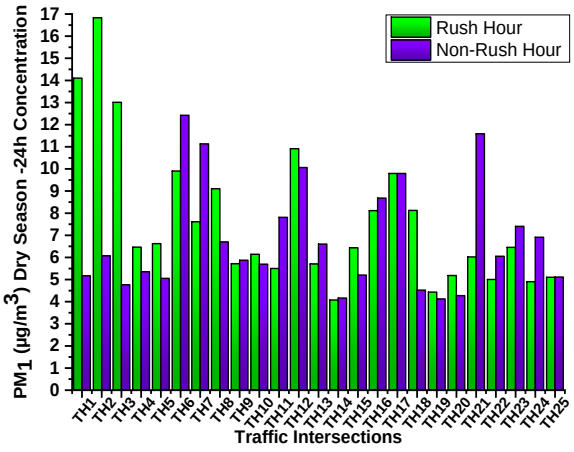

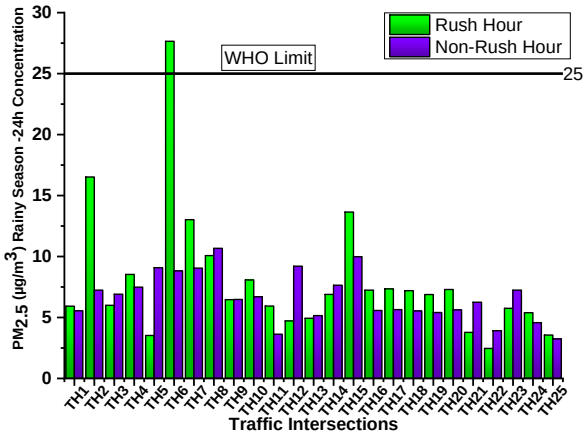

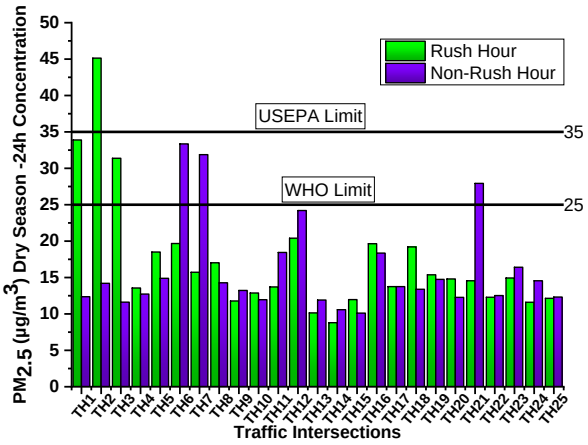

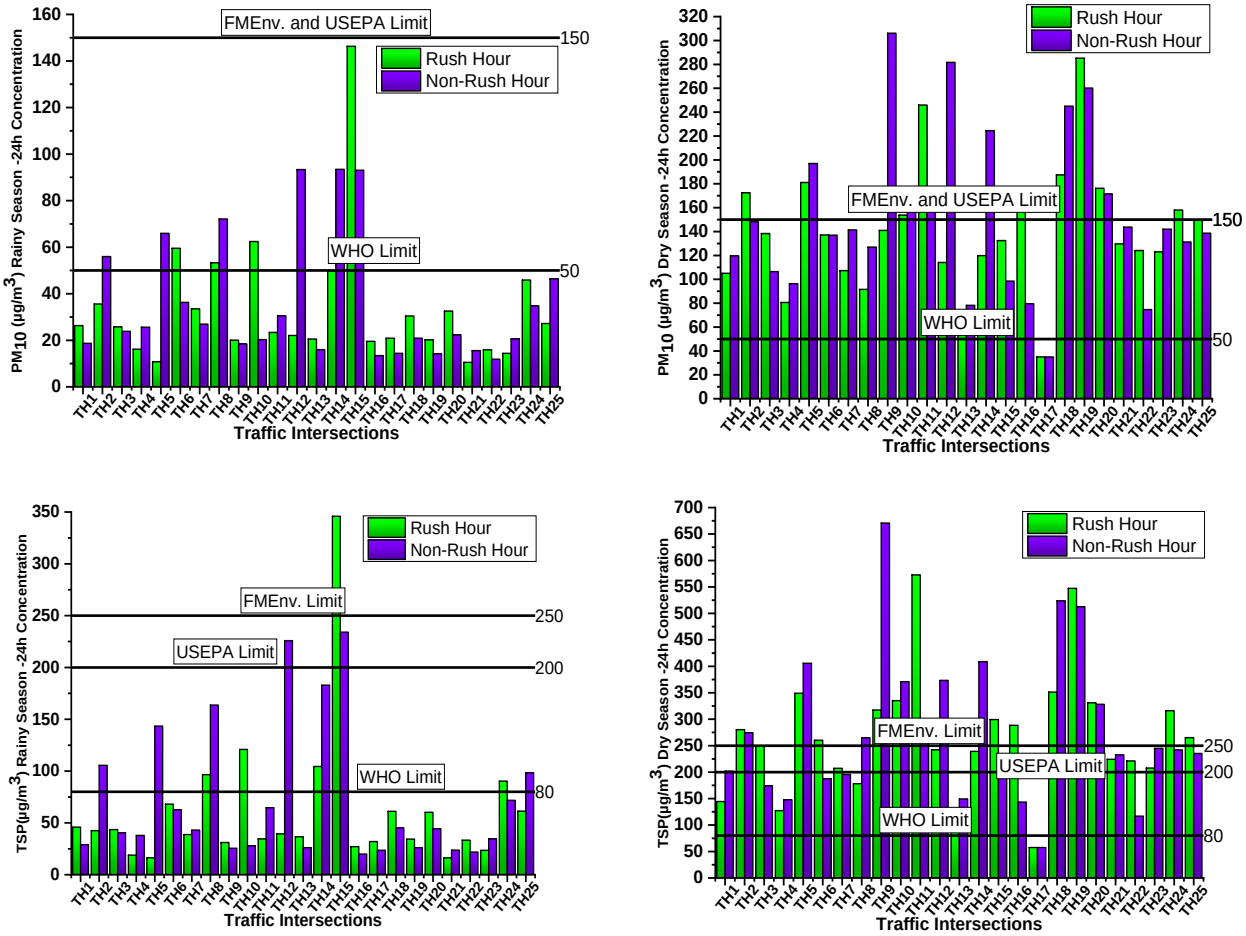

Figure 2: Seasonal variation of PM_1, $PM_{2.5}$, PM_{10} and TSP (24h) mass concentrations during Non-rush and Rush hour periods in Ibadan.

Temperature inversion contributes to higher PM concentrations during the early morning hours and late-night periods due to calmer night winds caused by an absence of solar irradiation, thus, leading to a lower temperature of the air which hinders the diffusion of PM having different densities (Saebo *et al.*, 2017).

The average concentration levels of PM_1, $PM_{2.5}$, PM_{10}& TSP during rush hour periods were higher than in non-rush hour periods at 64%, 60%, 60% and 56% of 25 TIs studied, respectively during the rainy season and correspondingly 52%, 52%, 44% and 48% of 25 TIs studied during the dry seasons. Apart from a few exceptions, PM during traffic congestion or rush hours was generally higher than those during free-flow traffic or non-rush hours in this study (Zhang *et al.*, 2017). The free movement of vehicles on the road results in the re-suspension of road dust while the slow movement of vehicles at traffic intersections (TIs) causes incomplete combustion of fuel (Gokhale and Raokhande, 2008; Shirmohammadi *et al.*, 2017).

3.3 Seasonal Variations in Concentrations of PM

According to Chowdhury *et al.* (2019), ambient PM loads are usually influenced by seasonal variation effects. In this study, the 24h mean concentrations of PM_1, $PM_{2.5}$, PM_{10} and TSP sampled at 25 TIs in Ibadan during the dry season were 1.57, 2.29, 4.19 and 4.09 times their corresponding values during the rainy season (Supplementary Table S3). Many related studies reported that re-suspended particles have varied impacts during the rainy and dry seasons, due to many factors including relative humidity, wind speed, rainfall, sunshine, categories of vehicles and traffic flow type (Adeniran *et al.*, 2018; Fernandez *et al.*, 2017). Forced deposition of particles may be accelerated during the rainy season than the dry season as a result of high relative humidity, temperature drop, rainfall, wind speed and lush vegetation (Chate, 2005; Jones and Harrison, 2004; Ranjan *et al.*, 2016).

3.4 PM Ratios

In this study, the ratios of PM_1 to $PM_{2.5}$, $PM_{2.5}$ to PM_{10} and PM_{10} to TSP were estimated to assess the ambient PM fractions and their exposure consequences on residents as shown in Supplementary Figure S1. In the rainy season $PM_1/PM_{2.5}$ ratio ranged from 0.5 to 0.74, $PM_{2.5}/PM_{10}$ ratio varied from 0.09 to 0.39 and PM_{10}/TSP ratio extended from 0.41 to 0.74. Similarly, during the dry season, $PM_1/PM_{2.5}$ ratios varied from 0.28 to 0.56; $PM_{2.5}/PM_{10}$

ratios stretched from 0.05 to 0.21 and PM_{10}/TSP ratios extended from 0.4 to 0.65. High ratios of $PM_1/PM_{2.5}$ and PM_{10}/TSP were observed during both rainy and dry seasons, implying particulate levels in Ibadan may generally influenced by emissions from crustal particles, automobile exhausts, road dust resuspension in addition to brake, tyre and engine wears during rainy and dry seasons in Ibadan (Odediran *et al.*, 2021).

The high percentages of ultrafine particles (PM_1) in respirable (fine) PM fractions ($PM_{2.5}$) during the two seasons studied confirmed that ultrafine particles are the main contributor to urban air pollution from fine particles. PM outdoor emissions are majorly caused by human activities which include fossil fuel combustion in internal combustion engines of generators and vehicles in addition to industrial activities at and around TIs (Adeniran *et al.*, 2018). Similarly, the high percentage of coarse particles (PM_{10}) in total suspended particles (TSP) during the two seasons implies coarse particles were formed from particulates coagulation, accretion, agglomeration and other processes of secondary formation. Thus, demonstrating the dominant contribution of non-exhaust sources (such as road dust suspension and re-suspension, crustal particles, wear of brake, tyre, engine and vehicle body parts) to PM_{10} urban air pollution in this study.

3.5 Statutory Limit Breach (SLB) for PM

The SLB results of PM sampled in 25 TIs in Ibadan were presented in Figure 2, In the rainy season, The SLB of $PM_{2.5}$ with reference to FMENV Standard of 25 µg/m^3 (Gazette FRN, 1991) at one TI (TH6) during rush hour only. Emissions of PM_{10} exceeded WHO limits of 50 µg/m^3(WHO, 2006) at 4 TIs (TH6, TH8, TH10 & TH15) during the rush hour and 6 TIs during the non-rush hour. SLB results of TSP show that 1 TI (TH15) breached FMENV limit of 250 µg/m^3(NESREA, 2020) during rush hour only, USEPA limits of 200 µg/m^3 for TSP (USEPA, 2012) were exceeded at 1 TI (TH15) during rush hour and 2 TIs (TH12 and TH15) during non-rush hour. In addition, 5 TIs (TH8, TH10, TH14, TH15 & TH24) during rush hour and 7 TIs (TH2, TH5, TH8, TH12, TH14, TH15, TH25) during non-rush hour breached WHO concentrations limit (80 µg/m^3) of TSP (WHO, 2006) in this study.

In the dry season, SLB estimates as shown in Figure 2 indicated that $PM_{2.5}$ limits (35 µg/m^3) of USEPA were breached at 1 TI (TH2) during rush hour while the $PM_{2.5}$ WHO limit (25 µg/m^3) was exceeded at 3 TIs each during the rush and non-rush hour periods. FMENV and USEPA limits (150 µg/m^3) of PM_{10} were breached at 8 and 7 TIs during the rush and non-rush hours, respectively. The standard WHO limits of PM_{10} (50 µg/m^3) and TSP (80 µg/m^3) were exceeded at 24 TIs out of 25 TIs studied during the rush and non-rush hour periods whereas FMENV limits (250 µg/m^3) of TSP were breached at 13 and 10 TIs during the rush and non-rush hours, respectively.

3.6 Total Respiratory Deposition Dose (TRDD) of PM

The average on-road TRDD rates estimates at TIs during the rainy season were 19±6.68, 62.57±27.6, and 289.72±197.30µg/day for PM_1, $PM_{2.5}$, and PM_{10}, respectively while the corresponding values at TIs during the dry season were 29.3±8.7, 145.15±45.45 and 1333.28±569.55µg/day. Figure 3 illustrates the average TRDD for PM_1, $PM_{2.5}$, and PM_{10} for the two seasons studied and different traffic flow intensities. The average on-road TRDD rates of PM_1, $PM_{2.5}$, and PM_{10} at all TIs during the dry season were higher than those during the rainy season by 35.16%, 56.89% and 78.27%.

Likewise, the TRDD rates for PM_1, $PM_{2.5}$, and PM_{10} at TIs during the rush hours were 25.88±9.93, 109.43±46.86, and 755±234.76 µg/day, respectively, and the corresponding non-rush hours TRDD rates were 22.61±6.20, 98.30±30.91 and 868.38±436.12 µg/day. Rates of average TRDD estimated for PM_1 and $PM_{2.5}$ during rush hours were found to be 12.64% and 10.18% greater than those estimated during the non-rush hours while the average TRDD rate of PM_{10} during non-rush hours was higher than that obtained during rush hours by 13.02%. This implies that faster movement of on-road vehicles during non-rush hours results in re-suspension of more coarse particulates from road dust during non-rush hours than rush hours. TRDD estimates were used to evaluate the exposure of pedestrians, roadside traders, traffic wardens, vehicle inspection officers and road safety professionals who regularly spend long hour at TIs. RDD and TRDD rates may be high and severe during traffic congestion (rush hour), triggering serious health ailments such as asthma, sneezing and coughing (Day, 2006). Ultrafine particulates (PM_1) and fine particulates ($PM_{2.5}$) could cause widespread adverse respiratory-related ailments when inhaled deeply into the lungs reaching the Alveoli while inflammatory responses are associated with inhalation of coarse particulates (Zwozdziak *et al.*, 2017).

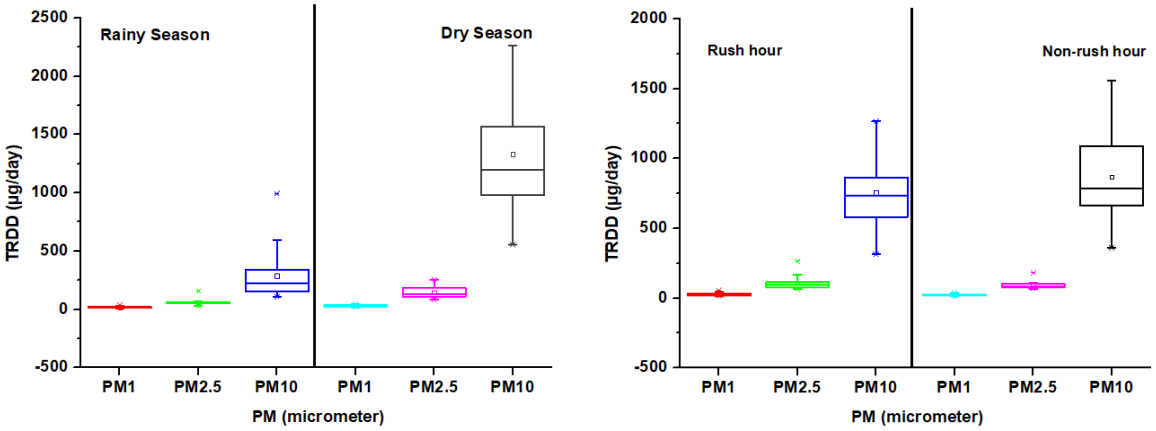

(a) (b)

Figure 3: Average TRDD rate of PM_1, $PM_{2.5}$ and PM_{10} for (a) seasonal variation and (b) traffic flow intensity

3.7 Effect of Climatic Parameters on Urban Air Pollution

Pearson's correlation presented in Supplementary Table S4 was used to test the relationship of the PM mass concentration levels (PM_1, $PM_{2.5}$, PM_{10} and TSP) with meteorological parameters (temperature, Relative Humidity, Atmospheric pressure, wind speed and wind direction) and vehicle traffic density (cars, buses, trucks, bicycles, tricycles and total vehicle on road per hour). The correlation coefficient obtained among all the PM sizes ranging from 0.53 to 1 showed a positive strong relationship signifying smaller particles are fragments of larger particles. Results showed that positive and negative correlations existed among the PM sizes, vehicle traffic densities and meteorological parameters. Effects of wet deposition may cause the negative coefficients obtained from the correlations of particulates with relative humidity during the washout process. Rainfall limits the possibility of PM re-suspension by increasing the humidity of the ecosystem and triggering a drop in outdoor PM concentrations. Wind speed interrupts the turbulence close to the land, thus reducing fine particulates in the air compared to coarse particulates. The rise or decline in wind speed determines the rate of PM dilution and dispersion in the air (Mkoma and Mjemah, 2011; Owoade *et al.*, 2012). Furthermore, wind direction enhances PM variation and movement from various upwind regions to the TIs. Ambient temperature and atmospheric pressure stimulate warmer air masses, which aids PM dispersion more than cold air masses.

As anticipated, relative humidity and wind speed showed positive correlations. A strong negative correlation of -0.82 was exhibited between temperature and relative humidity. The relationships of total vehicle on-road with PM_1 and $PM_{2.5}$ were positive whereas the correlation of total vehicle on-road with PM_{10} and TSP gave negative correlations (Supplementary Table S4). This demonstrates that ultrafine (PM_1) and fine ($PM_{2.5}$) particle emissions from vehicle exhausts rise as the time that vehicles spend in rush hours traffic increases whereas coarse (PM_{10}) particle rises more from road dust resuspension instigated by high-speed vehicles during non-rush hours.

4. CONCLUSION

This study revealed the seasonal variation in exposure to particulate matter (PM_1, $PM_{2.5}$, PM_{10} & TSP) at and around traffic hotspots in a model African metropolitan area. Pollutant concentration levels measured at and around twenty-five major traffic Intersections (TIs) in Ibadan was considerably more hazardous to public health during the dry season than the rainy season. Dispersion of particulates was influenced by the dominating northern wind during the rainy season while the blend of northern and southern wind-aided pollutant dispersion in the dry season. Estimates of Statutory Limit Breach (SLB) showed that the average concentrations of PM pollutants exceeded the threshold limits set by environmental regulatory agencies at many TIs. Total Respiratory Deposition Dose (TRDD) of PM_1, $PM_{2.5}$& PM_{10} were higher during the dry season by 35.15%, 56.89% and 78.27% than those during the rainy season. In this study, TRDD estimates during traffic congestion (Rush hour) for PM_1& $PM_{2.5}$ were greater than those during traffic free- flow (non-rush hour) by 12.64% and 10.18%, respectively whereas TRDD values for PM_{10} during non-rush hour were higher than rush hour TRDD by 13.02%. Pearson's correlation indicated that PM_1& $PM_{2.5}$ emissions from vehicle exhausts increased as traffic congestion rose whereas PM_{10} emission increased with road dust re-suspension during free-flow traffic. SLB and TRDD values indicated that pedestrians, road professionals and residents at and around the studied 25 TIs in Ibadan were exposed to particulate emissions considered harmful during the two seasons studied. Data

of this study are suitable for developing integrated traffic pollution abatement policies for a model African metropolis. Alternate routes for traffic reduction, usage of cleaner combustible fuels from sustainable renewables and the enforcement of obligatory automobile inspection and maintenance schedules could be incorporated as essential (quick fix) remedies to Africa's urban air pollution.

5. REFERENCES

Adeniran, J., Yusuf, R.& Olajire, A. (2017). Exposure to coarse and fine particulate matter at and around major intra-urban traffic intersections of Ilorin metropolis, Nigeria. *Atmospheric environment, 166*, 383-392.

Adeniran, J. A., Aremu, A. S., Saadu, Y. O.& Yusuf, R. O. (2018). Particulate matter concentration levels during intense haze event in an urban environment. *Environmental monitoring and assessment, 190*(1), 41.

Adiang, C. M., Monkam, D., Lenouo, A., Njeugna, E.& Gokhale, S. (2017). Evaluating impacts of two-wheeler emissions on roadside air quality in the vicinity of a busy traffic intersection in Douala, Cameroon. *Air Quality, Atmosphere & Health, 10*(4), 521-532.

Ajayi, O. O., Charles-Davies, M. A.& Arinola, O. G. (2012). Progesterone, selected heavy metals and micronutrients in pregnant Nigerian women with a history of recurrent spontaneous abortion. *Afr Health Sci, 12*(2), 153-159. doi:10.4314/ahs.v12i2.12

Ayeni, B. (1994). The metropolitan area of Ibadan: its growth and structure. *Ibadan region*, 72-84.

Chate, D. (2005). Study of scavenging of submicron-sized aerosol particles by thunderstorm rain events. *Atmospheric environment, 39*(35), 6608-6619.

Chowdhury, S., Dey, S., Di Girolamo, L., Smith, K. R., Pillarisetti, A.& Lyapustin, A. (2019). Tracking ambient PM2. 5 build-up in Delhi national capital region during the dry season over 15 years using a high-resolution (1 km) satellite aerosol dataset. *Atmospheric environment, 204*, 142-150.

Das, R., Khezri, B., Srivastava, B., Datta, S., Sikdar, P. K., Webster, R. D.& Wang, X. (2015). Trace element composition of PM2. 5 and PM10 from Kolkata–a heavily polluted Indian metropolis. *Atmospheric Pollution Research, 6*(5), 742-750.

Day, R. J. (2006). Traffic-related air pollution and perceived health risk: lay assessment of an everyday hazard. *Health, Risk & Society, 8*(3), 305-322.

Delkash, M.& Mir, H. M. (2016). Examining some potential actions in mitigating gaseous emissions from vehicles, case study: Tehran. *Air Quality, Atmosphere & Health, 9*(8), 909-921.

Djossou, J., Akpo, A. B., Liousse, C., Yoboué, V., Bedou, M., Bodjrenou, M., Chiron, C., Galy-Lacaux, C., Gardrat, E.& Abbey, M. (2018). Mass concentration, optical depth and carbon composition of particulate matter in the major southern West African cities of Cotonou (Benin) and Abidjan (Côte d'Ivoire). *Atmospheric Chemistry and Physics, 18*(9), 6275-6291.

Dockery, D. W.& Evans, J. S. (2017). Tallying the bills of mortality from air pollution. *Lancet, 389*(10082), 1862-1864. doi:10.1016/S0140-6736(17)30884-X

Doumbia, M., Toure, N. D. E., Silue, S., Yoboue, V., Diedhiou, A.& Hauhouot, C. (2018). Emissions from the Road Traffic of West African Cities: Assessment of Vehicle Fleet and Fuel Consumption. *Energies, 11*(9), 2300.

Essiet, U.& Mmom, P. C. (2014). Spatio-temporal variations in urban vehicular emissions in Uyo City, Akwa Ibom State, Nigeria. *Journal of Sustainable Development, 7*(4), 272-281.

Etim, E. U. (2016). Air pollution emission inventory along a major traffic route within Ibadan Metropolis, southwestern Nigeria. *African Journal of Environmental Science and Technology, 10*(11), 432-438.

Fenech, S.& Aquilina, N. J. (2020). Trends in ambient ozone, nitrogen dioxide, and particulate matter concentrations over the Maltese Islands and the corresponding health impacts. *Sci Total Environ, 700*, 134527. doi:10.1016/j.scitotenv.2019.134527

Fernandez, J.-M., Meunier, J.-D., Ouillon, S., Moreton, B., Douillet, P.& Grauby, O. (2017). Dynamics of suspended sediments during a dry season and their consequences on metal transportation in a coral reef lagoon impacted by mining activities, New Caledonia. *Water, 9*(5), 338.

Gazette FRN. (1991). Federal Republic of Nigeria Official Gazette.

Gokhale, S.& Raokhande, N. (2008). Performance evaluation of air quality models for predicting PM10 and PM2. 5 concentrations at urban traffic intersection during winter period. *Science of the Total Environment, 394*(1), 9-24.

Gordian, M. E., Haneuse, S.& Wakefield, J. (2006). An investigation of the association between traffic exposure and the diagnosis of asthma in children. *Journal of exposure science & environmental epidemiology, 16*(1), 49-55.

Gunawardena, J., Egodawatta, P., Ayoko, G. A.& Goonetilleke, A. (2013). Atmospheric deposition as a source of heavy metals in urban stormwater. *Atmospheric environment, 68*, 235-242.

Han, X.& Naeher, L. P. (2006). A review of traffic-related air pollution exposure assessment studies in the developing world. *Environ Int, 32*(1), 106-120. doi:10.1016/j.envint.2005.05.020

Hinds, W. C. (1999). *Aerosol technology: properties, behavior, and measurement of airborne particles*: John Wiley & Sons.

Jones, A. M.& Harrison, R. M. (2004). The effects of meteorological factors on atmospheric bioaerosol concentrations—a review. *Science of the Total Environment, 326*(1-3), 151-180.

Kumar, A.& Barrett, F. (2008). Stuck in traffic: Urban transport in Africa. *AICD Background paper, 1*.

Kumar, P.& Goel, A. (2016). Concentration dynamics of coarse and fine particulate matter at and around signalised traffic intersections. *Environmental Science: Processes & Impacts, 18*(9), 1220-1235.

Kumar, P., Hama, S., Nogueira, T., Abbass, R. A., Brand, V. S., Andrade, M. F., Asfaw, A., Aziz, K. H., Cao, S. J., El-Gendy, A., Islam, S., Jeba, F., Khare, M., Mamuya, S. H., Martinez, J., Meng, M. R., Morawska, L., Muula, A. S., Shiva Nagendra, S. M., Ngowi, A. V., Omer, K., Olaya, Y., Osano, P.& Salam, A. (2021). In-car particulate matter exposure across ten global cities. *Sci Total Environ, 750*, 141395. doi:10.1016/j.scitotenv.2020.141395

Liu, E., Wang, X., Liu, H., Liang, M., Zhu, Y.& Li, Z. (2019). Chemical speciation, pollution and ecological risk of toxic metals in readily washed off road dust in a megacity (Nanjing), China. *Ecotoxicol Environ Saf, 173*, 381-392. doi:10.1016/j.ecoenv.2019.02.019

Mkoma, S. L.& Mjemah, I. C. (2011). Influence of meteorology on ambient air quality in Morogoro, Tanzania. *International Journal of Environmental Sciences, 1*(6), 1107-1115.

Morakinyo, O. M., Adebowale, A. S., Mokgobu, M. I.& Mukhola, M. S. (2017). Health risk of inhalation exposure to sub-10 µm particulate matter and gaseous pollutants in an urban-industrial area in South Africa: an ecological study. *BMJ open, 7*(3), e013941.

NESREA. (2020). NESREA, 2020 National Environmental (Air Quality Control) Regulations, 2020 Schedule XIII Ambient Air Quality Standards.

NIMET. (2019). Nigerian Meteorological Agency (NiMeT) 2019 Seasonal Rainfall Prediction (SRP). Retrieved from https://fscluster.org/nigeria/document/nigerian-meteorological-agency-nimet website:

Njoku, K. L., Rumide, T. J., Akinola, M. O., Adesuyi, A. A.& Jolaoso, A. O. (2016). Ambient air quality monitoring in metropolitan city of Lagos, Nigeria. *Journal of Applied Sciences and Environmental Management, 20*(1), 178–185-178–185.

NPC. (2006). National Population Commission (2006). *Federal Republic of Nigeria Official Gazette, 96*(2).

Odediran, E. T., Adeniran, J. A., Yusuf, R. O., Abdulraheem, K. A., Adesina, O. A., Sonibare, J. A.& Du, M. (2021). Contamination Levels, Health Risks and Source Apportionment of Potentially Toxic Elements in Road Dusts of a Densely Populated African City. *Environmental Nanotechnology, Monitoring & Management*, 100445. doi:10.1016/j.enmm.2021.100445

Olajire, A., Azeez, L.& Oluyemi, E. (2011). Exposure to hazardous air pollutants along Oba Akran Road, Lagos–Nigeria. *Chemosphere, 84*(8), 1044-1051.

Owoade, K. O., Hopke, P. K., Olise, F. S., Ogundele, L. T., Fawole, O. G., Olaniyi, B. H., Jegede, O. O., Ayoola, M. A.& Bashiru, M. I. (2015). Chemical compositions and source identification of particulate matter ($PM_{2.5}$ and $PM_{2.5–10}$) from a scrap iron and steel smelting industry along the Ife–Ibadan highway, Nigeria. *Atmospheric Pollution Research, 6*(1), 107-119. doi:10.5094/apr.2015.013

Owoade, O., Olise, F., Ogundele, L., Fawole, O.& Olaniyi, H. (2012). Correlation between particulate matter concentrations and meteorological parameters at a site in Ile-Ife, Nigeria. *Ife Journal of Science, 14*(1), 83-93.

Pal, S. K., Wallis, S. G.& Arthur, S. (2012). Emission patterns of traffic-related metals and associated contamination in road deposited sediment. *International journal of global environmental issues, 12*(2-4), 229-241.

Polednik, B.& Piotrowicz, A. (2020). Pedestrian exposure to traffic-related particles along a city road in Lublin, Poland. *Atmospheric Pollution Research, 11*(4), 686-692.

Police, S., Sahu, S. K.& Pandit, G. G. (2016). Chemical characterization of atmospheric particulate matter and their source apportionment at an emerging industrial coastal city, Visakhapatnam, India. *Atmospheric Pollution Research, 7*(4), 725-733.

Ranjan, O., Menon, J. S.& Nagendra, S. S. (2016). Assessment of air quality impacts on human health and vegetation at an industrial area. *Journal of Hazardous, Toxic, and Radioactive Waste, 20*(4), A4016002.

Saebo, A., Janhäll, S., Gawronski, S.& Hanslin, H. M. (2017). Urban forestry and pollution mitigation. *Routledge Handbook of Urban Forestry. Routledge, London*, 112-122.

Shirmohammadi, F., Wang, D., Hasheminassab, S., Verma, V., Schauer, J. J., Shafer, M. M.& Sioutas, C. (2017). Oxidative potential of on-road fine particulate matter (PM2. 5) measured on major freeways of Los Angeles, CA, and a 10-year comparison with earlier roadside studies. *Atmospheric environment, 148*, 102-114.

Singh, P., Saini, R.& Taneja, A. (2014). Physicochemical characteristics of PM2. 5: Low, middle, and high–income group homes in Agra, India–a case study. *Atmospheric Pollution Research, 5*(3), 352-360.

Torkmahalleh, M. A., Hopke, P. K., Broomandi, P., Naseri, M., Abdrakhmanov, T., Ishanov, A., Kim, J., Shah, D.& Kumar, P. (2020). Exposure to particulate matter and gaseous pollutants during cab commuting in Nur-Sultan city of Kazakhstan. *Atmospheric Pollution Research*.

Triantafyllou, E., Diapouli, E., Korras-Carraca, M., Manousakas, M., Psanis, C., Floutsi, A., Spyrou, C., Eleftheriadis, K.& Biskos, G. (2020). Contribution of locally-produced and transported air pollution to particulate matter in a small insular coastal city. *Atmospheric Pollution Research, 11*(4), 667-678.

Ugbebor, J.& John, I. L. (2018). Impact of vehicular traffic on ambient air quality in selected junctions in Port Harcourt, Nigeria. *Science World Journal, 13*(4), 39-43.

USEPA. (2012). Integrated Risk Information System.

Vallero, D. A. (2014). *Fundamentals of air pollution*: Academic Press.

Wei, C., Bandowe, B. A., Han, Y., Cao, J., Zhan, C.& Wilcke, W. (2015). Polycyclic aromatic hydrocarbons (PAHs) and their derivatives (alkyl-PAHs, oxygenated-PAHs, nitrated-PAHs and azaarenes) in urban road dusts from Xi'an, Central China. *Chemosphere, 134*, 512-520. doi:10.1016/j.chemosphere.2014.11.052

WHO. (2006). *Air quality guidelines: global update 2005: particulate matter, ozone, nitrogen dioxide, and sulfur dioxide*: World Health Organization.

Yusuf, R. O., Odediran, E. T., Adeniran, J. A.& Adesina, O. A. (2022). Polycyclic aromatic hydrocarbons in road dusts of a densely populated African city: spatial and seasonal distribution, source, and risk assessment. *Environmental Science and Pollution Research*, 1-16.

Zhang, H., Huang, B., Dong, L., Hu, W., Akhtar, M. S.& Qu, M. (2017). Accumulation, sources and health risks of trace metals in elevated geochemical background soils used for greenhouse vegetable production in southwestern China. *Ecotoxicol Environ Saf, 137*, 233-239. doi:10.1016/j.ecoenv.2016.12.010

Zhang, J. J.& Day, D. (2015). Urban air pollution and health in developing countries *Air Pollution and Health Effects* pp. 355-380: Springer.

Zwozdziak, A., Gini, M. I., Samek, L., Rogula-Kozlowska, W., Sowka, I.& Eleftheriadis, K. (2017). Implications of the aerosol size distribution modal structure of trace and major elements on human exposure, inhaled dose and relevance to the PM2. 5 and PM10 metrics in a European pollution hotspot urban area. *Journal of Aerosol Science, 103*, 38-52.

DOI: 10.51975/23380106.som
Journal of the Nigerian Society of Chemical Engineers, 38(1), 2023

OPTIMIZATION OF AVOCADO SEED OIL EXTRACTION USING FIVE-LEVEL RESPONSE SURFACE METHODOLOGY DESIGN

[*]Giwa, S.O.[1], Abdullahi, F. Y.[2], Oloyede, O. G.[3], Ibrahim, S.[4] and Giwa, A.[5]

[1,23,4]Department of Chemical Engineering, Abubakar Tafawa Balewa University, Bauchi, Nigeria
[5]Department of Chemical and Petroleum Engineering, Afe Babalola University, Ado-Ekiti, Ekiti State, Nigeria

[1*]sogiwa@atbu.edu.ng, [2]fatimayakmut@gmail.com, [3]ogoloyede.pg@atbu.edu.ng, [4]saiduibrahim65@gmail.com, [5]agiwa@abuad.edu.ng
[*]Corresponding author

ABSTRACT

In this work, optimization of avocado seed oil extraction was carried out with the aid of Design Expert 7.0.0. The effects of particle size, extraction temperature and extraction time on the percentage yield of oil and cake were considered. Experiments were designed according to central composite method. With n-hexane as the solvent, each experimental run was carried out in a Soxhlet apparatus. Thereafter, experimental data were modelled. The analysis of variance results showed that the model developed for oil yield was statistically significant with p-value of 0.0277. The R-squared value of the model was found to be 0.6722 which was an indication that the quadratic model developed fairly represented the experimental data. The cake yield model was also significant and had an R-squared value of 0.6459. However, based on the adjusted R-squared value obtained, overall mean was observed to be a better predictor of the cake data. The numerical optimization results predicted 0.74 mm, 55 ^oC and 5 h as the optimum conditions to achieve 13.21% and 74.63% oil and cake yields respectively. On validation using the same conditions, 17.54% oil yield was obtained. The physicochemical properties of the extracted oil were also investigated.

Keywords: *Avocado seed oil, extraction, Central Composite Design (CCD), cake weight, oil yield.*

1. INTRODUCTION

In 2011, the global avocado production was about 4.4 million, with 20% increase recorded between 2007 and 2011 (Duarte *et al.*, 2016). The rise in productivity of the plant can be linked to high nutrition value and various health- related claims.

Avocado is an energetic fruit with high nutritional value and is considered a major tropical fruit, since it is rich in protein and contains fat-soluble vitamins lacking in other fruits, including Vitamins A and B, and median levels of vitamins D and E. It contains different oil levels in the pulp, thus it is widely used in pharmaceutical and cosmetic industries, and for obtaining commercial oils similar to olive oil, because of their similarity in fatty acid composition. In addition, this fruit has been recognized for its health benefits, especially due to the compounds present in the lipid fraction (Santos *et al.*, 2014).

Avocado oil is well known for its various health benefits. But the oil is mostly extracted from the pulp of the fruit while the skin and seeds are usually discarded (Gomez *et al.*, 2014). The seed of this plant is considered underutilised; thus, it attracts the attention of the researchers. Many of the works available on avocado seed involve extraction and/or optimization of phytochemicals (Gomez *et al.*, 2014; Adaramola *et al.*, 2016; Noorul *et al.*, 2017; Ong *et al.*, 2022). Also, there is a few studies on the seed oil extraction and its use for biodiesel production and the yield of oil extracted in these works were in the range of 3 % (Dagde, 2019) and 13. 4% (Deepalkshmi *et al.*, 2014). However, no work could be found on optimization of n-hexane extraction of avocado seed oil. Hence, the research was carried out to maximize the yield of oil extraction from the seed within the selected ranges of particle size, temperature and extraction time, using response surface methodology. The effects of variation of the extraction factors on the yield of the cake was also investigated as the by-product can be valuable. Moreover, the extracted oil at the optimum conditions was characterized to evaluate the suitability of the oil for various applications.

2. MATERIALS AND METHODS

2.1 Sample Collection and Preparation

Avocado fruits were procured from Muda Lawal market, in Bauchi metropolis. The seeds were ripped off from the fruit and were washed manually with water and sundried

for 7 days followed by oven drying at 40 ^{o}C for 72 h until their moisture content became constant, after which they were crushed and sieved to different particle sizes in the desired range given in Table 1.

2.2 Experimental Design and Oil Extraction

Previous study has shown that n-hexane extraction are significantly affected by particle size, extraction time and extraction temperature (Yahaya *et al.,* 2016). Based on this, 18 experiments were designed with the aid of Design Expert 7.0.0 using the central composite design (CCD) of Response Surface Methodology (RSM) for the extraction of avocado seed oil. The maximum and the minimum levels of the factors used were as given in Table 1.

Table 1: Maximum and minimum level of experimental factors

Variable	Unit	Maximum	Minimum
Particle Size (A)	mm	1.18	0.3
Temperature (B)	^{o}C	70.00	40.00
Time (C)	h	5.00	3.00

Thereafter, oil extraction experiments were performed according to the CCD matrix. For each experimental run, 10 g of the grounded avocado seed was wrapped in a filter paper and placed inside the thimble chamber which was placed into the extractor. A round bottom flask containing 150 ml n-hexane was coupled with the extractor connected to a condenser. Cool water (from a chiller at temperature of 10 ^{o}C) was passed through the condenser to condense the evaporating solvent back into the flask. The extraction was carried out according to the conditions specified for each run in the design matrix. Thereafter, the resulting mixture of n-hexane and the extracted oil was separated by distillation to recover the solvent. At the end of each experiment, the yield of the oil was obtained in percentage by dividing the amount of oil extracted by the weight of the seed and multiplying by 100. Also, the cake obtained was dried and later weighed. The cake weight was expressed as percentage of the feedstock.

2.3 Analysis of Experimental Data and Optimization

The experimental data were entered into the design matrix and the modelling of both the oil and cake yield data were performed. Each of the responses was model using a second-order polynomial equation which was later modified to improve its statistical importance. The significance of these models was evaluated using Analysis of Variance (ANOVA) results. Based on the fact that an experiment was performed at 0.74 mm, 55 ^{o}C and 5 h, numerical optimization criteria for particle size and temperature were set to be a target of 0.74 mm and 55 ^{o}C respectively and that of time was set to be in range. The objective of the oil yield was to maximize while the cake yield was set to be in range. This was done because our aim was to extract almost all the oil in the feedstock.

2.4 Characterization of the Avocado Seed Oil

The physicochemical properties of the oil determined were, density, viscosity, pour point, flash point, cloud point, acid value, iodine value, peroxide value and saponification. The density of the extracted oil was measured using the gravimetric method in which a known volume of the oil sample was placed in a pre-weighed bottle and the weight of oil was obtained by subtracting the weight of the empty bottle from the overall weight of the bottle with the oil. The density was later obtained as the ratio of the weight of the oil to its volume. The viscosity was measured as the ratio of the absolute viscosity of the oil to its density. The absolute viscosity was obtained by finding the difference between time (in sec) taken by 2 mL of the oil sample to flow through a burette and time spent by the same volume of water to flow through the burette, divided by the flow time of 2 mL of the sample already obtained.

The flash point of the oil was measured according to the method described by Akaagerger et al. (2016). By this approach, the minimum temperature that caused the ignition of the vapour escaping from a gradually heated oil sample, on exposure to a test flame was recorded as a flash point. The pour point was obtained as the temperature at which a previously cooled (-20 ^{o}C) amount of oil placed in a cylindrical bottle began to melt. The cooling was achieved by using a water bath. Cloud point was measured as the temperature at which distinct cloudiness appeared at the bottom of the test tube placed vertically inside a beaker (Akaagerger et al., 2016). The acid and free fatty acid values were obtained in accordance to British Standard Institute reported in the work of Akaagerger et al. (2016) in which the former was measured by titrimetric approach and the latter was calculated by multiplying the FFA value by 1.99. Iodine, peroxide and saponification values were respectively determined using the titrimetric method of Person 1970, ISO 1975 and AOAC 1990 explained by Adaramola *et al.* (2016) with slight modification.

3. RESULTS AND DISCUSSION

3.1 Oil Extraction

Conventionally, efficiency of extraction process which is usually defined using the yield of the product is affected by factors such as particle size of the solute, temperature and time. As shown in Table 2, at various extraction conditions, yield of both the oil and the cake was observed to vary. However, that of the former was more significant. The oil yield was in the range of 4.07 and 14.02%; the minimum and maximum cake yield obtained were 88.212 and 97.377%. As it can be noticed from Table 2, Run 1 gave the minimum amount of cake and maximum amount of oil, however, the sum of the two products is greater than 100 by 2.232. The increment may be as result of presence of residual n-hexane in both the cake and oil. Also, the cake might have more moisture. Similar trend can be observed in Run 2 where the minimum oil and maximum cake yields were obtained.

3.2 Statistical Analysis and Optimization

In order to understand the effects of the selected factors on the oil and cake yields, the experimental data were modelled using a second-order polynomial equation for each of the responses. The models were later modified to improve their performances. Given in Table 3 are the results of ANOVA obtained for oil yield. The reduced quadratic model was significant based on the fact that the probability of error value (p-value= 0.0277) was less than 0.05 (on 95% confidence level). Also, using the same criterion, the significant terms for this model were C, AB, BC and C^2 which implied that the oil extraction was significantly affected by variation of time at both linear and quadratic level, interaction of particle size and temperature, and interaction of temperature and time. Also, the model had predicted R-squared value of 0.6722, adjusted R-squared of 0.4934, Predicted R-squared of 0.2460 and adequate prediction of 7.951. Though, Predicted and adjusted R-squared were not very close, the results still demonstrated the validity of the model.

Table 2: The central composite design (CCD) experimental design matrix and the responses

Run No	A:Particle size (mm)	B: Temperature (^oC)	C: Time (h)	Y_1: Oil yield (%)	Y_2: Cake Yield (%)
1	0.74	55.00	5.00	14.02	88.212
2	1.00	46.08	4.59	4.07	97.377
3	0.48	46.08	3.41	9.54	90.408
4	0.74	40.00	4.00	7.13	93.694
5	0.74	55.00	4.00	9.49	92.627
6	0.48	46.08	3.41	7.74	92.078
7	0.74	63.92	3.41	6.15	94.095
8	0.74	70.00	4.00	8.37	94.065
9	1.18	55.00	4.00	8.28	91.654
10	1.00	55.00	4.00	6.86	93.505
11	0.30	63.92	4.59	8.15	91.332
12	0.74	55.00	4.00	8.60	92.80
13	0.74	55.00	3.00	7.33	94.123
14	0.74	55.00	4.00	5.03	96.151
15	1.00	63.92	3.41	9.34	90.577
16	0.48	63.92	4.59	9.35	90.897
17	0.74	55.00	4.00	4.50	95.309
18	0.48	46.08	4.59	8.01	92.536

Table 3: ANOVA results for Oil Yield Model

Source	Sum of Squares	df	Mean Square	F Value	p-value Prob > F
Model	58.7	6	9.78	3.76	0.0277
A-Particle size	3.25	1	3.25	1.25	0.2876
B-Temperature	12.18	1	12.18	4.68	0.0534
C-Time	24.07	1	24.07	9.25	0.0112
AB	27.21	1	27.21	10.46	0.008

Source	Sum of Squares	df	Mean Square	F Value	p-value Prob > F
BC	16.64	1	16.64	6.39	0.028
C^2	19.15	1	19.15	7.36	0.0202
Residual	28.63	11	2.6		
Lack of Fit	8.15	7	1.16	0.23	0.9568

Similarly, the results of ANOVA obtained for cake yield model is given in Table 4. As it can be seen from the Table, the reduced quadratic model developed for the response was significant and had among its important terms, time (C), the interaction of particle size and temperature (AB), and temperature and time (BC), indication that the variation of the selected factors affected the response. These interaction effects are also evident in Figures 1 and 2 respectively for AB and BC. As shown in Figure 1, at a low temperature (40 ^{o}C) oil yield improved with decreasing particle size. This can be explained using the knowledge of mass transfer, the lower the particle size, the higher the rate of diffusion of oil to the external surface of seed particles, which improves the yield of oil. The reversed case observed at high a temperature (70 ^{o}C) can be related to the higher rate of evaporation of solvent to the extraction chamber which later improved the mass transfer rate (Figure 1). Also, increasing temperature led to increasing oil yield at maximum extraction of 5 h, this may be due to the longer contact time that occurred between the solvent and the solute coupled with increasing temperature which improved mass transfer and consequently the oil yield. However, the reverse was the case at 3 h (Figure 2).

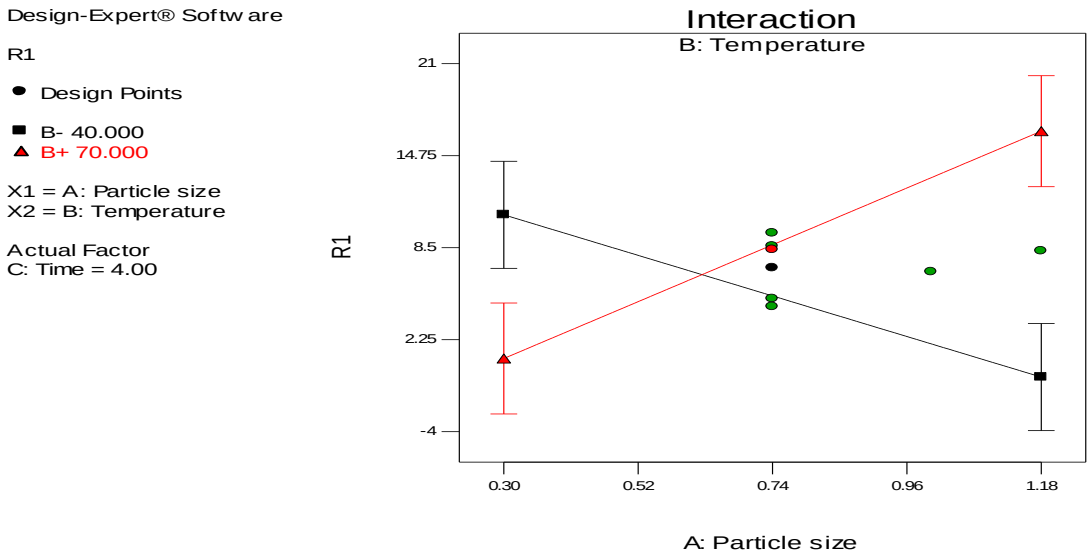

Figure 1: Interactive effect of Particle size and Temperature on Oil Yield

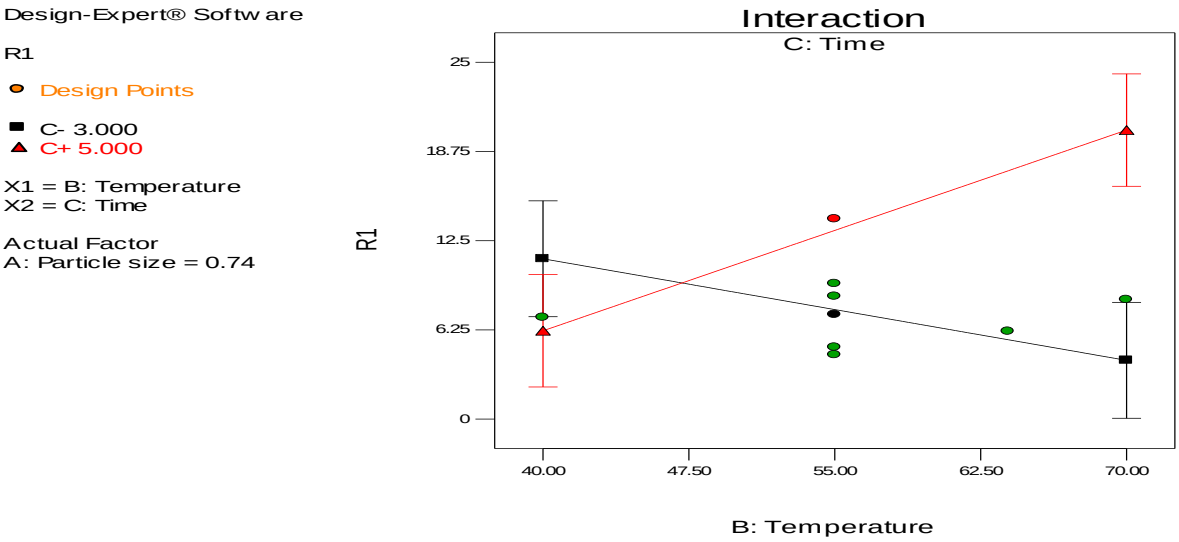

Figure 2: Interactive effect Temperature and Time on Oil Yield

The R-squared, its adjusted and predicted values were 0.6459, 0.4527 and-0.0163 respectively. The wide margin between the adjusted and predicted R-squared values and the negative nature of the former can be attributed to the fact that obtained cake yield values were in close range. This means that the overall mean could be a better predictor of the cake yield data.

Numerical optimization carried out based on criteria explained earlier showed that the predicted optimum conditions for obtaining maximum yield of oil of 13.21% with the cake yield of 74.63.4% were 0.74 mm, 55 ^{o}C and 5 h of particle size, temperature and time respectively at 91.9% desirability. Validating these conditions experimentally yielded 17.54% oil yield. The obtained yield was observed to be close to 17.9% reported by Musa *et al.* (2016) who optimized avocado seed oil extraction using petroleum ether as solvent. Also, the optimum conditions achieved in this work were in agreement with 0.5 mm, 60 ^{o}C and 5 h of particle size, temperature and time obtained in the previous study (Musa *et al.*, 2016).

Table 4: ANOVA results for Cake yield Model

Source	Sum of Squares	Df	Mean Square	F-Value	p-value Prob > F
Model	59.47	7	8.5	3.44	0.0382
A-Particle size	0.66	1	0.66	0.27	0.6176
B-Temperature	10.29	1	10.29	4.17	0.0685
C-Time	13.71	1	13.71	5.55	0.0402
AB	27.91	1	27.91	11.31	0.0072
BC	12.95	1	12.95	5.24	0.045
A^2	5.11	1	5.11	2.07	0.1806
C^2	13.96	1	13.96	5.65	0.0388
Residual	24.69	10	2.47		
Lack of Fit	13.83	6	2.3	0.85	0.5925

3.3 Physicochemical Properties of Avocado Seed Oil

The characteristics of the oil extracted at the optimum conditions were investigated. The characterization results obtained were as given in Table 5. As it can be seen in the Table, the avocado seed oil extracted at 0.74

mm, 55 ^{o}C and 5 h with the yield of 17.54wt% had the density of 0.8709 g/cm^3, kinematic viscosity of 27.1 cSt (2.71 mm^2/s), cloud point of 6 ^{o}C, pour point -2 ^{o}C and flash point of 187 ^{o}C. Based on the fact values of flash point, viscosity and density obtained were within EN 14214:2012 standard for biodiesel, the oil can be a good feedstock for biodiesel production or may be used as biodiesel if other fuel properties can be determined to conform to appropriate standards. However, the quantity of the oil in the seed may be its impediment for this application on industrial scale. The seed oil had free fatty acid of 1.592%, acid value of 3.168 mgKOH/g, peroxide value of 16.5 meq/kg, iodine value of 66.3 mgI/g, and saponification value of 143 mg KOH/g. The acid value and peroxide value obtained for this oil were higher than 0.6 mg KOH/g and up to 10 meq/kg specified standard for edible oil (Codex Stan 19-1981 Rev. 2-1999). The higher acid value may be associated with presence of unsaturated fatty acid which can make the oil to be susceptible to oxidative degradation (Negash *et al.*, 2019). Also, higher peroxide amount may indicate rancidity of the oil which can decrease the nutritional value of the oil (Negash *et al.*, 2019). High peroxide and acid values make the oil not a good choice for consumption.

Also, based on the fact that the saponification value of the oil was not to close 200 mg KOH/g, it may not be suitable for soap production (Musa *et al.*, 2016; Adaramola *et al.*, 2016). Thus, the extracted oil can be useful for cosmetics production as its saponification is close to that of baobab seed oil reported to be in the range of 140-205 mg KOH/g (Wright, 2021). Also, many studies (Adaramola *et al.*, 2016; Gomez *et al.*, 2014; Ong *et al.*, 2022) have confirmed that the seed extracts are rich in phytochemicals and antioxidants, thus, the oil may be useful for manufacturing of body-friendly cosmetic products. However, the characteristic of the extracted oil obtained in this study were observed not to be in line with the ones reported by Musa *et al.* (2016). The difference in the parameters may be as a result of different solvent types used, petroleum ether was adopted for their study.

Table 5: Physicochemical properties of avocado seed oil

Parameter	Values obtained
Density (g/cm^3)	0.8709
Kinematic Viscosity (mm^2/s)	2.71
Cloud point (^{o}C)	6
Pour point (^{o}C)	-2
Flash point (^{o}C)	187
Free Fatty Acid (%)	1.592
Acid value (mgKOH/g)	3.168
Peroxide value (meq/kg)	16.5
Iodine value (mg I/g)	66.3
Saponification value ((mgKOH/g)	143.055

4. CONCLUSION

In this study, Optimization of operating conditions for extraction of avocado seed oil was investigated using response surface methodology. The oil and the cake yields were found to be affected by the selected factors singly and/or interactively. Also, the models developed were observed to be statistically significant. The optimum conditions determined for the oil extraction using n-hexane as solvent, were 0.74 mm, 55 ^{o}C and 5 h of particle size, temperature and time respectively. Experimentally, the maximum oil yield obtained was 17.54%. Analysis of the physicochemical properties of the oil obtained at the optimum conditions revealed that the oil was suitable for biodiesel and cosmetics production.

REFERENCES

Adaramola. B., onigbinde, A. and Shokunbi, O. (2016). Phytochemical Properties and Antioxidant Potentials of Persea Americana Seed Oil, *Chemistry International*, 2, 168-175.

Akaagerger, S. M., Giwa, S. O**.,** Ibrahim, M. and Giwa, A. (2016). Production of Biodiesel from Desert Date Seed Oil. *International Journal of ChemTech Research*, 2455-9555), 9(6), 453-463.

Codex Stan 19-1981 Rev. 2-1999, available at https://www.fao.org/3/y2774e/y2774e03htm . [Accessed on 24 August, 2022].

Dagde, K. K., (2019). Extraction of Vegetable Oil from Avocado Seed Oil for Production of Biodiesel, *J. Appl. Sci. Environ. Manage*, *23* (2) 215-221.

Deepalkshmi, S., Sivalingam, A., Thirumarimurugan, M.,Yasvanthrajan, N.and Sivakumar, P. (2014). In-situ Transesterification and Process Optimization of Biodiesel from Waste Avocado Seed, National Conference on Green Engineering and Technologies for Sustainable Future-2014, *Journal of Chemical and Pharmaceutical Sciences*, 115-118.

Duarte, F. F.,Borgas, C. D. and Mendonca, C. R. B. (2016). Avocado Characteristics, Health Benefit and Uses, *Food Technology. Cienc. Rural*, *46*(4).

Gomez, F. S., Peirosanchez, S., Iradi, M.G.G., Azman, N.A.M. and Almajano, M. P. (2014). Avocado Seeds: Extraction Optimization and Possible Use as Antioxidant in Food, *Antioxidant*, *3*, 439-454.

Musa, U., Mohammed, I.A., Suleiman, B., Isah, A.G., Garba M.U., and Mohammed, A. (2016). Response Surface Optimization of Avocado Pear (*Persea americana*) Seed Oil Extraction and Characterization as Potential Industrial Feedstock. 37th Annual Conference and Annual General Meeting –Minna 2016 Proceedings Book, 590-596.

Nagash, Y. A., Amare, D. E., Bitew, B. D. and Dagne, H. (2019). Assessment of Quality of Edible Oils Accessed in Gondar City, Northwest Ethopia, BMC Res. Notes, 12, 793.

Noorul, H., Mujahid, M., Badruddeen. Khalid, M., Vartika, S., Nesar, A., Zafar, K., Zohrameena, S. (2017). Physico-phytochemical Analysis and Estimation of Total Phenolic, Flavonoids and Proantocyanidin Content of *Persea Americana* (Avocado) Seed Extracts, *World Journal of Pharmaceutical Sciences, 5* (4), 70-77.

Ong, E. S., Low, J., Tan, J. C. W., Foo, S. U., Leo and C. H. (2022). Valorisation of Avocado Seeds with Antioxidant Capacity using Pressurized Hot Water Extraction, *Scientific Reports*, *12*,13036.

Santos, M.A.Z., Alicieo, T,V. R., Pereira, C. M.P. Ramis-Ramos, G. and Mendonca, C. R. B. (2014). Profile of Bioactive Compounds in Avocado Pulp oil Influence of Drying Process and Extraction Method, *Journal of the American Oil Chemists' Society*, 91(1), 3776-3779.

Wright, R. (2021), Baobab Seed Oil, available at https://www.botanicalformulations.com/oil-monographs/baobab-seed-oil. [Accessed on 25tAugust, 2022].

Yahaya, S., Giwa, S.O., Ibrahim, M. and Giwa, A. (2016). Extraction of Oil from Jatropha Seed Kernels: Optimization and Characterization, *International Journal of ChemTech Research*, *9*, 758-770.

DOI: 10.51975/23380107.som
Journal of the Nigerian Society of Chemical Engineers, 38(1), 2023

MODELLING OF GASEOUS POLLUTANT EMISSIONS FROM SAVANNAH VEGETATION FIRES

***Abdulraheem, K. A. [1,2], Adeniran, J. A. [3] And Aremu, A. S. [1].**

[1] Department of Civil Engineering, University of Ilorin, Ilorin, Nigeria.

[2] Department of Water Resources and Environmental Engineering, Ahmadu Bello University, Zaria, Nigeria.

[3] Environmental Engineering Research Laboratory, Department of Chemical Engineering, University of Ilorin, Ilorin, Nigeria.

*khadijatabdulkareem2102@yahoo.com

ABSTRACT

The concentration and transport dynamics of emissions during savannah vegetation fires are not well-understood. This study aims at modelling the ground level concentrations (GLC) of gaseous pollutants on the receptor environment using the American Meteorological Society/Environmental Protection Agency Regulatory Model (AERMOD). Three (3) scenarios were investigated based on the vegetation density of the savannah grasses. The model revealed that the 24-hour averaging period for CO, NO_2, SO_2 and volatile organic compounds (VOC) ranged from 50 – 5,046 µg/m^3; 0.049 – 4.97 µg/m^3; 0.6 - 55.9 µg/m^3 and 63 – 6,253 µg/m^3 for Scenario 1; 288 – 28,825 µg/m^3; 0.08 – 8.31 µg/m^3; 2 – 203 µg/m^3 and 65 – 6,498 µg/m^3 for Scenario 2; 394 and 39,435 µg/m^3; 0.2 and 22.3 µg/m^3; 4 – 419 µg/m^3; and 118 - 11,782 µg/m^3 for Scenario 3, respectively. The study revealed that the World Health Organization (WHO) guideline of 4 mg/m^3 for the 24-hour concentration of CO was breached under Scenarios 2 and 3 by 150%. The findings of this study will help in the accurate estimation of emissions from the savannah fires and in the development of appropriate mitigation strategies for emission control.

Keywords: *Ground level concentrations; gaseous pollutants; modelling; emissions.*

1. INTRODUCTION

Vegetation fires have been identified as one of the sources of gaseous pollutants in the environment. Gaseous pollutants such as CO, SO_2, NO_2, and VOCs emitted during vegetation fires change the chemical composition of the atmosphere which has detrimental effects on the environment, human health, and climate. Savannah landscapes are noted to experience the highest frequency and intensity of fires globally (Sun *et al.*, 2019) with about 20% of nitrogen oxides (NO_X) and one-third of global CO emissions attributed to it (Andreae, 2019). Abdulraheem *et al*. (2022) reported that approximately 167 Tg of CO and 10 Tg of NO_X were emitted from savannah vegetation fires in the West Africa region between 1990 – 2019 while Akagi *et al.* (2011) disclosed that the vegetation fire is the second largest contributor of volatile organic carbons to the atmosphere.

High concentrations of gaseous pollutants in the atmosphere have adverse effects on the environment and human health when above the thresholds established by air quality regulatory bodies. The short-term Air Quality Guideline levels recently released by the WHO 2021 have replaced the 2005 levels where tolerable pollutants levels were reviewed. To ascertain the concentrations of pollutants emitted during vegetation fires on the receptor environment, dispersion models have been employed by researchers. One of such models is the American

Meteorological Society/Environmental Protection Agency Regulatory Model (AERMOD) as recommended by the United States Environmental Protection Agency (USEPA) (de Ferreyro Monticelli *et al.*, 2020). AERMOD is a near-field steady-state Gaussian Plume model that is based on planetary boundary layer (PBL) structure and scaling concepts over simple and complex terrains (Holmes and Morawska, 2006; ul Haq *et al.*, 2019). AERMOD calculates meteorological profiles with the use of measurements and similarity parameterizations to estimate adjacent vertical measurements (Cimorelli *et al.*, 2005). The model is relevant to a variety of pollutant sources in a wide range of settings such as rural, urban, flat, and complex terrain (Jampana *et al.*, 2004). The model has been used to analyze pollutant emissions in the environmental impact assessment study (Seangkiatiyuth *et al.*, 2011).

Researchers have used AERMOD models in the past for the determination of GLC of pollutants. In the study of Adeniran *et al.* (2018), air quality at the Ibese Cement factory in Ogun state Nigeria was assessed using the AERMOD model under four scenarios. The results revealed that particulates and gaseous pollutants from

simultaneous operations of all point sources of air emissions are within stipulated limits in the neighboring communities except for the 24-h concentration values of NO_X and SO_2 which breached their limits in a few locations. Afzali *et al*. (2017) predicted air pollutant concentrations from multiple sources with the use of AERMOD coupled with Weather Research Forecasting. Their findings indicated good agreement between predicted and observed concentrations. Rangel *et al*. (2018) estimated the concentrations of air pollutants emitted from the burning of sugarcane biomass using AERMOD software in Brazil. The study revealed that the highest dispersion was observed in February while April was observed to have the highest concentrations of pollutants.

Annual burning of vegetation is a prevalent practice in the savannah region of the country. The concentrations and transport dynamics of the pollutants emitted during this process are fairly understood and might exceed the acceptable levels stipulated by the regulatory guidelines. Therefore, this study aims at determining the GLC of pollutants emitted during savannah vegetation fires and their impacts on the receptor environment.

2. METHODOLOGY

The AERMOD model is a steady-state Gaussian dispersion model developed for air quality regulations. The gaseous pollutants emitted during the burning of savannah grasses were simulated using the AERMOD model over a flat/undulated terrain and under known meteorological conditions in three different scenarios. The impacts on receptor locations were observed under each scenario. The AERMOD model flowchart process is presented in Figure 1.

The licensed version of Lakes Environmental AERMOD View (version 8.9) was used for simulation in this study. The input data includes the source data, geological data i.e., the map of source location, and the meteorological data that are defined under various pathways.

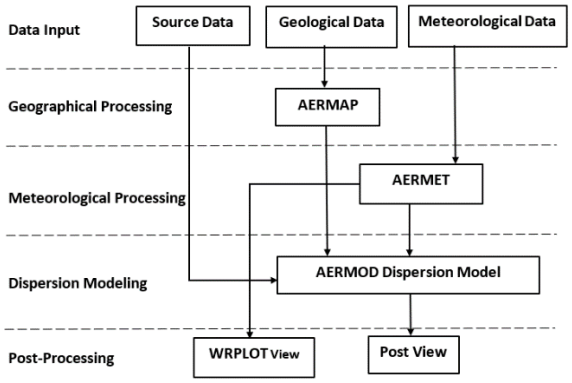

Figure 1: Process Flowchart for AERMOD model
Adapted from: Seangkiatiyuth *et al.* (2011)

The source location selected for modelling was selected based on the Moderate Imaging Spectoradiometer (MODIS) satellite observations detected by the Aqua satellite which shows the active fire hotspots. For this study, the savannah region that is susceptible to annual vegetation fires in Nigeria was used for the modelling. The area source was selected in the Mariga Local Government Area of Niger State, at a geographical location of 10.508°N and 5.853°E. Figure 2 shows the active fire hotspots detected in Niger State in the first week of January 2021 and the selected source location used for the AERMOD model.

The model input includes the air emission rate, release height, area of dimension, orientation angle, and base elevation. The air emission rate is given as:

$$AE = (\text{EF}\times\text{FC})/\text{t} \qquad (1)$$

where AE = Area emission rate (g/m^2 s); EF = Emission Factor (g/kg); FC = Fuel consumption (kg/m^2) and t = average burning time (sec).

For the determination of GLC of pollutants from burning of savannah grasses using the AERMOD model, three (3) scenarios of air emission from savannah burnings were considered in this study which was based on the emission rate and grass density, they are: Low Emission - Scenario 1; Moderate Emission – Scenario 2; and High Emission - Scenario 3.

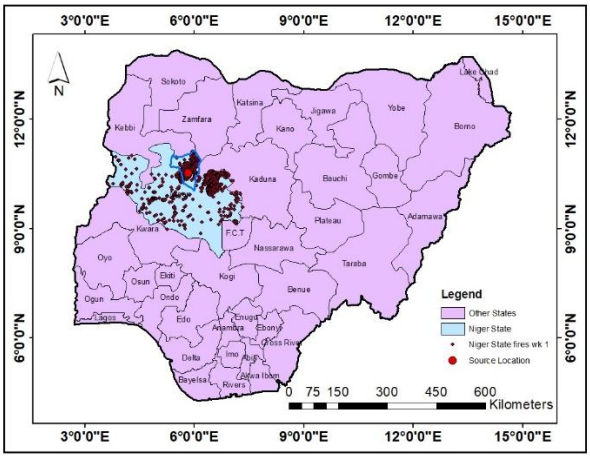

Figure 2: Map of Nigeria showing the source location used for the AERMOD model

3. RESULTS

The AERMOD air quality dispersion model was performed to predict the GLC of CO, NO_2, SO_2, and VOC around the selected burned area in Niger State, Nigeria. The GLCs CO, NO_2, SO_2, and VOC were considered for the 1-hour, 8-hour, and 24-hour averaging period using the Industrial Source Complex (ISC)-AERMOD view. The minimum and maximum GLC of the pollutants from burned vegetation were computed and compared with the NAAQS - FMEnv and NESREA; WHO Air Quality Guidelines; and the NAAQS - USEPA to determine their level of compliance.

Scenario 1: The minimum 1-hour averaging concentration for CO, NO_2, SO_2, and VOC are 908, 0.8, 11 and 986 µg/m^3, respectively while the maximum of 90835, 84.9, 1110, and 98637 µg/m^3 were observed, respectively. The minimum 8-hour averaging concentration for CO, NO_2, SO_2, and VOC are 140, 0.1, 2, and 201 µg/m^3, respectively while the maximum of 14011, 11.8, 185, and 20135 µg/m^3 are observed respectively. The minimum 24-hour averaging concentration for CO, NO_2, SO_2, and VOC are 50, 0.049, 0.6, and 63 µg/m^3 while the maximum of 5046, 4.97, 55.9, and 6,253 µg/m^3 are observed respectively. The isopleth of the 24-hour averaging of the predicted concentrations of CO in Scenario 1 is shown in Figure 3.
Scenario 2: For CO, the 1-hour averaging concentration ranges from 3,761 – 376,061 µg/m^3; the

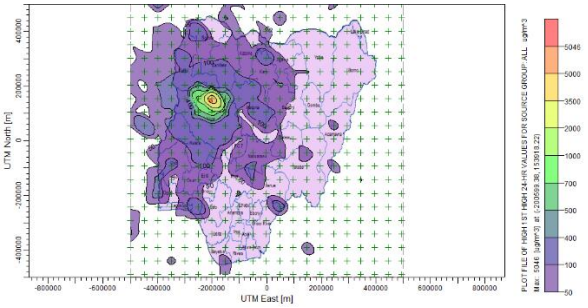

Figure 3: CO concentration profile for 24-hr averaging for Scenario 1

8-hour averaging concentration ranges from 1,242 – 124,160 µg/m^3 while the 24-hour averaging concentration ranges from 288 – 28,825 µg/m^3. For NO_2, the 1-hour averaging concentration ranges from 2 – 151 µg/m^3; the 8-hour averaging concentration ranges from 0.3 –25.2 µg/m^3 while the 24-hour averaging concentration ranges from 0.08 – 8.31 µg/m^3. For SO_2, the 1-hour averaging concentration ranges from 41 – 4,103 µg/m^3; the 8-hour averaging concentration ranges from 6 – 586 µg/m^3 while the 24-hour averaging concentration ranges from 2 – 203 µg/m^3. For VOC, the 1-hour averaging concentration ranges from 1,495 – 149,473 µg/m^3; the 8-hour averaging concentration ranges from 188 – 18,759 µg/m^3 while the 24-hour averaging concentration ranges from 65 – 6,498 µg/m^3. Figure 4 shows the isopleth of the 24-hour averaging of the predicted concentrations of CO in Scenario 2.

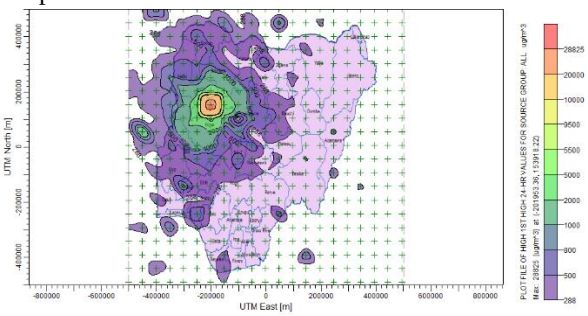

Figure 4: CO concentration profile for 24-hr averaging for Scenario 2

Scenario 3: The 1-hour, 8-hour and 24-hour averaging concentrations of CO was observed to be between 6,271 and 627,140 µg/m^3; 1,045 and 104,523 µg/m^3; 394 and 39,435 µg/m^3, respectively. For NO_2, the 1-hour, 8-hour, and 24-hour averaging concentrations observed are between 4 and 433 µg/m^3; 0.7 and 67 µg/m^3; 0.2 and 22.3 µg/m^3, respectively. For SO_2, the concentrations were in the range of 90 – 8,961 µg/m^3; 15 – 1,493 µg/m^3; and 4 – 419 µg/m^3 for 1-hour, 8-hour and 24-hour averaging, respectively. Lastly, the 1-hour, 8-hour and 24-hour averaging concentration for VOC are observed to be between 2,606 and 260,555 µg/m^3; 412 and 41,237 µg/m^3; 118 and 11,782 µg/m^3, respectively. The isopleth

of the 24-hour averaging of the predicted concentrations of CO is shown in Figure 5.

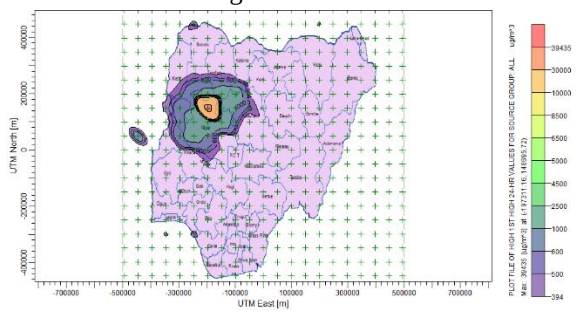

Figure 5: CO concentration profile for 24-hr averaging for Scenario 3

Table 1: The Nigerian States and their average distance from the source location

State	The average distance from the source (km)	State	The average distance from the source (km)
Kwara	197.33	Kano	272.6
Ekiti	307.62	Plateau	329.65
FCT	199.23	Kogi	261.24
Kebbi	61.93	Nasarawa	274.52
Sokoto	146.76	Osun	318.43
Kaduna	41.47	Oyo	270.45
Jigawa	376.34	Ondo	334
Bauchi	326.95	Benue	408.05
Katsina	152.75	Gombe	525.8
Ogun	468.114	Yobe	568.89
Zamfara	47.75		

Table 1 presents the distances of the pollution source point to the receptor locations, i.e., the states in the country where the impacts of the burning activity were observed. Table 2 displays the minimum and maximum GLC of the selected pollutants under the three scenarios considered while the percentage increase in average concentration of CO above the statutory limits are presented in Table 3.

Table 2: Ground-level concentrations of pollutants from the AERMOD model

	Pollutant concentrations (µg/m³)					
	Scenario 1		Scenario 2		Scenario 3	
	Min	Max	Min	Max	Min	Max
CO (1-hr)	908	90,835	3761	376,061	6,271	627,140
CO (8-hr)	140	14,011	1,045	104,523	1,242	124,160
CO (24-hr)	50	5,046	288	28,825	394	39,435
NO_2 (1-hr)	0.8	84.9	2	151	4	433
NO_2 (8-hr)	0.1	11.8	0.3	25.2	0.7	67
NO_2 (24-hr)	0.049	4.97	0.08	8.31	0.2	22.3
SO_2 (1-hr)	11	1,110	41	4,103	90	8,961
SO_2 (8-hr)	2	185	6	586	15	1,493

	Pollutant concentrations (µg/m³)					
	Scenario 1		Scenario 2		Scenario 3	
	Min	Max	Min	Max	Min	Max
SO_2 (24-hr)	0.6	55.9	2	203	4	419
VOC (1-hr)	986	98,637	1,495	149,473	2,606	260,555
VOC (8-hr)	188	18,759	201	20,135	412	41,237
VOC (24-hr)	63	6,253	65	6,498	118	11,782

Table 3: Percentage increase in average concentrations of CO above regulatory guidelines

	WHO guideline		**USEPA Standards 10 mg/m3**	
	4 mg/m3			
	(24-hr)		(8-hr)	
States	Scenario 2	Scenario 3	Scenario 2	Scenario 3
Kebbi	150%	150%	387%	385%
Kaduna	150%	150%	387%	191%
Zamfara	150%	138%	193%	191%

4. DISCUSSION

The distances from the source point to the receptor locations are shown in Table 1. It was observed that the dispersion of pollutants was in all directions of burned area for all the pollutants investigated. The pollutants disperse to several states in Nigeria and their concentrations depended on the distances between the source and the receptor states. The closest states to the source such as Kebbi, Zamfara, and Kaduna were observed to have the highest impacts.

In Table 2, the minimum and maximum GLC of the pollutants considered under the three scenarios are shown. The impacts of vegetation burning in the savannah on ambient air quality were investigated by comparing the hourly, 8-hourly, and daily maximum GLC of each of the investigated pollutants with the Nigerian NAAQS of the FMEnv and NESREA, WHO Air Quality Guidelines, and the NAAQS of the USEPA. For Scenario 1, the 1-hour, 8-hour and 24-hour maximum emission emitted for CO, NO_2, and SO_2 were within the standards sets by the regulatory organizations. Statutory guidelines for VOCs are not available, hence GLC of VOCs was not compared.

For Scenario 2, the 1-hour, 8-hour and 24-hour maximum emissions emitted for NO_2 and SO_2 were within the standards sets by the regulatory organizations. The WHO guideline of 4 mg/m^3 for the 24-hour concentration of CO was breached under this scenario by 150% in Kebbi, Kaduna, and Zamfara States whereas the USEPA standards of 9 ppm (approximately 10.3 mg/m^3) for the 8-hour concentration of CO was breached by 387% in Kebbi and Kaduna states and by 193% in Zamfara State. The breakdown of the percentage increase in average concentrations of CO above the WHO and USEPA thresholds is presented in Table 3**.**

For Scenario 3, the 24-hour concentration of CO breached the WHO guideline of 4 mg/m^3 and the 8-hour concentration of USEPA standard of 10.3 mg/m^3 in the three closest states to the source location as presented in Table 3. This study observed high concentrations of CO in the 24-hour averaging concentrations in scenarios 2 and 3 which exceeded the WHO and USEPA statutory guidelines. The high concentrations of this pollutant may be attributable to the quantity of biomass burned and the season of burning i.e., dry season. The severity of biomass burning in a location is usually measured with the concentration of CO (Kganyago and Shikwambana, 2020) since CO emission is generally an indicator of biomass burning (Scholes *et al*., 1996). CO and other non-methane volatile organic carbon are often released during the smoldering stage of a burning process whereas a significant fraction of well-oxidized species such as CO_2 or NO_X is released during the flaming stage (Manojkumar and Srimuruganandam, 2019).

The burning season in Nigeria coincides with the dry harmattan period associated with narrow planetary

boundary layer and poor mixing of air masses causing high concentrations of atmospheric gases including CO. Besides, low inversion and low wind speed usually experienced during the burning season reduce ventilation and dispersion of pollutants (Toro *et al.*, 2018) leading to their high concentrations. Increased concentrations of CO in the atmosphere may impact significantly on human health through the displacement of oxygen in the bloodstream and deprivation of the heart, brain, and other vital organs of oxygen which may lead to loss of consciousness and suffocation (Kampa and Castanas, 2008).

Smoke from wildfire plumes not only impacts the immediate environment but also has impacts on far locations at high concentrations. Alonso-Blanco *et al.* (2017) revealed that substantial concentrations of pollutants were observed in an area of Leon city in Spain, about 70km away from the source of fire due to intense subsidence inversion caused by a high-pressure system that prevented vertical dispersion. A similar observation was noted in this study, Kebbi State is approximately 62km away from the fire location and had a CO concentration of 1.5 folds of the WHO guideline for the 24-hr average concentration.

5. CONCLUSION

High concentrations of CO in the 24-hour averaging were detected from the AERMOD dispersion model in Scenarios 2 and 3. These values exceeded the WHO guideline of 4 mg/m^3 for 24-hr and the USEPA standard of 10 mg/m^3 for 8-hr which have negative implications on human health and the environment. The findings from this study have significantly advanced the understanding of savannah ecosystem and the characteristics of the pollutants emitted during biomass burning. The results would be useful in the estimation of emissions specific to the region and help in the development of appropriate mitigation strategies for the control.

Nomenclature

AERMOD	American Meteorological Society/Environmental Protection Agency Regulatory Model
CO	Carbon monoxide
FCT	Federal Capital Territory
FMEnv	Federal Ministry of Environment
GLC	Ground level concentration
NAAQS	National Ambient Air Quality Standards
NESREA	National Environmental Standards and Regulations Enforcement Agency
NO	Nitric oxide
NOx	Nitrogen Oxide
USEPA	United State Environmental Protection Agency
VOC	Volatile organic compounds
WHO	World Health Organization

REFERENCES

Abdulraheem, K., Adeniran, J., & Aremu, A. (2022). Carbon and precursor gases emission from forest and non-forest land sources in West Africa. *International Journal of Environmental Science and Technology*, Vol. 19: 12003-12018.

Adeniran, J. A., Yusuf, R. O., Fakinle, B. S., & Sonibare, J. A. (2019). Air quality assessment and modeling of pollutants emission from a major cement plant complex in Nigeria. *Atmospheric Pollution Research,* Vol. 10 (1): 257-266.

Afzali, A., Rashid, M., Afzali, M., & Younesi, V. (2017). Prediction of air pollutants concentrations from multiple sources using AERMOD coupled with WRF prognostic model. *Journal of Cleaner Production,* Vol. 166: 1216-1225.

Akagi, S., Yokelson, R. J., Wiedinmyer, C., Alvarado, M., Reid, J., Karl, T., Crounse, J., & Wennberg, P. (2011). Emission factors for open and domestic biomass burning for use in atmospheric models. *Atmospheric Chemistry and Physics*, Vol. 11(9): 4039-4072.

Alonso-Blanco, E., Castro, A., Calvo, A. I., Pont, V., Mallet, M., & Fraile, R. (2018). Wildfire smoke plumes transport under a subsidence inversion: Climate and health implications in a distant urban area. *Science of the Total Environment*, Vol. 619: 988-1002.

Andreae, M. O. (2019). Emission of trace gases and aerosols from biomass burning–an updated assessment. *Atmospheric Chemistry and Physics*, Vol. 19(13): 8523-8546.

Cimorelli, A. J., Perry, S. G., Venkatram, A., Weil, J. C., Paine, R. J., Wilson, R. B., Lee, R. F., Peters, W. D., & Brode, R. W. (2005). AERMOD: A dispersion model for industrial source applications. Part I: General model formulation and boundary layer characterization. *Journal of Applied Meteorology*, Vol. 44(5):682-693.

De Ferreyro Monticelli, D., Santos, J. M., Dourado, H. O., Moreira, D. M., & Reis Jr, N. C. (2020). Assessing particle dry deposition in an urban environment by using dispersion models.

Atmospheric Pollution Research, Vol. 11(1): 1-10.

Holmes, N. S., & Morawska, L. (2006). A review of dispersion modeling and its application to the dispersion of particles: an overview of different dispersion models available. *Atmospheric Environment*, Vol. 40(30): 5902-5928.

Jampana, S. S. (2004). Comparison, Evaluation and Use of AERMOD Model for Estimating Ambient Air Concentrations of Sulfur Dioxide, Nitrogen Dioxide and Particulate Matter for Lucas County. University of Toledo.

Kampa, M., & Castanas, E. (2008). Human health effects of air pollution. *Environmental Pollution*, Vol. 151(2): 362-367.

Kganyago, M., & Shikwambana, L. (2021). Did COVID-19 Lockdown Restrictions have an Impact on Biomass Burning Emissions in Sub-Saharan Africa? *Aerosol and Air Quality Research*, Vol. 21(4): 200470.

Manojkumar, N., & Srimuruganandam, B. (2019). Assessment of gaseous emissions and radiative forcing in Indian forest fires. *International Journal of Environmental Studies*, Vol. 76: 541-557.

Rangel, M. G. L., Henríquez, J. R., Costa, J. A., & de Lira Junior, J. C. (2018). An assessment of dispersing pollutants from the pre-harvest burning of sugarcane in rural areas in the northeast of Brazil. *Atmospheric Environment*, Vol. 178: 265-281.

Scholes, R., Ward, D., & Justice, C. (1996). Emissions of trace gases and aerosol particles due to vegetation burning in southern hemisphere Africa. *Journal of Geophysical Research: Atmospheres*, Vol. 101(D19): 23677-23682.

Seangkiatiyuth, K., Surapipith, V., Tantrakarnapa, K., & Lothongkum, A. W. (2011). Application of the AERMOD modeling system for environmental impact assessment of NO2 emissions from a cement complex. *Journal of Environmental Sciences*, Vol. 23(6): 931-940.

Sun, Q., Miao, C., Hanel, M., Borthwick, A. G., Duan, Q., Ji, D., & Li, H. (2019). Global heat stress on health, wildfires, and agricultural crops under different levels of climate warming. *Environment international*, Vol. 128: 125-136.

Toro, R., Kvakić, M., Klaić, Z. B., & Koračin, D. (2019). Exploring atmospheric stagnation during a severe particulate matter air pollution episode over complex terrain in Santiago, Chile. *Environmental pollution*, Vol. 244: 705-714.

Ul Haq, A., Nadeem, Q., Farooq, A., Irfan, N., Ahmad, M., & Ali, M. R. (2019). Assessment of AERMOD modeling system for application in complex terrain in Pakistan. *Atmospheric Pollution Research*, Vol. 10(5): 1492-1497.

DOI: 10.51975/23380108.som
Journal of the Nigerian Society of Chemical Engineers, 38(1), 2023

ELECTROCHEMICAL AND THERMODYNAMIC EVALUATIONS OF *SPONDIAS MOMBIN* LEAVES EXTRACT AS GREEN INHIBITOR FOR MILD STEEL CORROSION IN ACIDIC MEDIUM

***Adama K. K.[1], Onyeachu B. I.[2]** and **Igho E. M.[1]**
[1] *Department of Chemical Engineering, Faculty of Engineering, Edo State University Uzairue, Edo State, Nigeria*
[2] *Department of Industrial Chemistry, Faculty of Science, Edo State University Uzairue, Edo State, Nigeria*
*Corresponding author: adama.kenneth@edouniversity.edu.ng

ABSTRACT

Acid corrosion of steel-based structural equipment is a serious challenge for the chemical industry, especially, during descaling practices. Adding efficient corrosion inhibitors into the acid solution can significantly mitigate against this phenomenon. Currently, greener corrosion inhibitors, such as extracts of plant parts, have gained outstanding attention because they impact minimally when discharged into the environment. In this work, electrochemical and thermodynamic methods were employed to investigate the inhibitive efficiency of the water and ethanol extracts of Spondias mombin leaves against the corrosion of typical industrial steel (C1020) in 1.0M HCl. Both extracts protect the steel surface by blocking anodic and cathodic reactions on the steel surface, and lowering the capacitive behavior of the steel-acid interface. The extracts adsorb according to the models of Langmuir and Freundlich isotherms. The ethanol extract performs better (with an efficiency 96–98 %) than the water extract (efficiency 36–38 %), and exhibits more negative ΔG (-28.00 KJ/mol.) which is synonymous with more feasible and spontaneous adsorption.

Keywords: *Electrochemical, Thermodynamics, Corrosion inhibition, Green product, Spondias mombin extracts.*

1. INTRODUCTION

Carbon steel constitutes the most abundantly used alloy for fabricating major equipment in the chemical process industry due to its natural abundance, cheapness and strength (Palaniappan et al., 2020; Verma et al., 2019). Over time, inorganic scales would percolate on the surface of the steel-based equipment; interfering with production and diminishing the structural integrity of the equipment. Acid-cleaning, with dilute mineral acids like hydrochloric acid (HCl), is a common industrial practice that dislodges these scales and restores the efficiency of the equipment. However, the acid solution eventually impacts severe corrosion attack on the steel surface during acid-cleaning. Globally, the financial and material losses associated with this acid corrosion is enormous (Alrefaee et al., 2020; Marzorati et al., 2019; Verma et al., 2019). One of the most conventional ways to mitigate against this corrosion is to add effective corrosion inhibitors into the acid-cleaning solution.

Most chemical process industries usually add toxic chemicals to acid-cleaning solutions (Alrefaee et al., 2020; Muthukumarasamy et al., 2020; Fouda et al., 2019; Ishak et al., 2019), but these chemicals impact dangerously on the environment (Alrefaee et al., 2020; Belakhdar et al., 2020; Berrissoul et al., 2020; Chen et al., 2020; Asfia et al., 2020; Bidi et al., 2020). Identifying greener alternatives, with high inhibition efficiency, is important for the chemical industry since they would be excellent replacements for the toxic chemicals. The extracts of plant parts are remarkable in this regard (Ahanotu et al., 2020, Akinbulumo et al., 2020). They are naturally abundant, cheap and environmentally safe. They also contain phytochemicals which offer enormous active sites for interaction with metal atoms (Alrefaee et al., 2020; Chaudhary and Tak 2022). Several research works exist on the use of plant extracts as corrosion inhibitors for steel in acidic solutions (Marzorati et al., 2019; Verma et al., 2019; Ishak et al., 2019; Chen et al., 2020; Asfia et al., 2020; Alrefaee et al., 2020; Ahanotu et al., 2020). However, majority of reported works used only single (and toxic) solvents for their extraction. We have a concept that the amount/characteristics of phytoconstituents extracted from a plant part would influence its corrosion inhibition efficiency, and depends on the extracting solvent. Knowledge of this will guide the industry on the most preferable solvent for extraction.

It is important, also, that these solvents (like water and ethanol) also exhibit green properties in case of eventual discharge to environment.

This work reports a study conducted to investigate the capability of water and ethanol extracts of *spondias mombin* leaves to ameliorate the acid corrosion of carbon steel C1020. Potentiodynamic polarization (PDP) and electrochemical impedance spectroscopy (EIS) were utilized as electrochemical methods to understand the effect of extracts on the kinetics and mechanism of the steel corrosion in 1 M HCl solution. Thermodynamic assessment was performed based on adsorption isotherm and ΔG calculations.

2. MATERIALS AND METHODS

2.1 Materials

The materials used include fresh samples of *spondias mombin* leaves, sterile plastic bags, industrial blender, solvents: acetone, distilled water and ethanol (98 %), rotary evaporator, steel coupons and polishing papers, acid/extract concentrations tested: 1 M HCl /100, 200, 300, and 500 ppm.

2.2 Methods

2.2.1. Sample preparation

Coupons with surface area of 1.0 x 1.0 cm^2 were used for electrochemical measurement. Prior to use, they were abraded mechanically using abrasive polishing papers (successively) with 400 and 600 grit sizes, rinsed with distilled water and acetone, and dried using a Buchler Torramet specimen dryer. Analytical grade HCl (36 wt. %) was dissolved in distilled water to prepare the corrodent (1 M HCl). Fresh samples of *spondias mombin* leaves were obtained from the campus of Edo State University Uzairue and was validated accordingly in Biological Science Department, Edo State University Uzairue, Nigeria. The leaves were thoroughly washed with distilled water, dried at room temperature for fourteen days and then ground to powdered form using an industrial blender. The extraction was performed by soaking the powder for 72 h in ethanol and water as solvent in the ratio of 1:10 (plant powder (g): solvent volume (mL)). Thereafter, the mixture was filtered and the filtrate was concentrated using a rotary evaporator. The powder residue was also air-dried until a constant mass was obtained. The difference in powder mass before and after extraction was utilized to calculate the amount of plant phytochemical extracted by each solvent.

2.2.2 Electrochemical and thermodynamic investigations

The electrochemical experiments were conducted on a Gamry Potentiostart/Galvanostat/ZRA Reference 600 work station following the method reported previously by Ahanotu et al. 2020. The setup comprises a three-electrode system where an epoxy-encapsulated C1020 steel functioned as the working electrode, the auxiliary electrode was a graphite rod, and the reference electrode was a Ag/AgCl electrode. The electrochemical experiments were performed after monitoring the variation of open circuit potential (OCP) for an hour. The electrochemical impedance spectroscopy (EIS) measurements were performed, at OCP, within the frequency range of $10^5\ Hz\ to\ 10^{-3}\ Hz$ with $\pm 10\ mV$ amplitude signal. The signal amplitude perturbation was $\pm 10\ mV$. On the other hand, the potentiodynamic polarization (PDP) measurements were conducted by polarizing the working electrode within $\pm 0.25\ V$ versus OCP using a scan rate of 0.166 mVs^{-1}. The analysis of EIS data was done using Echem analyst while EC-lab software was used for PDP data analysis. The experiments were conducted in triplicates to achieve reproducibility. The inhibition efficiency (from EIS and PDP results) was calculated according to Solomon et al., 2018 and Fang et al., 2019, based on Equations (1) and (2), where R_{ct} is the resistance to charge transfer and i_{corr} is the corrosion current density.

$$\%\ IE_{EIS} = 1 - \frac{R_{\mathrm{ct(without\ inhibitor)}}}{R_{\mathrm{f(with\ inhibitor)}} + R_{\mathrm{ct(with\ inhibitor)}}} \times 100\% \quad (1)$$

$$\%\ IE_{PDP} = 1 - \frac{i_{corr(with\ inhibitor)}}{i_{corr(without\ inhibitor)}} \times 100\% \quad (2)$$

Different adsorption isotherm models were adopted to investigate the thermodynamic interactions and properties of the inhibitor. From the investigated isotherm models, the Gibbs free energy was evaluated to understand the spontaneity and feasibility of inhibitor protection.

3. RESULTS AND DISCUSSION

3.1. Electrochemical studies

3.1.1 Electrochemical impedance spectroscopy (EIS)

The analysis of the EIS is presented in the form of a Nyquist, Absolute impedance and Phase angle plots as shown in Figure 1. The addition of different concentrations of the *spondias mombin* leave extracts caused the size of the Nyquist arcs to expand significantly in comparison to the size displayed by the uninhibited

solution (blank solution). This is shown in Figure 1(a). This enlargement of the Nyquist arc size depicts lower rate of corrosion and increase in corrosion resistance. It can be seen that, at 500 ppm, the ethanol extract (with charge transfer resistance, R_{ct}, of 2004.10 Ω cm^2) shows larger sizes than the water extract (with charge transfer resistance, R_{ct}, of 121.00 Ω cm^2), which confirm that the ethanol extract exhibits greater protection of the steel surface than the water extract.

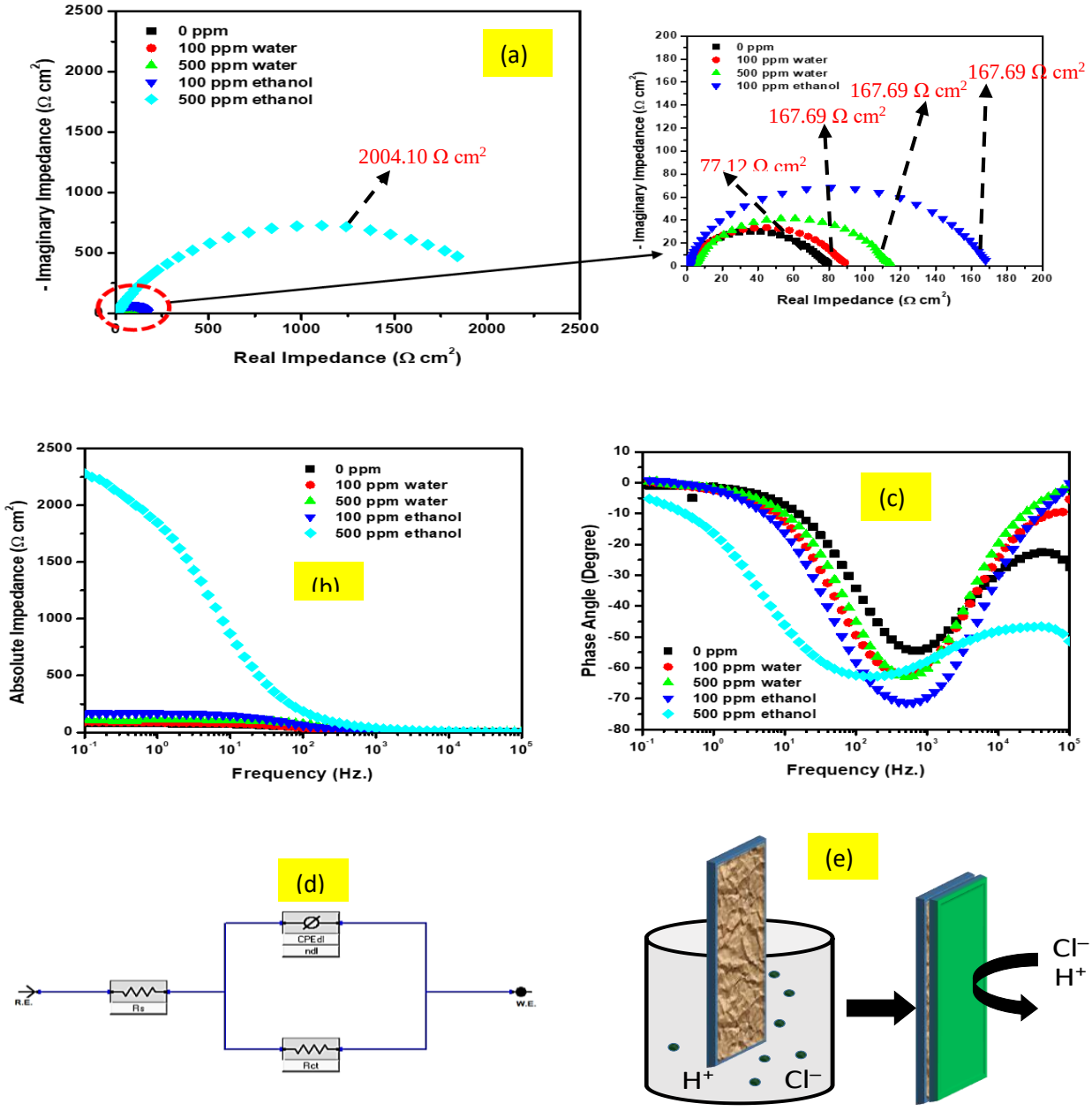

Figure 1: EIS analysis shown as (a) Nyquist (R_{ct} values in red font) (b) absolute impedance and (c) phase angle plots, along with (d) electrical equivalent circuit model and (e) schematic illustration of inhibition mechanism.

The Nyquist trend is also supported by the absolute impedance plots in Figure 1(b) whereby the addition of inhibitor extracts continuously increases the value of impedance at low frequency, compared with the blank solution. Also, the phase angle plots of Figure 1(c) reveal higher peaks in the presence of inhibitor extract. Higher peaks depict greater corrosion resistance. Consequently, the impedance behavior of the inhibited and uninhibited steel is modeled using the one-time electrical equivalent circuit in Figure 1(d). The model depicts that the extracts effectively modify the electric double layer at the steel-solution interface, by repelling water and chloride ions from the acid away from the steel surface, as depicted in Figure 1(e).

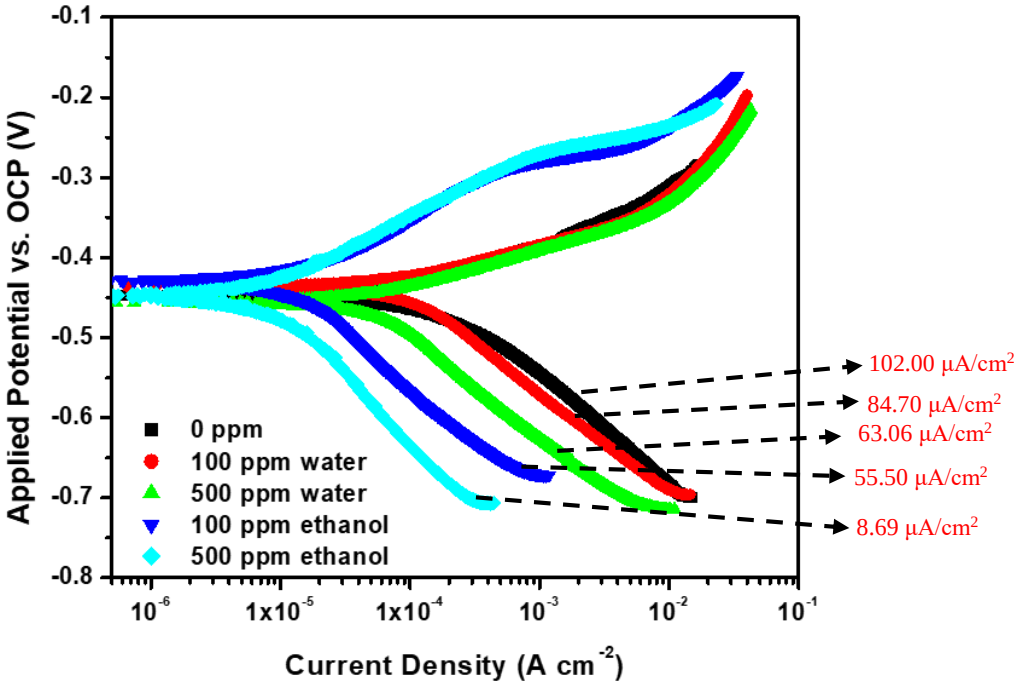

Figure 2: PDP analysis of C1020 steel in 1 M HCl containing water and ethanol extracts of *Spondias mombin* leaves at 25 °C (corrosion current, i_{corr}, values given in red font).

3.1.2 Potentiodynamic polarization (PDP)

The influence of the extracts on the anodic and cathodic reactions on the steel surface during the corrosion in the acid solution was investigated using the PDP technique. In the present study, the predominant anodic reaction is the oxidation of Fe to Fe^{2+} while that of the cathodic reaction is the reduction of H^+ to $H_2(g)$. Figure 2 shows the result of the polarization of the steel samples in the acid solution without and with concentrations of 100 and 500 ppm of the different extracts. The influence of both extracts on the corrosion potentials of the steel was observed to be minimal. This implies that the extracts had minimal influence on the thermodynamic propensity of the steel to corrode in the acid solution. However, the extracts significantly shifted both anodic and cathodic current to lower values. The implication is that the extracts exhibited mixed-type inhibitions since they were able to lower both anodic and cathodic reactions.

3.2. Adsorption Isotherm Analysis

The electrochemical results confirm that the ethanol extract of *Spondias mombin* leave performed better than the water extract. This could be attributed to the fact the ethanol, being a more vigorous solvent, could extract more phytoconstituents from the leaves, compared with the less aggressive solvent (water). It has also been well documented that the plant constituents protect corroding metal surfaces by adsorbing on active sites to block the electrochemical reactions. Adsorption isotherms are usually employed to decipher the predominant adsorption mechanism by corrosion inhibitors. In this work, we have tested the extract adsorption using the Langmuir, Freundlich and Temkin isotherms (Equations (3)–(5), respectively), by focusing on the ethanol extract. The results are presented in Figure 3.

$$\frac{C}{\theta} = \frac{1}{K_{ads}} + C \quad (3)$$

$$\log\theta = \log K_{ads} + \frac{1}{n}\log C \quad (4)$$

$$\theta = -\frac{1}{2\alpha}\ln C - \frac{1}{2\alpha}K_{ads} \quad (5)$$

The most appropriate model is usually identified by the isotherm with the highest correlation coefficient (R^2). Figure 3 shows that the Freundlich isotherm (0.9975) exhibited the highest value of R^2. This indicates that the extract components adsorbed as single layer on roughened steel surface during the corrosion inhibition (Akinbulumo et al., 2020; Chaudhary and Tak 2022).

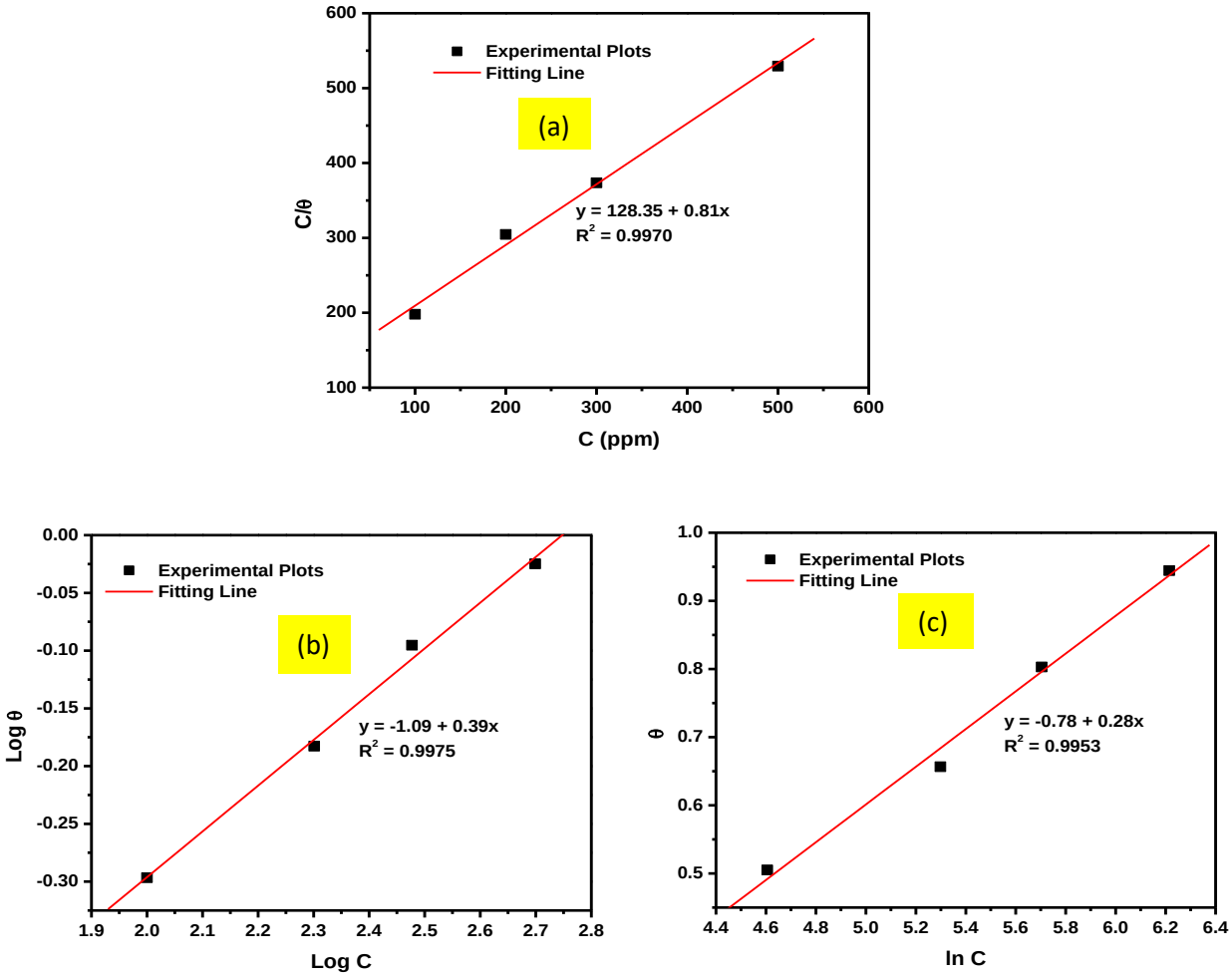

Figure 3: (a) Langmuir (b) Freundlich and (c) Temkin and isotherm plots for C1020 steel in 1 M HCl containing different concentrations of water extract of *Spondias mombin* leaves at 25 ℃.

The adsorption constant, K_{ads}, can be extrapolated from the intercept of the Freundlich plot, according the Equation (4), can be introduced into the following $\Delta G_{ads} = -RT(10^6 K_{ads})$ to calculate the thermodynamic Gibbs free energy change which describes the feasibility and spontaneity of inhibitor adsorption. The adsorption equilibrium constant was calculated as 0.081 ppm mol.$^{-1}$ and, from this value, the Gibbs' free energy was deduced as –28.00 KJ mol.$^{-1}$. The negative value confirms that the extract adsorption was spontaneous and feasible.

4. CONCLUSIONS

This study examines current developments in the use of plant extracts as corrosion inhibitors based on the use of *Spondias mombin* leave extracts. Several plant extracts have been evaluated as inhibitors against metallic corrosion due to their environmentally friendly behavior and excellent inhibitory efficiency. The adsorption of the *Spondias mombin* leave extracts on the mild carbon steel was via Langmuir and Freundlich isotherm indicating the components adsorbed as single layer on much roughened steel surface during the corrosion process. The water extract had dominant effect on the anodic corrosion reactions while the ethanol extract had major effect on the cathodic corrosion reactions. The electrochemical analysis revealed lower rate of corrosion and increase in corrosion resistance of the extracts.

REFERENCES

Ahanotu C.C., Onyeachu I.B., Solomon M.M., Chikwe I.S., Chikwe O.B., Eziukwu C.A. Pterocarpus Santalinoides Leaves Extract as Sustainable and Potent Inhibitor for Low Carbon Steel in a Simulated Pickling Medium, Sustainable Chemistry and Pharmacy, 15 (2020) 100196

Akinbulumo O.A., Odejobi O.J., Odekanle E.L. Thermodynamics and Adsorption Study of the Corrosion Inhibition of Mild Steel by Euphorbia heterophylla L. Extract in 1.5M HCl, Results in Materials, 5 (2020) 100074

Alrefaee S.H., Rhee K. Y., Verma C., Quraishi M. A., Ebenso E.E. Challenges and Advantages of Using Plant Extract as Inhibitors in Modern Corrosion Inhibition Systems: Recent Advancements, Journal of Molecular Liquids, (2020), 44-88.

Asfia M.P., Rezaei M., Bahlakeh G. Corrosion Prevention of AISI 304 Stainless Steel in Hydrochloric Acid Medium Using Garlic Extract as Green Corrosion Inhibitor: Electrochemical and Theoretical Studies, Journal of Molecular Liquids, 315 (2020) 113679

Belakhdar A., Ferkous H., Djellahi S., Sahraoui R., Lahbib H., Amor Y.B., Erto A., Balsamo M., Benguerba Y. Computational and Experimental Studies on the Efficiency of Rosmarinus officinalis Polyphenols as Green Corrosion Inhibitors for XC48 Steel in Acidic Medium, Colloids and Surfaces A: Physicochemical and Engineering Aspects 606 (2020) 125458

Berrissoul A., Onarhach A., Benhiba F., Romane A., Zarrouk A., Guenbour A., Dikici B., Dafali A. Evaluation of Lavandula mairei Extract as Green Inhibitor for Mild Steel Corrosion in 1M HCl Solution – Experimental and Theoretical Approach, Journal of Molecular Liquids, (2020) 113493

Bidi M.A., Azadi M., Rassouli M. A New Green Inhibitor for Lowering the Corrosion Rate of Carbon Steel in 1M HCl Solution Using Hyalomma tick Extract, Materials Today Communication, 24 (2020) 100996

Chaudhary S., Tak R.K. Natural Corrosion Inhibition and Adsorption Characteristics of Tribulus terrestris Plant Extract on Aluminum in Hydrochloric Acid Environment. Biointerface Research in Applied Chemistry 12 (2) (2022) 2603-2617

Chen S., Chen S., Zhu B., Huang C., Li W. Magnolia grandiflora Leave Extracts as a Novel Environmentally Friendly Inhibitor for Q235 Steel Corrosion in 1M HCl: Combining Experimental and Theoretical Researches, Journal of Molecular Liquids (2020) 113312

Fang Y., Suganthan B., Ramasamy R.P. Electrochemical Characterization of Aromatic Corrosion Inhibitors from Plant Extracts. Journal of Electroanalytical Chemistry 840 (2019) 74-83

Fouda A., Shalabi K., Shaaban M. Synergistic Effect of Potassium Iodide on Corrosion Inhibition of Carbon by Achillea santolina Extract in Hydrochloric Acid Solution, Journal of Bio-and Tribo-Corrosion, 5 (2019) 71.

Ishak A., Adams F.V., Madu J.O., Joseph I.V., Olubambi P.A. Corrosion Inhibition of Mild Steel in 1M Hydrochloric Acid Using Haematostaphis barteri Leaves Extract, Procedia Manufacturing, 35 (2019) 1279-1285

Marzorati S., Verotta L., Trasatti S.P. Green Corrosion Inhibitors from Natural Sources and Biomass Wastes, Molecules, 24 (2019) 48.

Muthukumarasamy K., Pitchai S., Devarayan K., Nallathambi L. Adsorption and Corrosion Inhibition Performance of Tunbergia fragrans Extract on Mild Steel in Acid Medium, Materials Today: Proceedings, (2020) 23-31

Palaniappan N., Cole I., Caballero-Briones F., Manickam S., Thomas K.J., Santos D. Experimental and DFT Studies on the Ultrasonic Energy-assisted Extraction of the Phytochemicals of Catharanthus roseus as Green Corrosion Inhibitors for Mild Steel in NaCl Medium, Royal Society of Chemistry (RSC) Advances, 10 (2020) 5399-5411

Solomon M.M., Umoren S.A., Obot I.B., Sorour A.A. Gerengi H. Exploration of Dextran for Application as Corrosion Inhibitor for Steel in Strong Acid Environment: Effect of Molecular Weight, Modification and Temperature on Efficiency. ACS Applied Materials & Interfaces 10 (2018) 28112-28129

Verma C., Ebenso E.E., Bahadur I., Quraishi M.A. Alkaloids as Green and Environmental Benign Corrosion Inhibitors: An Overview, International Journal of Corrosion and Scale Inhibition, 8 (2019) 512-528

DOI: 10.51975/23380109.som
Journal of the Nigerian Society of Chemical Engineers, 38(1), 2023

AN APPROACH TO SCALE UP OF NEEM SEED OIL SOLVENT EXTRACTION PILOT PLANT

Usman, J. G.[1*], Okonkwo, P. C.[2], Mukhtar, B.[3], Baba, A. [4]
[1]*Department of Chemical Engineering, Kaduna Polytechnic, Nigeria.*
[2,3,4]*Department of Chemical Engineering, Ahmadu Bello University, Zaria , Nigeria.*

[1*]*johngoji@yahoo.com,* [2]*chemstprom@yahoo.com,*[3]*belloonline@yahoo.com, olubababdul@gmail.com*
*Corresponding author

ABSTRACT

The current mechanical expression of oil from neem seed cannot satisfy the ever-increasing demand of the neem oil. The futuristic solution to the shortage of neem oil is the successful scale up of the solvent extraction pilot plant to larger commercial plant to boost the production capacity. The scale up approach is based on the pilot plant study and the use of existing model equations. The similarities values for the scale up are 21.69 W/m^2, 0.125, 0.029, 0.21 and 7.5831× 10^{11} as power per volume, shape factor, Froude number, impeller speed and Reyleigh number respectively. Scaling up the agitation pilot plant, using ethanol at an extraction temperature of 50 ^{o}C and separation of the miscella at 50 ^{o}C under reduced pressure of 207.02 mmHg will reduce the recovery time and retain the oil quality. ASPEN PLUS V10 is recommended for simulation and the fractional compositions of neem seed kernel are 0.45% neem oil and 0.55% neem seed cake, while for ethanol are 96% pure ethanol and 4% water. The concept of overall heat transfer coefficient will be used for design and sizing of the condenser heat exchanger.

Keywords: *Neem tree, Solvent extraction, Scale up, Power per volume number and Reyleigh number*.

1. INTRODUCTION

The neem tree belongs to the mahogany family and its botanical name is *'Azadiracdita Indica'*. It is highly medicinal and extensively found in India and Indonesia (Oluwole *et al.,* 2015). The neem tree is found as plantation in Kano, Katsina and Jigawa states of Nigeria in West African subcontinent to check desertification and it provide materials base for industrial development (Nde & Foncha, 2020; Orsar *et al.,* 2016). The quality of neem oil is expressed in terms of iodine, acid and saponification values; and these values are affected by extraction temperature (Baboo, 2016; Workneh, 2011).

Agitation and mixing increase the mass and heat transfer (Usman *et al*., 2013) and two processes are considered similar if they possess geometric, kinematic and dynamic similarities (Belwal *et al.,* 2016). Simulation process is used to predict the performance of the scaled-up equipment before construction (Maria, 1997) and ASPEN PLUS V10 is suitable for the simulation. Despite the abundant availability of neem seed in Nigeria, the major problem and challenges of neem oil extraction is the lack of processing equipment (Oluwole *et al.,* 2015). The current extraction process (mechanical press) cannot meet the increasing demand due to low yield extraction rate (Nkouam *et al.,* 2017). The demand on neem oil is ever increasing (Orsar *et al.,* 2016) and scale up to large scale production will meet the ever-increasing demand for the neem oil (Nde & Foncha, 2020; Oluwole *et al.,* 2015). Scale up of the solvent neem seed oil extraction pilot plant to large scale will boost the production capacity to meet the increasing demand of neem seed oil.

The scaling up procedure will largely depends on the pilot scale plant study. Prospectively, a futuristic recommendation on how to scale up the process to large extraction plant in order to meet the ever – increasing demand and preserve the quality of the extracted oil is presented. The most conventional method of extracting neem seed oil is the mechanical expression which leaves 6% to 14% of oil in the cake (Workneh, 2011) and needs additional solvent extraction method to maximize yield (Tesfaye & Tefera, 2017). The solvent extraction method leaves 0.5% of oil in the cake (Workneh, 2011) and the Soxhlet apparatus is the most popular equipment use for continuous solid – liquid extraction of oil from seed (Subramanian *et al*., 2017). It gives higher yield and less turbid product when compared to mechanical method (Tesfaye & Tefera, 2017).

The neem kernel is dried in an oven at a temperature of 40 – 55 ^{o}C (Subramanian *et al.*, 2017; Tesfaye & Tefera, 2017; Jessinta *et al.*, 2014; Workneh, 2011). N-hexane and ethanol are the most commonly used solvent for extraction of neem seed oil. Subramanian *et al.* (2017) used n- hexane and ethanol in a Soxhlet apparatus at 70 ^{o}C and obtained percentage yield of 45, 46, 47.5 and 49%; 40, 42, 45 and 46% at extraction time of 120, 180, 240 and 300 minutes respectively. Tesfaye and Tefera, (2017) used ethanol at 70, 78 and 86 ^{o}C and obtained percentage yield of 41.08, 41.89 and 42.41% respectively. Workneh, (2011) extracted neem seed oil in an agitated laboratory vessel at an extraction temperature of 30, 40 and 50 ^{o}C using ethanol and n–hexane. The percentage yield obtained were 26.9, 31.1 and 33.2%; 39.2, 44.8 and 47.3% respectively. At same temperature and solvents the iodine values were 66.58, 65.79 and 61.32 I_2/g; 72.62, 68.41 and 62.83 I_2/g respectively. The acid values were 32.8, 36 and 40; 96.4, 102 and 122 mg KOH/g respectively. The saponification values were 175.71, 194.3 and 205.84 mgKOH/g; 184.03, 209.30 and 221.93 mgKOH/g respectively.

Table 1 shows the work done by Usman *et al*. (2013) and Workneh, 2011 to extract oil from neem seed in an agitated media. Usman *et al*. (2013) used an agitated ethanol pilot plant with capacity of 9.65 kg/day of neem seed kernel to extract oil at a rate of 174.33 g/h within 40 minutes at 50^{o}C with a maximum yield of 36.86% using flat blade turbine impeller at 84 rpm; while Workneh, (2011) reported an extraction rate of 6.63 g/h when agitated laboratory beaker was used at 50^{o}C, with a yield of 33.19 and 47.32% for using ethanol and n – hexane respectively as seen from Table 1. The extraction rate of 174.33 g/h of neem oil reported by Usman *et al*. (2013) is greater than 6.63 g/hr of neem oil reported by Workneh, (2011). The major components of the pilot plant are mixer (extractor), evaporator, double – pipe condenser and a chiller. A flat blade turbine impeller was shown to be better than the Rhuston blade turbine impeller at 84 rpm due to the absent of a disc on the flat blade turbine impeller. It took 4 hr 25 minutes to separate the oil from the miscella (Usman *et al*., 2013; Usman and Okonkwo, 2013).

Table 1: Effect of impeller speed and impeller type on the yield of oil from neem seed

Author	Solvent used	Impeller type	Impeller speed (RPM)	Extraction time	Yield	Extraction rate (g/hr)
Usman *et al*., 2013a; Usman and Okonkwo, 2013b.	Ethanol	Flat blade turbine impeller	37	20	24.28	
				40	28.64	
			84	20	29.32	
				40	36.86	174.3
		Rhuston turbine impeller	37	20	20.95	
				40	23.95	
			84	20	25	
				40	31.25	
Workneh, 2011.	Ethanol	Stirrer	-	180	33.19	6.633

ASPEN PLUS is simulation software that is used base on mass balance and application of property method. The property method is easily applied because it depends on process parameters such as temperature, flow rate and fractional composition of the materials (Hachhach *et al*., 2019).

Based on the published work by Usman *et al*. (2013), the following recommendations are made for scale up of the pilot plant.

DOI: 10.51975/23380109.som
Journal of the Nigerian Society of Chemical Engineers, 38(1), 2023

1.1 Scale – up of solid – liquid mixer (Extractor).

a. ***Geometric similarity:*** Geometric similarity is attained by keeping the ratios of different dimensions such as impeller diameter to vessel

diameter constant upon scale – up (Yavuz and Sandeep, 2019). The scale – up ratio in term of volume is expressed as:

$$R = (\frac{V_2}{V_1})^{1/3} \quad (1)$$

In Equation (1), R = scale – up ratio, V_1= volume of pilot plant and V_2= volume of larger plant (Yavuz and Sandeep, 2019). Geometric similarity is obtainable when the impeller speed is greater than just suspended speed (critical speed), the power per volume and shape factor of the pilot and large plants are equaled (Megawati *et al*., 2018; McCabe, 1993).

The impeller power number, N_p, is the flow of momentum associated with the bulk motion of the fluid. It is used to predict the power of the mixer, P directly.

$$N_p = \frac{P}{\rho N^3 D^5} \quad (2)$$

In Equation (2), N_p = Power number, P = Power of mixer (Watt), D = Diameter of impeller (m), N = Revolution per second and ρ = Density of the liquid, Kgm^{-3} (McCabe, 1993).

The power number at a given Reynolds number, number of baffles in the extractor, number of blade and shape factor is obtained using Figure 1.

b. ***Kinematic similarity:*** **Velocity ratios at corresponding points are same.**

The impeller tip speed is expressed as:

$$\pi D_1 N_1 = D_2 N_2 \quad (3)$$

In Equation (3), N_1 = impeller speed of pilot plant, N_2 = impeller speed of large scale and D_1 = impeller diameter of pilot plant and D_2 = impeller diameter of large plant.

Impeller Speed Scale up: $N_2 = N_1(\frac{1}{R})^n \quad (4)$

In Equation (4), n = $\frac{2}{3}$, for systems having equal rates of mass transfer (equal power per unit volume) (Scaleup of Mixing system (n.d))

c. ***Dynamic similarity:*** Similarities in internal collision energy or same ratio of forces between corresponding sites in two systems. The Froude number is use to evaluate the dynamic similarity (Jang *et al.*, 2020).

$$\text{Froude number, (Fr)} = \frac{\text{Inertia force}}{\text{Gravitational force}} = (\frac{N^2 \times D}{g})_{\text{pilotplant}} = (\frac{N^2 \times D}{g})_{\text{largeplant}} \quad (5)$$

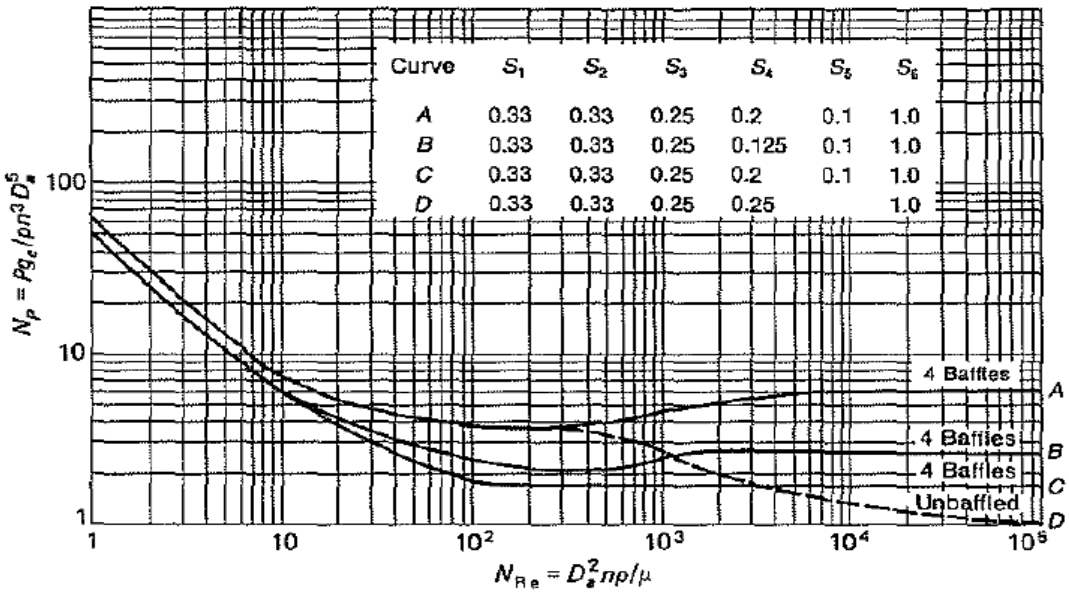

Figure 1: Chart for Power number, N_P versus Reynold number, N_{Re} for six-blade turbines.
Source: (McCabe, 1993)

1.2 Scale up of evaporator.

The mode of heat transfer during separation of solvent from the extracted neem oil is natural convention (Usman

et al., 2013). Fluid motion and heat transfer phenomena are related in the evaporator and governed by the dimensionless quantities such as Grashof and Prandtl numbers. The Grashof (Gr) and Prandtl (Pr) number are connected by the Rayleigh number (Ra) as shown in Equation (6) to (8).

$$Gr = \frac{g\beta(T_w - T_a){D_t}^3}{V^2} \quad (6)$$

$$Pr = \frac{v}{\alpha} \quad (7)$$

$$Ra = Gr \times Pr = \frac{g\beta(T_w - T_a){D_t}^3}{(v \times \alpha)} \quad (8)$$

In Equations (6) to (8), β = coefficient of thermal expansion = $1/T_a$ ($^oC^{-1}$), T_a = ambient temperature (^oC) , T_w = wall temperature (^oC), Dt = extractor diameter (m) , k = thermal conductivity of air at average temperature (W/m^{o}C), v = kinematic viscosity (m^2/s) and α = thermal diffusivity (m^2/s) (Janna, 1986).

The evaporator for separating the extracted oil required low heating temperature and short residence time of the miscella. This is achieved by minimizing the volume of the miscella and operating the evaporator at a reduced pressure (Glover, 2004). The vapour pressure of ethanol at 50^{o}C is 276 mbar (207.02 mmHg) (Rütti and Heierli, 2012).

1.3 Design of 1-2 shell-and-tube heat exchanger.

The pilot plant used by Usman *et al*. (2013) employs the usage of a double – pipe condenser. For scale up of the pilot plant to large plant, there is need for design of a condenser in the form of 1-2 shell-and-tube heat exchanger to reduce the condenser length and to enhance heat transfer for faster condensation. The 1 – 2 exchanger means one shell – side and two tube – side passes (Backhurst and Harker, 1983). The concept of overall heat transfer coefficient can be adopted for calculating the heat transfer area of the 1 – 2 shell-and-tube heat exchanger and its sizing. The basic equation for calculating heat transfer in a heat exchanger is

$$Q = UA\Delta Tm \quad (9)$$

In Equation (9), Q = Quantity of heat transferred (W), U = Design value of overall heat transferred coefficient (W/m^2^{o}C), A = Area for heat transfer (m^2) and ΔTm = Logarithmic mean temperature difference (^{o}C)

The approximate or assumed overall heat transfer coefficient is given by

$$U_a = \frac{0.7 \times h_i \times h_o}{h_i + h_o} \quad (10)$$

The overall design heat transfer coefficient is obtained from the individual film heat transfer coefficients. Neglecting pipe wall resistance and scale resistance, the equation is given as

$$\frac{1}{U_D} = \frac{1}{h_{io}} + \frac{1}{h_o} \quad (11)$$

In Equations (10) to (11), h_i = inside film coefficient (W/m^2 ^{o}C) and h_o = outside film coefficient (W/m^2 ^{o}C), h_{io} = inside film coefficient based on the outside diameter (W/m^2^{o}C) (Backhurst and Harker, 1983).

Data from the pilot plant used by Usman *et al*., (2013) for the purpose of scale up include the following:

Extractor

i. Number of blades on the flat blade turbine impeller = 6
ii. Extractor diameter = 0.300 m
iii. Impeller diameter = 0.150 m
iv. Height of mixture = 0.306 m
v. Height of extractor = 0.390 m
vi. Extractor volume = 0.02121 m^3
vii. Width of impeller = 0.0188 m
viii. Width of baffle = 0.025 m
ix. Number of baffles in the extractor = 4
x. Impeller speed = 84 rpm (1.40 rps)
xi. Density of ethanol at 35^{o}C ($\frac{20+50}{2}$) = 788.38 kg/m^3
xii. Viscosity of ethanol at 35^{o}C = 0.000882 kg/ms
xiii. Reynolds number = 28,155.71
xiv. Extraction temperature = 50^{o}C

Evaporator

i. Miscella temperature, T_w = 78^{o}C
ii. Ambient temperature, T_a = 20^{o}C
iii. Diameter of cylindrical evaporator, Dt = 0.2346 m
iv. Height of evaporator, H = 0.6744 m
v. Acceleration due to gravity, g = 9.81 m/s^2
vi. Coefficient of thermal expansion, β = 1/ T_a = 1/20 = 0.05 $^oC^{-1}$
vii. Kinematic viscosity of ethanol at 49^{o}C, v = 0.9198 × 10^{-6} m^2/s
viii. Thermal conductivity of ethanol at 49^{o}C, k = 1.0210 W/m^{o}C
ix. Density of ethanol at 49^{o}C, ρ = 679.98 kg/m^3
x. Specific heat capacity of ethanol at 49^{o}C, Cp = 2850.5 J/kg^{o}C
xi. Thermal diffusivity, α = 5.2675 × 10^{-7}(m^2/s)

2. METHODOLOGY

Based on the data obtained from the pilot plant used by Usman *et al.* (2013); the shape factor is evaluated based on the width and diameter of the impeller, the power number N_p is obtained from Figure 1 using curve B and shape factor of 0.125 at a Reynolds number of 28,155.71. The required power is evaluated using equation 2. The

geometric similarity based on powers per volume of 21.69 W/m^2 and shape factor of 0.125 were obtained for the pilot plant for comparison with the future scaled up plant. Similarly, the Froude Number, 0.029 (Dynamic similarity) and the impeller tip speed of 0.21 (Kinematic similarity) were calculated for comparing the dynamic and kinematic similarities of the scaled-up plant respectively. The scale up ratio is obtainable using equation 1 and is based on the known volume of solvent used in the pilot plant and the volume of solvent for the scaled-up plant. The evaporator Reyleigh number of 7.5831×10^{11} is evaluated for comparison with the scale up evaporator to ensure scale up similarity. The condenser can be designed using the concept of overall heat transfer coefficient to calculate the area and size the 1-2 shell-and-tube heat exchanger (condenser) while the chiller is replaceable with an independent cooling water supply.

The ASPEN – PLUS V10 is recommended for correlating the existing models used is scaled up calculations. The ASPEN – PLUS V10 will be used for simulation of the scaled up plant before construction based on the flow rate of neem seed kernel and ethanol solvent (flow rate values depend on the scaled up capacity of the future commercial plant), fractional composition of neem seed kernel (neem seed oil = 0.45% and neem seed cake = 0.55%) and fractional composition of ethanol solvent (96% pure ethanol and 4% water), operating temperature (50^{o}C) and operating pressures (760 mmHg for extraction in the extractor and 207.02 mmHg for separation in the evaporator) as requirement for running the ASPEN PLUS V10.

The 4hr 25 minutes used by Usman *et al.* (2013) for separating the miscella at 760 mmHg will be reduced in the scale up plant by incorporating a vacuum pump. Separation will take place at lower temperature of 50 ^{o}C under reduced pressure of 207.02 mmHg to reduce the recovery time and preserve the quality of the neem oil.

3. RESULTS AND DISCUSSION

The Geometric (Power per volume and shape factor), Dynamic (Froude number), Kinematic (Impeller tip speed) similarities and the Rayleigh number of the pilot plant are shown in Table 2.

Table 2: Calculated similarities values and Rayleigh numbers for future scale up

Plant	Power per Volume (W/m^3)	Shape factor	Froude number	Impeller Tip Speed	Rayleigh Number
Pilot Plant	21.69	0.125	0.029	0.21	7.5831×10^{11}

The oven drying at 50 ^{o}C is commonly used for drying the neem seed kernel because it preserves the quality of the neem seed (Azwanida, 2015) and the most commonly used solvents are ethanol and n – hexane with an extraction yield range of 26.9 - 46% and 39.2 – 49% respectively within the extraction temperature range of 30 – 86 ^{o}C. The quality of neem oil is affected by extraction temperature as seen from the work of Workneh, (2011). The iodine, acid and saponification values changes from 66.58 to 61.32 gI_2/g, 32.8 to 40 mg KOH/g and 175.71 to 205.84 mg KOH/g as extraction temperature increases from 30 to 50 ^{o}C respectively using ethanol as the extraction solvent. The increase in temperature brings about decrease of iodine value due to formation of more saturate compounds, and this will make the oil less reactive. Extraction yield of neem oil in an agitation vessel is affected by the level of agitation. This is clearly seen from the work of Usman *et al*. (2013) in Table 1; at 84 rpm for 40 minutes extraction time, a yield of 36.86% was achieved as compared to 28.64% yield at 37 rpm for 40 minutes extraction time.

The successful operation and calculation of geometric, dynamic, kinematic and Reyleigh values of the pilot plant for similarities comparison potent the success toward the scale up of the pilot plant to commercial scale.

4. CONCLUSION

The scale up of the pilot plant used by Usman *et al.* (2013) to commercial scale is possible due to successful calculated values for similarity comparison. Such values include: 21.69 W/m^2 (Power per volume) and 0.125 (Shape factor) for geometric similarity; 0.029 (Froude number) for Dynamic similarity; 0.21 (Impeller tip speed) for kinematic similarity and 7.5831×10^{11} as Reyleigh number for the evaporator scaled up. The 1-2 shell – and – tube heat exchanger (condenser) can be designed and sized using the overall heat transfer coefficient technique. For future extraction of large quantity of good neem seed oil; the geometric, dynamic and kinematic similarities

should be implored for the scale up of the pilot plant to commercial plant.

NOMENCLATURE

Symbols

R Scale – up ratio
V_1 Volume of pilot plant and
V_2 Volume of larger plant
N_p Power number
P Power of mixer
D Diameter of impeller
N Revolution per second and
ρ Density of the liquid
N_1 Impeller speed of pilot plant
N_2 Impeller speed of large scale
D_1 Impeller diameter of pilot plant
D_2 Impeller diameter of large plant
n Constant for equal rates of mass transfer
g Acceleration due to gravity
β Coefficient of thermal expansion
T_a Ambient temperature
T_w Wall temperature.
Dt Extractor diameter
K Thermal conductivity of air
ν Kinematic viscosity
α Thermal diffusivity
Q Quantity of heat transferred
U or U_D Design value of overall heat transferred coefficient
U_a Approximate or assumed overall heat transfer coefficient
A Area
ΔTm Logarithmic mean temperature difference
h_i Inside film coefficient
h_o Outside film coefficient
h_{io} Inside film coefficient based on the outside diameter

ACKNOWLEDGEMENT

The authors are grateful to Kaduna Polytechnic, Kaduna and Ahmadu Bello University Zaria, for being sources of encouragement to carry out this futuristic study.

REFERENCES

Azwanida, N. N. (2015). A Review on The Extraction Methods Use in Medicinal Plants, Principle, Strength and Limitation. *Journal of Medicinal and Aromatic Plants*, 4(3). DOI:10.4172/2167-0412.1000196

Baboo, P. (2016). Advancement In Neem Oil Extraction Process. Downloaded From https://Www.Researchgate.Net/Publication/292392229_Advancement_In_Neem_Oil_Extraction_Process/Link/56ae169f08ae19a38515f831/Download on 17/7/2020 By 10:08am.

Backhurst, J.R. and Harker, J.H. (1983). *Process Plant Design*. Heinemann Chemical Engineering Series, London, Pp. 64 - 71.

Belwal, S., Revanth, V., Dinesh, K.S.V.V., Reddy, B.V. And Bhagvanth, M. R. (2016). Development And Scale Up of A Chemical Process In Pharmaceutical Industry: A Case Study. *International Journal of Engineering Research And Application*, 6(7), Pp. 81-88.

Hachhach,M., Akram, H., Hanafi, M., Achak, Q And Chafik, T. (2019). Simulation And Sensitivity Analysis of Molybdenum Disulfide Nanoparticle Production Using Aspen Plus. *International Journal of Chemical Engineering.* Volume 2019, Article Id 3953862, 8 Pages. https://Doi.Org/10.1155/2019/3953862.

Jang, E.H, Park, Y.S, Kim, M And Choi, D.Y. (2020). Model-Based Scale-Up Methodologies For Pharmaceutical Granulation. *Journal of Pharmaceutics*. 12, 453; Doi:10.3390/Pharmaceutics12050453.

Janna, W.S. (1986). *Engineering Heat Transfer*. Pws Publishers, United States of America. Pages 453 - 454.

Jessinta, S., Azhari, H.N., Saiful, N.T. And Abdurahman, H. N. (2014). Impact of Geographic Variation on Physicochemical Properties of Neem (*Azadirachta Indica*) Seed Oil. *International Journal of Pharmaceutical Sciences And Research*, 5(10), Pp. 4406-4413.

Maria, A. (1997). Introduction To Modeling and Simulation. Proceedings of the 1997 Winter Simulation Conference. State University of New York At Binghamton. Department of Systems Science and Industrial Engineering, Binghamton, Ny 13902-6000, U.S.A. Pages 7 – 13. Available on www.acqnotes.vom.

Mccabe, W.L., Smith, J.C., and Harriott, P. (1993). Unit Operation of Chemical Engineering. 5th Edition, Mcgraw-Hill Book Company, Singapore. Pages 248 – 250, 429 – 440.

Nde, D.B. and Foncha, A.C. (2020). Optimization Methods For The Extraction of Vegetable Oils: A Review. *Journal of Processes.* 8(209), Doi:10.3390/Pr8020209 vwww.mdpi.Com/Journal/Processes.

Nkouam, G.B., Musongo, B., Bouba, A. A., Tchatchueng, J. B., Kapseu, C. and Barth, D. (2017). Traditional Techniques of Oil Extraction from

Kapok (Ceiba Pentandra Gaertn), Mahogany (Khaya Senegalensis) and Neem (*Azadirach Indica A. Jus.*) Seeds From The Far-North Region of Cameroon. *International Journal of Environment, Agriculture and Biotechnology*, 2(4), Pp. 2207 – 2213.

Oluwole, F.A; Oumaru, M.B. and Abdulrahim, A.T. (2015). Traditional Method of Neem Seed Oil Extraction In Northeastern Nigeria: Challenges and Prospect. *Continental Journal of Engineering Sciences*, 10(1), Pp. 1 – 8.

Orsar, T. J., Tyowua, B. T. and Asemave, J.T. (2016). Neem (*Azadirachta Indica A. Juss*) Fruit Yield Determination in Makurdi, Benue State, Nigeria. *Journal of Research In Forestry, Wildlife & Environment*, 8(2), Pp. 145 – 156.

Rütti, D. and Heierli, M. (2012). Multivapor Application Guide. Buchi Labortechnik Ag, Switzerland, Pp. 6 & 39. Retrieved From https://static1.buchi.com/sites/default/files/application_guide_multivapor_1205... on 25/04/2020 By 3.53 P.M.

Subramanian, S., Salleh, A. S., Bachmann, R. T., Idrus, N. M. and Hossain, M. S. (2017). Optimising *Azadirachtin* Yield from Neem Tree Seeds and Leaves using a Binary Solvent System for Potential Pest Control Application. *International Conference on Environmental Research and Technology.* Universiti Kuala Lumpur, Malaysian Institute of Chemical and Bioengineering Technology, Gajah, Malaysia, Pp. 481 – 486.

Tesfaye, B. and Tefera, T. (2017). Extraction of Essential Oil from Neem Seed By Using Soxhlet Extraction Methods. *International Journal of Advanced Engineering, Management and Science*, 3(6), Pp. 646 – 649.

Usman, J.G., Okonkwo, P.C. and Mukhtar, B. (2013a). Design and Construction of Pilot Scale Process Solvent Extraction Plant For Neem Seed Oil. *Nigerian Journal of Technology (Nijotech,)* 32(3), Pp. 528 – 537.

Usman J.G. and Okonkwo P.C. (2013b). Pilot Scale Extraction of Neem Oil Using Ethanol As Solvent. International Journal of Engineering Research & Technology, 2(9), Pp. 1716 – 1733.

Workneh, W. (2011). Extraction and Characterization of Essential Oil From Morgosa Seed. Addis Ababa University, School of Graduate Studies, Addis Ababa Institute of Technology, Department of Chemical Engineering, Ethopia, Retrieved From www.libsearch.com/search/soxhlet%25.

Yavuz, N. and Sandeep, K.P. (2019). Scale-Up of Shear Thinning Fluid Mixing In An Unbaffled Stirred Vessel With Eccentrically Located and Modified Impellers. *International Journal of Chemical Reactor Engineering, Doi*: 10.1515/Ijcre-2018-0205

Scaleup of Mixing System (N.D). From http://www.uobabylon.edu.iq/uobcoleges/ad_downloads/5_4801_857.pdf. Downloaded on 5/5/2020 By 9.05p.m.

DOI: 10.51975/233801010.som
Journal of the Nigerian Society of Chemical Engineers, 38(1), 2023

METHYLENE BLUE ADSORPTION BY *VITEX DONIANA* ACTIVATED CARBON: EQULIBRIUM ISOTHERM STUDY

***Francis, A. O.[1] and Jock, A. A.[2]**
[1]*Department of Chemical Engineering, Edo State University, Uzairue, Nigeria*
[2]*Department of Chemical and Petroleum Engineering, University of Uyo, Nigeria*
*Email: francis.asokogene@edouniversity.edu.ng

ABSTRACT

Vitex doniana activated carbon modified with zinc chloride ($VDZnCl_2$) was synthesized for the removal of methylene blue. $VDZnCl_2$ was characterized for textural properties, surface morphology and surface chemistry. The textural properties revealed increased surface area from 14.02 to 933.25 m^2/g, the surface morphology showed pores with widened cavities, and the surface chemistry showed the inclusion of O—H group and a characteristics C=C group commonly found in carbonaceous materials. Adsorption study showed increased removal of methylene blue as concentration increased from 1 to 800 mg/L until equilibrium was attained. Sips isotherm model had the best fittings with the equilibrium data (R^2 = 0.938 and SSE = 7016.14), thereby suggesting physical adsorption onto the heterogeneous surface of $VDZnCl_2$. However, the maximum adsorption capacity was 238 mg/g. The performance put up by $VDZnCl_2$ suggested that it is a possible /suitable alternative adsorbent for textile and dyeing industries wastewater.

Key words: *Activated carbon, synthesized, adsorbent, methylene blue, characterized*

1. INTRODUCTION

Most paper, pulp, textile and dyeing industries either permanently or temporarily empty their waste into water bodies, which in turn contaminates them and other adjoining streams and tributaries, thereby reducing the dissolved oxygen and restricting the penetration of sunlight and aerobic activities. These phenomena render the waters unfit for drinking and irrigation, and ultimately posing serious hazards to human life and aquatic system (Ertugay and Acar 2017; Asokogene et al. 2019; Iqbal et al. 2019; Piriya et al. 2021). Exposure to dyes results in several health challenges like dyscrasia, leukocytosis, anemia, cyanosis, vomiting, convulsion, methemoglobinemia, liver, heart, spleen, kidney, lungs, and bone damage, (Miyah et al. 2018; Alipour et al. 2019; Iqbal et al. 2019; Piriya et al. 2021). Methylene blue ($C_{16}H_{18}CIN_3S$) is a cationic dye commonly used in textile industries for cotton, wool and silk (Miyah, Idrissi, and Zerrouq, 2015; Thakur, Pandey, and Arotiba, 2016). Therefore, its treatment in wastewater has become an issue of great concern.

Notable among the treatment methods for methylene blue in wastewater include extraction, membrane separation, coagulation, ozonation, flocculation and adsorption (Aslam et al. 2017; Wang et al. 2017; Asokogene et al. 2019). Adsorption is low cost, possess the potential to selectively adsorb certain molecules and excellent at dyes removal from wastewater (Asokogene et al. 2019; Naushad et al. 2019; Pandey et al. 2020; Piriya et al. 2021).

The quest for low-cost, and available adsorbents has made scientists to turn to a variety of natural and synthetic biomass waste materials as adsorbents. Activated carbon, has gained wide attention as adsorbent due to its high content of hydroxyl functional group which reflects significant potential for the removal of several aquatic pollutant. It also possesses high surface area and good pore architectures (Afshin et al. 2019). Activated carbon can be made from several biomass waste materials such as coconut shell (Singh et al. 2017), bamboo (Zhao et al. 2017), palm shells (Zhao et al. 2018), woods (Nowicki, 2016), sawdust (Zhu et al. 2014), apricot stones (Djilani et al. 2015), grape seeds (Okman et al. 2014), rice husk (Li et al. 2015) and empty fruit bunche (Zaini and Shaid, 2016).

Research has shown that activated carbon adsorbents which are chemically modified with metal salt possess improved porosity, better specific surface area and better adsorption potential for dyes, metals and other aqueous contaminants (Piriya et al. 2021). Rangabhashiyam and Selvaraju (2015), reported that $ZnCl_2$ activated carbon derived from sterculia gulata shells showed an adsorption capacity of 90.90 mg/g, compared to 45.45 mg/g of its precursor for hexagonal chromium removal from

wastewater. Zhang et al. 2020 also found that $ZnCl_2$ treated activated carbon from rice husk had a larger surface area than its precursor at a 1:1 impregnation ratio.

Meanwhile, *vitex doniana* seeds and its modified adsorbent have not gained wide recognition in dye (methylene blue) removal from wastewater, except as activated carbon adsorbent for Zn (II) and Pb (II) removal (Ameh, Odoh and Oluwaseye 2012.), and as phosphoric acid (H_3PO_4) modified activated carbon for Cr (II) removal (Yusuf, Muhammed and Grace, 2020) from wastewater. However, the availability at little cost of *vitex doniana* seeds (Kapooria and Aime, 2005) which is the raw materials for this adsorbent could be promising alternative to present day adsorbents. Therefore, this work was aimed at evaluating the adsorptive characteristics of zinc chloride ($ZnCl_2$) activated *vitex doniana* for methylene blue removal from wastewater. The activated carbon adsorbent was characterized and its adsorption for methylene blue in batch mode was performed. Equilibrium isotherm models were adopted to evaluate the adsorption data, from which the possible adsorption behavior was discussed.

2. MATERIALS AND METHODS

Seeds *of vitex doniana* were collected around Auchi Polytechnic community in Edo State, Nigeria. Methylene blue powder (98.5%) was supplied by BDH, England and zinc chloride pellet (99%) was supplied by Merck, Germany. All chemicals are of analytical reagent grade.

2.1 Adsorbent preparation and characterization

The exocarp and associated impurities of *vitex doniana* seed were washed off with running water. The seed was sun-dried for seven days, crushed, ground and sieved to 355 µm (Ameh et al. 2012). A 100 g pulverized *vitex doniana* was chemically activated using $ZnCl_2$ ($VDZnCl_2$) at 800^{o}C for 2 h in a TT-EF-12 muffle furnace (Techmel, USA). The activated sample was allowed to cool before it was soaked in HCl (3 wt%) for 12 h to remove surface ash and then washed in distilled water to a pH of 7 (Jaria et al. 2015; Khadiran et al., 2015; Mkungunugwa et al. 2021).

The surface functional groups of $VDZnCl_2$ and VDC adsorbent samples were determined using FTIR analyzer from Thermo Scientific Nicolet ISI 10, USA at wavenumber range of 4000-500 cm^{-1}. The textural properties were measured using a Thermo Scientific, USA model surface area analyzer (single point Brunauer-Emmett-Teller (BET) method. The SEM image of the adsorbent surface and texture was obtained by Karl Zeiss (Germany) instrument.

2.2 Batch adsorption studies

One gram (1 g) of methylene blue powder was dissolved in 1000 mL of distilled water to make stock solution. Following that, working concentrations of 1–800 mg/L were created by serial dilution. In Beatson bottles, 50 mL of each concentration was added to 50 mg of adsorbent, the bottles were sealed, shaken, and kept at 28^{o}C for 72 h. The contact time was assumed to be long enough to achieve equilibrium adsorption (Asokogene et al. 2019). The residual concentrations were obtained by measuring absorbance at 620 nm with an Angstrom Advanced Inc. (model 752) scientific ultra violet-visible (UV-Vis) spectrophotometer. The pH of the methylene blue solution was kept in its natural form of 4.8±0.3. The adsorption capacity, q_e (mg/g), was determined from a mass balance equation,

$$q_e = \left(\frac{C_o - C_e}{m}\right) x \quad V \qquad (1)$$

where $C_o$and C_e (mg/L) are the initial and equilibrium concentrations, respectively, V (L) is the volume of solution, and m (g) is the mass of the adsorbent.

3. RESULTS AND DISCUSSION

3.1 Adsorbent characterization

Figures 1 and 2 present the FTIR spectrum of $VDZnCl_2$ and VDC adsorbents across a frequency range of 4000-500 cm^{-1}, revealing the surface functional groups. The functional groups contained in $VDZnCl_2$ and VDC revealed that majority of the peaks in both adsorbent materials were comparable, with the exception of a peak at 1551.37 cm^{-1} (Figure 1), which corresponds to C=C stretching vibrations in the aromatic ring of alkenes and is commonly detected in carbonaceous materials like activated carbon (Mkungunugwa et al. 2021). The signals at 3625.27 cm^{-1} and 3605.53 cm^{-1} in the FTIR spectrum of $VDZnCl_2$ and VDC, respectively, correspond to the intermolecular hydrogen bonding of polymeric compounds such as alcohols, phenols, and carboxylic acids, showing the presence of free hydroxyl groups on the carbon surface. C=C stretching vibration of alkenyl, unconjugated ketone, carbonyl, and ester groups has a peak at 2611.08 cm^{-1} (Figure 1) and 1903.27 cm^{-1} (Figure 2).

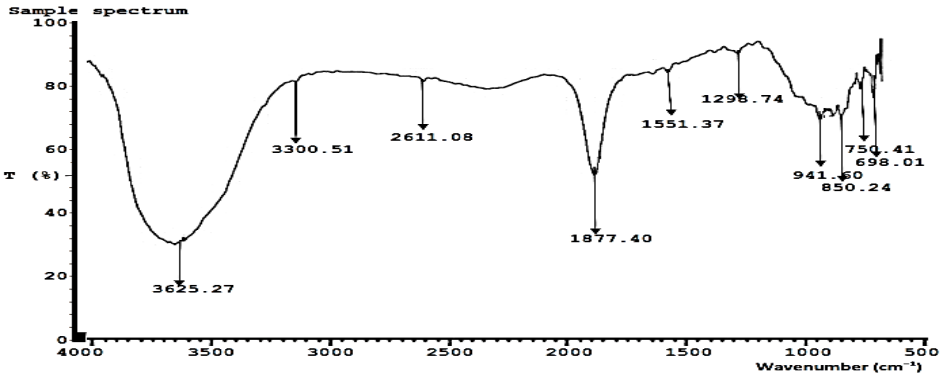

Figure 1: FTIR spectrum of vitex doniana activated carbon treated with zinc chloride ($VDZnCl_2$)

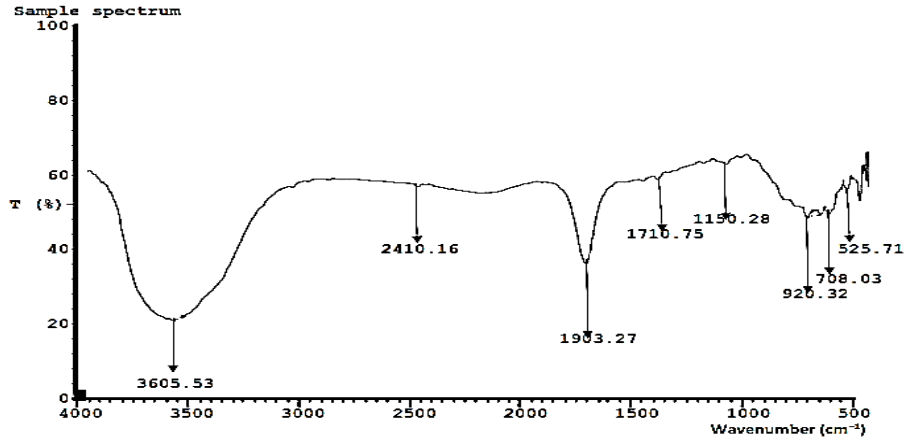

Figure 2: FTIR spectrum of untreated vitex doniana (VDC)

Table 1 presents the textural properties of $VDZnCl_2$ and VDC. The surface area of $VDZnCl_2$ increased dramatically from 14.02 to 933.3 m^2/g. This pattern is consistent with other materials after activation (Gonzalez, 2018; Mistar, Alfatah and Supardan, 2020). Accordingly, the pore volume increased by about three times, from 0.07 to 0.21 cm^3/g. After activation, the pore size increased from 0.92 t0 18.9Å. Therefore, $VDZnCl_2$ will allow for pore fillings of numerous molecules inside its carbon matrix during adsorption (Thommes et al. 2015; Sethia and Sayari, 2016; Mistar, Alfatah and Supardan, 2020).

Table 1: Surface Textural Properties of $VDZnCl_2$ and VDC

BET Parameters	Samples	
	VDC	$VDZnCl_2$
Surface area ($m^2\ g^{-1}$)	14.02	933.3
Pore volume ($cm^3\ g^{-1}$)	0.07	0.21
Pore size (A)	0.92	18.9

DOI: 10.51975/233801010.som
Journal of the Nigerian Society of Chemical Engineers, 38(1), 2023

The SEM result of $VDZnCl_2$ adsorbent material which was characteristics of its surface morphology and texture at ×500 magnification is shown in Figure 3.

Figure 3: $VDZnCl_2$ adsorbent SEM micrograph

The SEM micrograph showed thin plant boundary walls due to modification and the presence of varieties of pores with widened cavities which could be due to the removal of volatile matter and production of fixed carbon after activation (Ohimor, Temisa, and Ononiwu, 2021).

3.2 Equilibrium adsorption isotherm

Figure 4 presents the adsorption isotherm model fittings of methylene blue onto $VDZnCl_2$ when 50 mg of adsorbent was brought into contact with 50 mL of the solution (initial concentration, 1–800 mg/L) at 28°C for 72 h, while the summarized models' constants are presented in Table 2. Until maximum methylene blue adsorption occurred and adsorption equilibrium was reached, there was increased adsorption capacity as the solution concentration increased from 1 to 400 mg/L. This is because active adsorption sites of adsorbent were easily occupied and saturated by adsorbate molecules at low initial concentrations, resulting in low adsorption capacity; meanwhile, at high initial concentrations, a higher fractional adsorbent-adsorbate adsorption ratio occurred which resulted in increased methylene blue adsorption (Luo et al. 2019; Zhao et al. 2022). Meanwhile, nonlinear Langmuir, Freundlich, and Sips isotherm models were used for the validation of the adsorption experimental data. Equations (2), (3), and (4), respectively, define these models., and Microsoft Excel Solver 2019 was used to solve the model equations through non-linear regression.

$$q_e = \frac{Q_m K_L C_e}{1 + K_L C_e} \quad (2)$$

$$q_e = K_F C_e^{\frac{1}{n}} \quad (3)$$

$$q_e = \frac{Q_m (K_S C_e)^{ns}}{1 + (K_S C_e)^{ns}} \quad (4)$$

where q_e (mg/g) is the amount of dye removed by the adsorbent, C_e (mg/L) is the equilibrium dye concentration in solution, K_L (L/mg) is the Langmuir equilibrium constant, Q_m (mg/g) is the maximal monolayer adsorption capacity. The Freundlich adsorption constant of adsorption capacity and the frequency of surface heterogeneity are defined as K_F (mg/g)(L/mg)$^{1/n}$ and *1/n*, respectively. Sips constant is K_S (L/mg), and surface heterogeneity is *ns*. The Langmuir isotherm model assumes a one-molecule thick adsorbed layer and sorbate removal at defined and definite sites with no lateral or steric interference. Only low concentrations and multilayer adsorption are covered by Freundlich isotherm model (Fosso-Kankeu et al., 2014; Vhahangwele and Mugera, 2015). Sips isotherm model combines Langmuir and Freundlich models in forecasting heterogeneous surface adsorption (Elmorsi 2011; Chen, 2012).

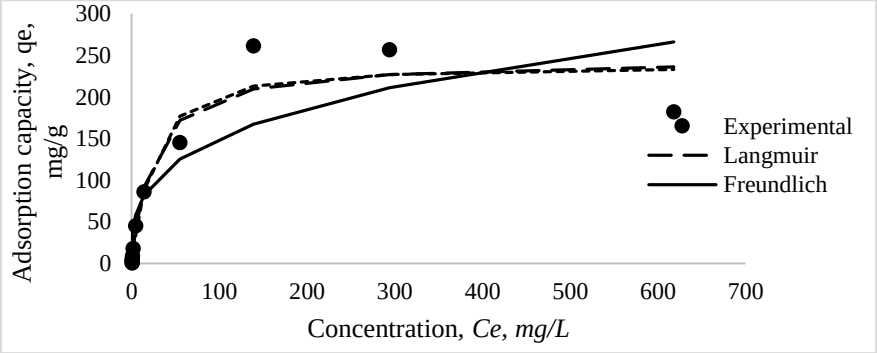

Figure 4: Equilibrium curve of methylene blue adsorption (Lines and isotherm models)

Table 2: Parameters of Isotherm Models for Methylene Blue Adsorption on $VDZnCl_2$

Isotherm model	Parameters	Adsorbent ($VDZnCl_2$)
Langmuir	$Q_m\ (mg/g)$	244.901
	$K_L\ (L/mg)$	0.043
	R^2	0.936
	R_L	0.087
	SSE	7240.47
Freundlich	$K_f\ (mg/g)(L/mg)^{1/n}$	35. 988
	$1/n$	0.311
	R^2	0.813
	SSE	22663.4
Sips	$Q_m\ (mg/g)$	237.631
	$K_s\ (L/mg$	0.046
	n_s	1.168
	R^2	0.938
	SSE	7016.14

Both the Langmuir and Sips models fit the experimental data well; However, the Sips isotherm model fit better due to its closeness to the experimental data under experimental conditions (Figure 4), its highest regression coefficient (R^2) value of 0.938, and least error function (SSE) value of 7016.14. (Table 2). As a result, the Sips model best described this adsorption behavior at equilibrium, implying a heterogeneous methylene blue adsorption process onto $VDZnCl_2$ involving pore filling and ionic interaction (Kumar et al., 2010; Luo et al. 2019; Mistar, Alfatah and Supardan, 2020). Maximum adsorption capacity (Q_m) of methylene blue was, 238 mg/g.

3.4 Comparison of various adsorbents capacity for methylene blue

Comparison of the equilibrium adsorption capacities of various adsorbents to that used in this study are presented in Tables 4. The highest adsorption capacity of methylene blue as predicted by Sips model is 238 mg/g. However, adsorbent such as hazelnut activated carbon (Karacet, Sezen and Mustafa, 2014) presented higher adsorption performance than $VDZnCl_2$ due to its higher specific surface area. Meanwhile, that was not the case for other adsorbents (Moosa, Ridha and Kadim, 2016; Islam et al. 2017; Marrakchi et al. 2017a). Methylene blue adsorption is a complex process which rely on adsorbent and adsorbate physicochemical properties, pH, concentration, adsorbent dosage, temperature etc. (Mistar, Alfatah and Supardan, 2020; Mkungunugwa et al. 2021).

Table 4: Comparison of Methylene Blue Adsorption by different Adsorbents Materials

Adsorbent	Surface area (m^2/g)	Adsorbent dosage (mg)	C_o (mg/L)	Ph	Temp. (^oC)	Q_m (mg/g)	Reference
$VDZnCl_2$	933.25	50	1-800	4.8±0.3	28	244.9	This study
Hazelnut activated carbon	1369	50	50-800	7	25	476	Karacet, Sezen and Mustafa, (2014)
Activated carbon-clay composite	355	-	-	8.5	-	179	Marrakchi *et al.* (2017a)
Steam-activated lantana camara stem carbon	-	500	50	-	20	19.8	Amuda *et al*. (2014)
Fishery waste-based activated carbon	1867	-	-	11	-	184	Marrakchi, Bouaziz, and Hameed,. (2017b)
Chitosan/granulated activated carbon	795	800	20-200	7	25	12.0	Moosa, Ridha and Kadim, (2016)
Pongamia pinnata hulls-based activated carbon	828.30	-	-	7	-	239.4	Islam *et al*. (2017)

4. CONCLUSIONS

Zinc chloride modified activated carbon adsorbent ($VDZnCl_2$) was synthesized from *vitex doniana* (black plum) seed for methylene blue removal from simulated wastewater. The textural properties and functional group of $VDZnCl_2$ revealed increased surface area from 14.02 to 933.25 m^2/g and porosity, and the inclusion of O—H group and a characteristics C=C group commonly found in carbonaceous materials, respectively. Adsorption study showed increased removal of methylene blue as concentration increased from 1 to 800 mg/L until equilibrium was attained. Sips isotherm model had the best fittings with the equilibrium data. However, the maximum adsorption capacity was 244.90 mg/g.

ACKNOWLEDGEMENT

We wish to acknowledge the support made by our 2022 project students and the department of Chemical Engineering laboratory of Auchi Polytechnic.

REFERENCES

Afshin, S., Rashtbari, Y., Shirmardi, M., Vosoughi, M. and Hamzehzadeh, A. (2019). Adsorption of basic violet 16 dye from aqueous solution onto mucilaginous seeds of Salvia sclarea: kinetics and isotherms studies. *Desalination and Water Treatment*, 161, pp. 365–375.

Alipour, M., Vosoughi, M., Mokhtari, S. A., Sadeghi, H., Rashtbari, Y., Shirmardi, M. and Azad, R. (2021). Optimising the basic violet 16 adsorption from aqueous solutions by magnetic graphene oxide using the response surface model based on the Box–Behnken design. *International Journal of Environmental Analytical Chemistry*, *101*(6), pp. 758-777.

Ameh, P. O., Odoh, R. and Oluwaseye, A. (2012). Equilibrium study on the adsorption of Zn(II) and Pb(II) ions from aqueous solution onto *vitex doniana* nut. *International Journal of Modern Chemistry*, 3(2), pp. 82-97

Amuda, O. S., Olayiwola, A. O., Alade, A. O., Farombi, A. G. and Adebisi, S. A. (2014). Adsorption of methylene blue from aqueous solution using steam-activated carbon produced from lantana camara stem. *Journal of Environmental Protection*, 5, pp. 1352-1363.

Aslam, S., Zeng, J., Subhan, F., Li, M., Lyu, F., Li, Y. and Yan, Z. (2017). In-situ one-step synthesis of Fe_3O_4 @ MIL-100 (Fe) core-shells for adsorption of methylene blue from water. *Journal of Colloid and Interface Science*, 505, pp. 186–95.

Asokogene, F. O., Muhammad, A. A. Z., Misau, M. I., Surajudeen, A. and El-Nafaty, A. U. (2019). Methylene Blue Adsorption onto Neem Leave/Chitosan Aggregates: Isotherm, Kinetics and thermodynamics Studies. *International Journal of Chemical Reactor Engineering*, pp. 1–16.

Chen, C. (2012). Evaluation of equilibrium sorption isotherm equations. *Chemical Engineering Journal*, 7 (1), pp. 24–44.

Djilani, C., Zaghdoudi, R., Djazi, F., Bouchekima, B., Lallam, A., Modarressi, A. and Rogalski, M. (2015). Adsorption of dyes on activated carbon prepared from apricot stones and commercial activated carbon. *Journal of Taiwan Institute of Chemical Engineering*, 53, pp. 112–121.

Elmorsi, T. M. (2011). Equilibrium isotherms and kinetics studies of removal of methylene blue dye by adsorption onto Miswak leaves as a natural adsorbent. *Journal of Environmental Protection*, 2 (6), pp. 817–827.

Ertugay, N., and Acar, F.N. (2017). Removal of COD and color from direct blue 71 azo dye wastewater by fenton's oxidation: kinetic study." *Arabian Journal of Chemistry*, 10, pp. 1158–1163.

Fosso-Kankeu, E., Reitz, M. and Waanders, F. (2014). Selective adsorption of heavy and light metals by natural zeolites. *6th International Conference on Green Technology, Renewable Energy and Environmental Engineering, Cape Town* (SA), pp. 167–170.

Kapooria, R. G. and Aime, M. C. (2005). Report of oliver scitula on *vitex doniana* in Zambia. *Africa Journal of Science and Technology*, 3, pp. 57–60.

Karacet, G., Sezen, S. and Mustafa, I. (2014). Adsorption of methylene blue from aqueous solutions by activated carbon prepared from Hazelnut husk using zinc chloride. *Journal of Analytical and Applied Pyrolysis*, 110, pp. 270–276.

González, P. G. (2018). Activated carbon from lignocellulosics precursors: a review of the synthesis methods, characterization techniques and applications. *Renewable and Sustainable Energy Rev.*, 82(1), pp. 1393–1414.

Imran, M., Islam, A. U., Tariq, M. A., Siddique, M. H., Shah, N. S., Khan, Z. U. H., Amjad, M., Din, S. U., Shah, G. M., Naeem, M. A., Nadeem, M., Nawaz, M. and Rizwan, M. (2019). Synthesis of magnetite-based nanocomposites for effective removal of brilliant green dye from wastewater. *Environmental Science and Pollution Research*, 26 (24), pp. 24489–24502.

Islam, M. A, Sabar S, Benhouria A, Khanday, W. A, Asif M. and Hameed, B. H. (2017). Nanoporous activated carbon prepared from karanj (pongamia pinnata) fruit hulls for methylene blue adsorption. *Journal of the Taiwan Institute of Chemical Engineers*, 74, pp. 96–104.

Iqbal, M., Abbas M., Nisar J., Nazir A. and Qamar A. (2019). Bioassays based on higher plants as excellent dosimeters for ecotoxicity monitoring: A review. *Chemistry International*, 5(1), pp. 1–80.

Jaria, G., Calisto, V., Gil, M. V., Otero, M. and Esteves, V. I. (2015). Removal of fluoxetine from water by adsorbent materials produced from paper mill sludge. *Journal of Colloid and Interface Science*, 448, pp. 32–40.

Khadiran, T., Hussein, M. Z., Zainal, Z. and Rusli, R. (2015). Textural and chemical properties of activated carbon prepared from tropical peat soil by chemical activation method. *BioResources*, 10(1), pp. 986–1007.

Kumar, P. S., Ramalingam, S., Senthamarai, C., Niranjanaa, M., Vijayalakshmi, P. and Sivanesan, S. (2010). Adsorption of dye from aqueous solution by cashew nut shell: studies on equilibrium isotherm, kinetics and thermodynamics of interactions. *Journal of Desalination*, 261, pp. 52-60

Li, W., Ma, T., Zhang, R., Tian, Y. and Qiao, Y. (2015). Preparation of porous carbons with high and low pressure CO_2 uptake by KOH activation of rice husk char *Fuel*, 139, pp. 68–70.

Luo, L., Wu, X., Li, Z., Zhou, Y., Chen, T., Fan, M. and Zhao, W. (2019). Synthesis of activated carbon from biowaste of fir bark for methylene blue removal. *Royal Society Open Science*, 6(190523), pp. 1-14

Marrakchi F, Auta M, Khanday W. A and Hameed B. H. (2017b). High-surface-area and nitrogen-rich mesoporous carbon material from fishery waste for effective adsorption of methylene blue. *Powder Technology*, 321, pp. 428-434.

Marrakchi, F, Bouaziz, M and Hameed, B. H. (2017a). Activated carbon-clay composite as an effective adsorbent from the spent bleaching sorbent of olive pomace oil: Process optimization and adsorption of acid blue 29 and methylene blue. *Chemical Engineering Research and Design*, 128, pp. 221-230.

Mistar, E. M., Alfatah, T. and Supardan, M. D. (2020). Synthesis and characterization of activated carbon from bambusa vulgaris striata using two-step KOH activation. *Journal of Materials Research and Technology*, 9(3), pp. 6278-6286.

Miyah, Y., M. Idrissi, and Zerrouq, F. (2015). Study and modeling of kinetics methylene blue adsorption on the clay adsorbents (pyrophillite, calcite). *Journal of Materials and Environmental Sciences*, 6(3), pp. 699-712

Miyah, Y., A. Lahrichi, Idrissi, M., Khalil, A. and Zerrouq, F. (2018). Adsorption of methylene blue from aqueous solutions onto walnut shells powder: equilibrium and kinetic studies. *Surfaces and Interfaces*, 11, pp. 74-81

Mkungunugwa, T., Manhokwe, S., Chawafambira, A. and Shumba, M. (2021). Synthesis and characterisation of activated carbon obtained from Marula (sclerocarya birrea) nutshell. *Journal of Chemistry.*

Moosa, A. A., Ridha, A. M. and Kadim, N. A. (2016). Use of biopolymer adsorbent in the removal of phenol from aqueous solution. *American Journal of Materials Science*, 6(4), pp. 95-104.

Naushad, M., Alqadami, A. A., AlOthman, Z. A., Alsohaimi, I. H., Algamdi, M. S. and Aldawsari, A. M. (2019). Adsorption kinetics, isotherm and reusability studies for the removal of cationic dye from aqueous medium using arginine modified activated carbon. *Journal of Molecular Liquids*, 293, pp. 111442.

Nowicki P. (2016). Effect of heat treatment on the physicochemical properties of nitrogen enriched activated carbons. *Journal of Thermal Analysis and Calorimetry*, 125(3), pp. 1017-1024.

Ohimor, E. O., Temisa, D. O. and Ononiwu, P. I. (2021). Production of activated carbon from carbonaceous agricultural waste material: coconut fibres. *Nigerian Journal of Technology*, *40*(1), pp. 19-24.

Okman, I., Selhan, K., Tay, T. and Erdem, M. (2014). Activated carbons from grape seeds by chemical activation with potassium carbonate and potassium hydroxide. *Applied Surface Science*, 293, pp. 138-142.

Pandey, S., Do, J. Y., Kim, J. and Kang, M. (2020). Fast and highly efficient catalytic degradation of dyes using κ-carrageenan stabilized silver nanoparticles nanocatalyst. *Carbohydrate Polymers*, 230, pp. 115597.

Piriya, R. S., Jayabalakrishnan, R. M., Maheswari, M., Boomiraj, K. and Oumabady, S. (2021). Coconut shell derived $ZnCl_2$ activated carbon for malachite green dye removal. *Water Science & Technology*, pp 1-16

Rangabhashiyam, S. and Selvaraju, N. (2015). Adsorptive remediation of hexavalent chromium from synthetic wastewater by a natural and $ZnCl_2$ activated Sterculia guttata shell. *Journal of Molecular Liquids*, 207, pp. 39-49.

Sethia, G. and Sayari A. (2021). Activated carbon with optimum pore size distribution for hydrogen storage. *Nigerian Journal of Technology* 40 (1), pp. 19–24.

Singh, G., Kim, I. Y., Lakhi, K. S, Srivastava, P., Naidu, R. and Vinu, A. (2017). Single step synthesis of activated bio-carbons with a high surface area and their excellent CO_2 adsorption capacity. *Carbon*, 116, pp. 448–455.

Thakur, S., Pandey, S. and Arotiba, O. A. (2016). Development of a sodium alginate-based organic/inorganic superabsorbent composite hydrogel for adsorption of methylene blue. *Carbohydrate Polymers*, 153, pp. 34-46.

Thommes, M., Kaneko, K., Neimark, A. V., Olivier, J. P., Reinoso, F. R., Rouquerol, J. et al. (2015). Physisorption of gases, with special reference to the evaluation of surface area and pore size distribution (IUPAC Technical Report). *Pure and Applied Chemistry*, 87, pp. 1051–1069.

Vhahangwele, M. and Mugera, G. W. (2015). The potential of ball-milled South African bentonite clay for attenuation of heavy metals from acidic wastewater: simultaneous sorption of CO^{2+}, Cu^{2+}, Ni^{2+}, Pb^{2+} and Zn^{2+} ions. *Journal of Environmental Chemical Engineering*, 3 (4), pp. 2416–2425.

Wang, F., Zhang, L., Wang, Y., Liu, X., Rohani, S. and Lu, J. (2017). Fe_3O_4 @ SiO_2 @ CS-TETA functionalized graphene oxide for the adsorption of methylene blue (MB) and Cu(II). *Applied Surface Science*, 420, pp. 970–981.

Yusuf, J., Muhammed, M. and Grace, B.T. (2020). Preparation of activated carbon from syzygiumcumini seed for the removal of chromium (II) ion from aqueous solution. *Bayero Journal of Pure and Applied Sciences*, 13(1), pp. 158 - 163

Zaini, M. A. A., Shu-Hui, T., Lin-Zhi, L. and Alias, N., (2016). Fate of chemical activators in the aqueous environment: What should we do about it? *Aceh International Journal of Science and Technology*, 5(1), pp. 18-20.

Zhang, S., Zhu, S., Zhang, H., Liu, X. and Xiong, Y. (2020). Synthesis and characterization of rice husk-based magnetic porous carbon by pyrolysis of pretreated rice husk with $FeCl_3$ and $ZnCl_2$. *Journal of Analytical and Applied Pyrolysis*, 147, pp. 104806.

Zhao, H., Zhong, H., Jiang, Y., Li, H., Tang, P., Li, D. and Feng, Y. (2022). Porous $ZnCl_2$-activated carbon from Shaddock peel: methylene blue adsorption behavior. *Materials*, 15(895), pp. 1-16

Zhao, W., Luo, Lu., Wang, H. and Fan, M. (2017). Synthesis of bamboo-based activated carbons with super-high specific surface area for hydrogen storage. *Bioresources*, 12, pp. 1246–1262.

Zhao, W., Luo, L., Chen, T., Li, Z., Zhang, Z. and Fan, M. (2018). Activated carbons from oil palm shell for hydrogen storage. *Material Science Engineering*, 368, pp. 012031.

Zhu, X., Wang, P., Peng, C., Yang, J. and Yan, X., (2014). Activated carbon produced from paulownia sawdust for high-performance CO_2 sorbents. *Chin. Chem. Lett.*, 25, pp. 929–932.

DOI: 10.51975/233801011.som
Journal of the Nigerian Society of Chemical Engineers, 38(1), 2023

ASSESSMENT OF AFRICAN STAR APPLE (*CHRYSOPHYLLUM ALBIDUM*) FRUIT PULP AS A POTENTIAL FEEDSTOCK FOR BIOETHANOL PRODUCTION

***Ogbodo, N. J.[1], Esonye, C.[1] and Omotioma, M.[2]**
1 Department of Chemical Engineering, Alex Ekwueme Federal University,
Ndufu-Alike (AE-FUNAI), Ebonyi State, Nigeria.
2 Department of Chemical Engineering, Enugu State University of Science and Technology (ESUT),
Enugu State, Nigeria

Corresponding Author: nkirukaogbodo@yahoo.com

ABSTRACT

This study focused on production of bioethanol from ripped African star apple (Chrysophyllum albidum) pulp through hydrolysis and fermentation processes. The present work determines the potentials of African Star apple fruit pulp as a precursor for bioethanol production. The pre-treated African star apple fruit pulp was characterized by proximate analysis and Fourier transform infrared (FTIR) spectroscopic analysis. Diluted sulphuric acid was used to hydrolyse the dried pulp and the corresponding substrate was fermented under various conditions. Yeast was added which provided enzymes for the conversion of the glucose into ethanol. Effects of pH, yeast dosage, incubation temperature and fermentation time on the ethanol yield were determined. The fermentation process was optimized using Response Surface Methodology. The analysis showed that African star apple fruit pulp contains 54.97% carbohydrate. Predominant functional groups of the sample include; N-H stretch, O-H stretch, C≡C stretch, C-H out of plane, C=O stretch, N-H deforming, S=O stretch, N=O stretch and C-F stretch. The optimum ethanol yield of 9.89g/cm^3 was obtained at pH of 5, yeast dosage of 4.5 %wt/v, incubation temperature of 35^{o}C and fermentation time of 72 hrs. A quadratic model adequately described the relationship between the ethanol yield and the production process parameters.

***Keywords**: Bioethanol, African star apple, Chrysophyllum albidum hydrolysis, fermentation*

1.0 INTRODUCTION

Exploration for alternative source of energy is on the increase with the intention to overcome the challenges of over dependent on fossil fuel. It has been established that one of the ways to reduce energy insecurity and environmental pressure is by diversifying energy sources, hence research efforts are being made to generate biofuels from biomass. Biomass-based fuels (biofuels) are eco-friendly fuels derived from plant biomass and they are seen as a potential way to reduce energy insecurity and environmental pressure as well as diversifying transportation energy sources (Vertes et al., 2009; Kuhad et al., 2011). In recent times, bioethanol has recently attracted enormous attention in different countries throughout the world as the most promising biofuel for transportation, hence increasing research and development efforts have been conducted on the commercial production of bioethanol due to the global demand to reduce oil importation, thereby contributing towards boosting rural economies and improving air quality (Demirbas and Karslioglu, 2007). Accordingly, recent research works are concentrated on renewable energy from crops with lignocellulosic residues for bioethanol production (*Naik* et al., 2010; Oiwoh et al., 2018) because their availability and easy conversion into bioenergy is feasible without high capital investments.

Bioethanol(ethanol) is a biofuel made by microbial fermentation, mostly from carbohydrates rich in sugar or starch-bearing plants such as corn, sugarcane, sweet sorghum or lignocellulosic biomass and more recently from microalgae (Anyanwu et al., 2022). It is biodegradable, less toxic and oxygenated (35% oxygen). Thus, it provides the possibility of reducing automobile greenhouse gas emissions (generated in fossil fuel combustion) and lessening dependence on petrol diesel (Hahn-Hagerda et al., 2006; Farrell et al., 2006; *Zhang and Smith, 2007*; Ibeto et al., 2011; Ye et al., 2017). Numerous biomass resources have been investigated for bioethanol production such as: sugar juice, starchy crops, and lingocellulosic biomass (Balat, 2009; *Randor et al., 2010;* Summoogum et al., 2015; Silva et al., 2017). They

are broadly classified into: a) first generation, which involves the use of sugarcane, sugar beet, wheat, fruits, corn, potato, rice, sweet potato or barley (Cheng et al., 2007; Abdulkareem et al., 2015; Elemike et al., 2015); b) second generation, which involves lingo-cellulosic biomass (Segui et al., 2018); c) third generation comes from micro and micro algae biomass (Kumar et al,, 2018).

Bioethanol production involves a fermentation process that transforms carbohydrates into ethanol and among the second generation bioenergy crops used for bioethanol production, agricultural wastes and over ripped fruits such as African star apple (*Chrysophyllum albidum*) comprise up to 50% of agricultural production (Lafond, 2009), Citrus processing industry uses mainly citrus peel as their major solid by-product which comprises around 50% of the fresh fruit weight and can be utilized as substrate for bioethanol production (Alemayehu, 2014). Ethanol as a grain alcohol can be blended with gasoline and used in regular motor vehicles at a concentration of up to 10 percent. Gasoline- ethanol blended fuel reduces production energy and total greenhouse gas emission hence total hydrocarbon and nitrogen oxide emissions are decreased up to 34.5% - 35.6% with increased oxygenated fuel. This is one of the best tools to fight vehicular pollution, as it contains 35% oxygen that helps in the complete combustion of fuel which reduces harmful tailpipe emissions (Lee & Park, 2020; Khan, 2013).

Previously, production of bioethanol from some agro-based products such as African star apple (*Chrysophyllum albidum*) has not been fully explored. African star apple is from the *Sapotaceae* family, an order of *Ericales* (Adekanmi and Olowofoyeku, 2020). The family comprises seventy (70) genera and eight hundred (800) species. Nigeria has seven of the species which includes *albidum* and *africanum* which are widely found within the country (Omotioma et al., 2013; Bello et al., 2015). In Nigeria, the common name for African star apple includes *cherry, agbalumo* (Yoruba), *udara* (Ibo) and *ehya* (Igala) (Akubor et al., 2013). The ripe fruits are mostly available in the market between the periods of December and April every year. Amusa et al., (2003) reported that the deterioration of fruit pulp begins after about five days under ambient conditions and this leads to loss of huge amount of the fruits yearly during gathering, transportation and storage. Significantly, different parts of the *Chrysophyllum albidum* tree serve a number of important uses; the wood can be used to produce charcoal, the seed oil has proven to be a good precursor for industrial biodiesel production (Onukwuli et al., 2021), its pulp contains high amount of sugar that can be valorized for the production of a product with high added value such as bioethanol and the leaves are used for medicinal purpose (Odugbemi et al., 2007), hence the improved variety can strive in any agricultural sector if properly harnessed. Despite its multipurpose character, this species remains underutilized in the country and consequently, there is need to use over-ripen African star apple as raw materials for fermentation, enzymatic hydrolysis using microbial enzymes which could be a possible solution to reduce the input costs in bioethanol production (Hammond, et al., 1996). Mostly, for the production of bioethanol in commercial quantities, baker's yeast (*Saccharomyces cerevisiae*) can be used because of its high ethanol tolerance, rapid fermentation rates, insensitivity to temperature and substrate concentration (Linden, T & Hahn-Hägerdal, 1989).

Previously, Ureigho, (2010), Okwu *et al. (*2018) studied the organoleptic variation of species of African Star Apple fruits in contrast with their proximate parameters. From their research, the fruits have mean values of 73.33, 2.64, 3.61 and 16.99% for the moisture, ash, fibre and protein contents respectively. The seed shell pericarp has higher crude protein of (8.66%) and fat (8.07%) content while the fruit pulp has more carbohydrates (66.45%) and the fruit skin is copious in crude fibre (15.57%) (Aboaba & Olide, 2006; Ibrahim *et al.*, 2017). They also confirmed that the pulp was abundant in protein and carbohydrate content (4.1 and 60.1%). Ylitervo, (2008) used dried orange peels to produce bioethanol by enzymatic hydrolysis with the application of the *Mucor Indicus* fungus, hydrolyzing and converting into sugars, in the bioethanol production by two fermentable sugar process, and obtained a yield of 0.36g/g after 24 hrs. Azevedo, (2007) evaluated the production of bioethanol from the persimmon juice and observed that the factors of the initial concentration of inoculum, soluble solids and initial pH did not influence the alcoholic fermentation of the organic matter. Lima, (2015) in his study presented in terms of efficiency and yield of the process of obtaining cellulosic ethanol by means of alcoholic fermentation of the hydrolyzed liquors with the use of the yeast *Saccharomyces cerevisiae*. These authors obtained maximum yield and efficiency values of 0.445g of ethanol/g of bagasse and 87.1% for the hydrolyzed liquor with the addition of cashew juice. Bello & Henry, (2015) studied the effects of storage on the proximate composition of *Chrysophyllum albidum* under ambient conditions and reported an increase in moisture content and crude fibre in the pulp after 5 days from 36.45 to 46.69% and 2.54 to 2.89% respectively. This result

validates the findings of (Adeboyejo *et al.*, 2019) and suggest that fruits stored at ambient conditions for long loose nutritive value and become softer increasing their susceptibility to deterioration.

In order to harness and add more values to the sugar content of the over ripen African star apple fruit pulp, this research work focused on assessing the potentials of the fruit pulp as a second-generation bioethanol production so as to improve its valorization and evaluate it as a precursor for industrial production of bioethanol. For the possibility of maximizing bioethanol yield and minimizing the cost of bioethanol production, this work further optimized the process parameters such as pH, incubation temperature, fermentation time and yeast dosage. It is important to note that if proper attention is given to the use of African star apple as an alternate biofuel feedstock; it will become economically valuable, the greenhouse gas emissions in the environment and scarcity of fuel will be reduced drastically.

2.0 MATERIALS AND METHODS

2.1 Materials

The materials used in the fermentation of bioethanol include Dried African Star Apple fruit pulp, dilute Sulphuric acid (H_2SO_4), Hydrochloric acid (HCl), Baker's yeast (*Saccharomyces cerevisiae)*, sodium hydroxide. The chemicals used in this study were purchased from a local chemical shop in Enugu, Nigeria and were used without any pre-treatment.

2.2 Sample collection and preparation

The method employed by (Onukwuli et al, 2021) was used for the sample preparation. The over ripped African star apple were collected from local market in Ugwogo Nike, Enugu state of Nigeria and were washed to remove dirt and sand, the fruit pulps were carefully peeled to remove the seeds. The pulps were cut and chopped into the small slice. The pulps were air dried for seven (7) days to reduce the moisture content and to promote effective grinding with electric grinding machine into smaller particles before being sieved to obtain a finer particle size of 400µm. The residual moisture in the sieved grounded fruit pulp was removed by further sun drying for a period of five (5) days and stored in an air tight container until use.

Figure 1a: African Star Apple Fruit pulp and seed.

Figure 1b: African Star Apple Tree.

2.2.1 Determination of Moisture Content

Association of Official Analytical Chemist (AOAC method, 1990) was used for the proximate analysis of

the sample. For determination of moisture content, 5g of the sample was placed into weighed crucibles and then put inside the oven set at 105^{o}C for 4 hrs. The sample was removed from the oven, cooled and weighed. The drying continued until a constant weight was noticed. Then, the moisture content was calculated using Equation (1).

$$\% \text{ moisture} = \frac{A-B}{A} \times \frac{100}{1} \quad (1)$$

where A is the original weight of sample while B is the weight of dried sample.

Standard method (Kjeldahl method) was used in determination of the crude protein content. This method involves the estimation of the total nitrogen in the waste and the conversion of the nitrogen to protein with the assumption that all the protein in the sample is present as nitrogen. Using a conversion factor of 6.25, the actual percentage of protein in the sample was calculated using

% crude protein = % Nitrogen x 6.25

Titration was carried out using 0.01M standard HCl to first pink colour.

$$\% \text{ Nitrogen} = \frac{Titration\ vol. \times 0.014 \times M \times 100x\ 100}{wt.ofsample \quad 10} \quad (2)$$

where M is the molarity of standard HCl.

2.2.2 Determination of Crude Fibre Content

5g of the sample was weighed into a 500ml beaker and 150ml of preheated 0.128M H_2SO_4 was added to it. It was heated at 70°C for 30 minutes, filtered and washed with hot distilled water. The residue was then transferred to a beaker and was place in a heating mantle at 70°C for 30 minutes with 150ml of preheated 0.223M KOH. It was filtered and washed with hot water until the washings are no longer alkaline. The residue was washed three times with acetone and dried in an oven at 105°C for 1.5 hrs. It was then cooled in a desiccator, weighed and heated in a muffle furnace at 500°C for 4 hours. The ash obtained was cooled in a desiccator and weighed.

$$\% \text{ Crude fibre} = \frac{W_2 - W_3}{W_1} \times \frac{100}{1} \quad (3)$$

where W_1 is the weight of sample, W_2 is the weight of dry residue and W_3 is the Weight of ash.

For the determination of fat content, 5g of the ground sample was transferred into a rolled filter paper and then placed inside the extraction thimble. The thimble was placed inside the extractor. 180 ml of petroleum ether was poured inside the extraction flask. The condenser and the flask were connected to the extractor. The whole unit was placed on a heating mantle for 3 hrs after which the petroleum ether was recovered. The oil collected in the flask was dried in an oven at 105°C. It was then weighed and the percentage fat calculated using Equation (4):

$$\% \text{ fat} = \frac{C - A}{B} \times \frac{100}{1} \quad (4)$$

C is weight of flask + oil, A is weight of empty flask and B is weight of original sample.

In the determination of ash content of the sample, 5 g of the finely ground sample was weighed into porcelain crucibles which have been washed, dried in an oven at 100°C, cooled in a desiccator and weighed. It was then placed inside a muffle furnace and heated at 600°C for 3 hrs. It was then removed and cooled in a desiccator and weighed. The ash content was determined using Equation (5):

$$\% \text{ Ash} = \frac{A - B}{C} \times \frac{100}{1} \quad (5)$$

where A is the weight of crucible + ash, B is weight of crucible and C is the weight of original sample.

Total carbohydrate content was calculated Equation (6):

Total carbohydrate =100- (protein + fat + crude fiber +ash + water) (6)

2.3 Determination of the functional groups

Fourier transform infrared (FTIR) spectrophotometer (Cary 630, Agilent Technologies USA) was used to determine the functional groups of the African star apple fruit pulp. FTIR spectra were collected in transmission mode using the Br pellet method. In the process, Fourier transform converted raw data into actual spectrum (with various peaks). Analysis of the FTIR produced peaks were carried out so as to identify the appropriate functional groups (Onukwuli and Omotioma, 2016).

2.4 Experimental Design and Statistical Analysis

A standard response surface methodology (RSM) design using central composite design (CCD) was applied to develop the standard combinations of the process conditions for maximum yield of bioethanol from the African star apple fruit pulp. The three levels, four factors process conditions used for the optimisation are as follows:− Ph level: 4.0, 5.0 & 6.0; Incubation temperature, °C: 25, 35 & 45; Fermentation time, hrs: 24, 72 & 120; Yeast dosage, %w/v: 3.5, 4.5 & 5.5.

2.5 Bioethanol production and Characterization

Bioethanol was produced from African star apple fruit pulp by acid hydrolysis and enzymatic fermentation process. 15g of dry sample of African star apple fruit pulp was weighed into 250 ml conical flask. 200ml of 5% dilute sulphuric acid (H_2SO_4) was used to hydrolyse the samples. The flask was covered with cotton wool and wrapped with aluminium foil, and then heated at 50°C for

30 minutes. The sample was allowed to cool and filtered using whatman 42 filter paper. The pH value of the sample was adjusted with sodium hydroxide before addition of yeast to the hydrolysed sample. Baker's yeast (*Saccharomyces cerevisiae*) dosage was added to the flask containing the sample and stirred thoroughly. The substrate was fermented under various conditions. Effects of pH, yeast dosage, incubation temperature and fermentation time on the ethanol yield were determined. The added yeast provided enzymes (invertaze and zymaze) for the conversion of the sample into ethanol and carbon dioxide. The bioethanol yield was optimized using response surface methodology (RSM). In designing the experiment, central composite design tool of design expert software as used by Omotioma and Onukwuli (2015) was employed. At the end of fermentation, the produced bioethanol was distilled out at 78 ºC. The bioethanol was characterized to ascertain its properties in terms of specific gravity, flash and smoke points, viscosity, refractive index, cloud and pour points and sulphur.

3.0 RESULTS AND DISCUSSIONS

3.1 Characterisation of the Samples

3.1.1 Proximate Analysis

Results of proximate analysis of the sample are presented in Table 1. For the analysis, 20g of star apple fruit pulp was used. The moisture content of the dried African star apple fruit pulp was within the acceptable limit of not more than 10% for long term storage of flour (Akubor et al, 2013; Onimawo and Akubor, 2012). The low moisture content would enhance its storage stability by preventing mould growth and reducing moisture dependent biochemical reactions (Onimawo and Aklubor, 2012). It contains 54.97% carbohydrate which is close to the value of 60.01% obtained by (Asare et al, 2015). Crude fibre content of 6.03 is higher than that recorded by Bello et al (2015). Ash content of 5.12% was recorded, which indicates high mineral content of the African star apple fruit pulp.

Table 1. Proximate analysis of African star apple fruit pulp.

Composition (%)	Values
Ash	5.12
Crude fat	15.43
Crude fibre	6.03
Moisture content	7.85
Protein	10.6
Carbohydrate	54.97

3.2 Fourier transform infrared (FTIR) spectroscopy

The functional groups present in the sample of African star apple as determined by the use of FTIR spectrometer and the spectrum of the sample as determined by Fourier transform infrared spectroscopy is presented in Figure 1. The peaks as represented in brackets shows the functional groups of the sample (Onukwuli and Omotioma, 2016). The predominant functional groups of the African star apple fruit pulp as shown in Figure 1 confirms the presence of N-H (3295.0) stretch, O-H(2922.2) stretch, C≡C(2109.7) stretch, C-H(1990.4) out of plane, C=O(1729.5)stretch, N-H(1617.7) deforming, S=O(1375.4) stretch, N=O((1244.9) stretch and C-F(1025.0) stretch. Presence of the heteroatoms portrays that the African star apple fruit pulp is a potential source of bioethanol.

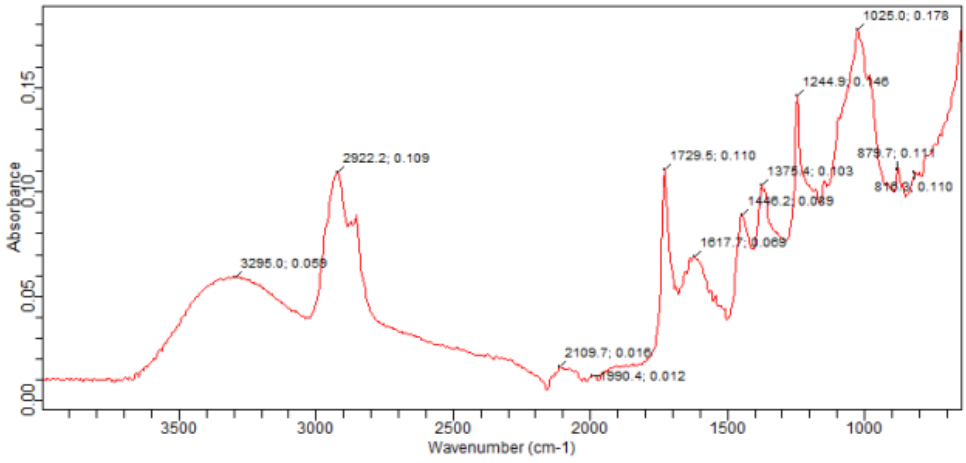

Figure 1: Spectrum of the functional groups of African star apple pulp

3.3 Characteristics of the bioethanol

Experimental values of various properties of produced bioethanol according to American Society for Testing and Materials standards (ASTM) methods using standard apparatus for the measurement are shown in Table 2.

The refractive index of the bioethanol produced indicates that the refractive index of the produced ethanol is 1.352 which is a little lower than the set limit of 1.36. The essence of measuring the refractive index of fuels is to verify the purity of the fuels, it can be deduced from the results obtained that the ethanol produced is pure bioethanol. Flash point is described as the lowest temperature at which the ethanol will ignite when exposed to an ignition source. The flash point of the produced bioethanol is 15.30. It is a bit lower compared to the set limit of 18.60, which implies that the bioethanol produced is within the standard bioethanol flammability. Also, ash content of bioethanol produced of 0.2% is within the acceptable limit. Fuels with high sulphur content impact negatively on environment. The bioethanol has sulphur content of 0.01%, which makes the bioethanol suitable for various applications. The specific gravity obtained was 0.858 which corroborates the results obtained in literature for bioethanol produced from fruits.

Table 2. Properties of ethanol produced from African star apple fruit pulp.

Parameters	Values
Refractive index	1.352
Specific gravity	0.858
Flash point (ºC)	15.30
Viscosity (mPas)	1.71
Sulphur content (%)	0.01
Ash content (%)	0.10
Cloud point (ºC)	19
Pour point (ºC)	4.82

3.4 Result of the Response Surface Methodology

The Interactive effects of process variables; pH, yeast dosage, incubation temperature and fermentation time on the ethanol yield are presented in Table 3. Highest value of the ethanol yield was recorded at the mid-points of the process variables. Maximum bioethanol yield occurred at the mid-points of the variables. This is an indication that the interactive effect of the variables on the ethanol yield is in parabolic form (Tripathi, 2018). Further analyses of the data are required for proper interpretation of the data. Such analysis include; analysis of variance, mathematical modeling, graphical analysis and optimization. Ethanol yield of 10.14 g/cm^2 was obtained from African star apple at pH of 5, yeast dosage of 4.5 %wt/v, temperature of 35ºC and fermentation time of 72 hrs.

Table 3. Interactive effects of process variables on the ethanol yield.

Std	Run	Factor 1 A: pH	Factor 2 B: Yeast dosage %wt/v	Factor 3 C: Incubation Temp. ºC	Factor 4 D: Fermentation Time Hr.	Response 1 Ethanol Yield g/cm^3
29	1	5	4.5	35	72	10.14
14	2	6	3.5	45	120	5.71
28	3	5	4.5	35	72	10.14
1	4	4	3.5	25	24	1.75
3	5	4	5.5	25	24	2.34
18	6	6	4.5	35	72	9.53
24	7	5	4.5	35	120	9.92
26	8	5	4.5	35	72	10.14
7	9	4	5.5	45	24	2.64
21	10	5	4.5	25	72	8.93
12	11	6	5.5	25	120	8.95
2	12	6	3.5	25	24	3.32

5	13	4	3.5	45	24	1.78
16	14	6	5.5	45	120	9.93
4	15	6	5.5	25	24	5.86
11	16	4	5.5	25	120	3.09
10	17	6	3.5	25	120	4.61
22	18	5	4.5	45	72	9.86
6	19	6	3.5	45	24	4.21
19	20	5	3.5	35	72	5.74
8	21	6	5.5	45	24	6.63
25	22	5	4.5	35	72	10.14
20	23	5	5.5	35	72	9.63
23	24	5	4.5	35	24	7.41
30	25	5	4.5	35	72	10.14
17	26	4	4.5	35	72	4.96
13	27	4	3.5	45	120	2.19
9	28	4	3.5	25	120	2.55
27	29	5	4.5	35	72	10.14
15	30	4	5.5	45	120	4.25

3.4.1 Fit summary of the model of the ethanol yield

Fit summary of the model of the ethanol yield is presented in Table 4. The experimental data was tested with linear, 2 factor indicators (2FI), quadratic and cubic models. Quadratic model is suggested as best fitted model because the predicted R^2 of 0.9366 is in reasonable agreement with the adjusted R^2 of 0.9748. The difference is less than critical value of 0.2 which is within the acceptable R^2 range for a suitable model.

Table 4. Fit Summary of the Model of the Ethanol Yield.

Source	Sequential p-value	Adjusted R^2	Predicted R^2	Remarks
Linear	**0.0280**	**0.2373**	**0.0661**	
2FI	**0.9834**	**0.0459**	**-1.3251**	
Quadratic	**< 0.0001**	**0.9748**	**0.9366**	**Suggested**
Cubic	**0.1220**	**0.9860**	**0.5571**	**Aliased**

3.4.2 Analysis of Variance (ANOVA) of the Quadratic Model of Ethanol yield

ANOVA of the quadratic model of the ethanol yield is presented in Table 5. The model F-value of 81.26 implies the model is significant. There is only a 0.01% chance that an F-value this large could occur due to noise. P-values less than 0.0500 indicate model terms are significant (Onukwuli and Omotioma, 2016). In this case A, B, C, D, AB, AD, BD, A^2, B^2, D^2 are significant model terms. Adequate precision measures the signal to noise ratio. A ratio greater than 4 is desirable. Ratio of 23.451 indicates an adequate signal. This model can be used to navigate the design space.

Table 5. Analysis of Variance of the Model

Source	Sum of Squares	Df	Mean Square	F-value	p-value	
Model	**292.86**	**14**	**20.92**	**81.26**	**<0.0001**	**Significant**
A-Ph	**61.24**	**1**	**61.24**	**237.87**	**<0.0001**	
B-Yeast dosage	**25.59**	**1**	**25.59**	**99.39**	**<0.0001**	
C-Incubation temperature	**1.87**	**1**	**1.87**	**7.26**	**0.0166**	
D-Fermentation time	**12.94**	**1**	**12.94**	**50.26**	**< 0.0001**	
AB	**5.61**	**1**	**5.61**	**21.77**	**0.0003**	

AD	**1.97**	**1**	**1.97**	**7.64**	**0.0145**
BC	**0.1502**	**1**	**0.1502**	**0.5833**	**0.4569**
BD	**1.41**	**1**	**1.41**	**5.48**	**0.0335**
A^2	**14.82**	**1**	**14.82**	**57.57**	**<0.0001**
B^2	**9.87**	**1**	**9.87**	**38.34**	**<0.0001**
C^2	**0.1513**	**1**	**0.1513**	**0.5878**	**0.4552**
D^2	**2.45**	**1**	**2.45**	**9.50**	**0.0076**
Residual	**3.86**	**15**	**0.2574**		
Lack of Fit	**3.86**	**10**	**0.3861**		
Pure Error	**0.0000**	**5**	**0.0000**		
Cor Total	**296.72**	**29**			
Std. Dev.	**0.5074**	**-**	**R^2**		**0.9870**
Mean	**6.55**	**-**	**Adjusted R^2**		**0.9748**
C.V. %	**7.74**	**-**	**Predicted R^2**		**0.9366**
			Adeq Precision		**23.4507**

3.4.3 Mathematical model of the yield

Model of the ethanol yield (Y) in terms of coded and actual factors are expressed in Figures (7) and (8) respectively. The equation in terms of coded factors can be used to make predictions about the response for given levels of each factor. By default, the high levels of the factors are coded as +1 and the low levels are coded as -1. The coded equation is useful for identifying the relative impact of the factors by comparing the factor coefficients (Omotioma and Onukwuli, 2019). The equation in terms of actual factors can be used to make predictions about the response for given levels of each factor.

$$Y = +9.89 + 1.84A + 1.19B + 0.3222C + 0.8478D + 0.5919AB + 0.3506AD + 0.2969BD - 2.39A^2 - 1.95B^2 - 0.2417C^2 - 0.9717D^2 \quad (7)$$

$$Y = -88.93464 + 22.00080pH + 15.01347Yeast\ dosage + 0.067889Incubation\ temperature + 0.009980Fermentation\ time + 0.591875pH * Yeast\ dosage + 0.007305pH * Fermentation\ time + 0.006185Yeast\ dosage * Fermentation\ time - 2.39167pH^2 - 1.95167Yeast\ dosage^2 - 0.002417Incubation\ temperature^2 - 0.000422Fermentation\ time^2 \quad (8)$$

3.4.4 Graphical RSM result

Predicted versus actual ethanol yield is displayed in Figure 2. The points clustered along the line of best fit, showing that the generated model adequately predicted the experimental data. This assertion is in agreement with the report of Oiwoh et al (2018). 3-D plots of the interactive effects of the variables on the ethanol yield are shown in Figures 3 -8. Each plot showed a parabolic curve, which is typical of quadratic model. Also, optimum ethanol yield of 9.89 g/cm^3 was obtained at pH of 5, yeast dosage of 4.5 %wt/v, incubation temperature of 35^{o}C and fermentation time of 72 hrs. This value competes favourably with the report of Oiwoh et al (2018).

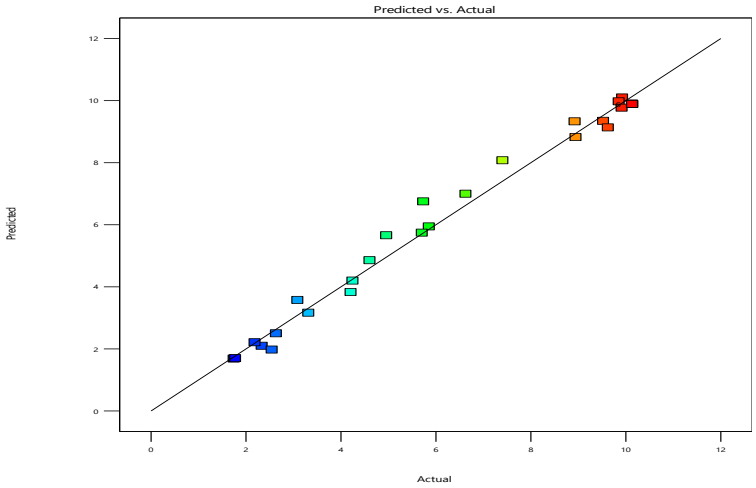

Figure 2: Predicted versus actual ethanol yield

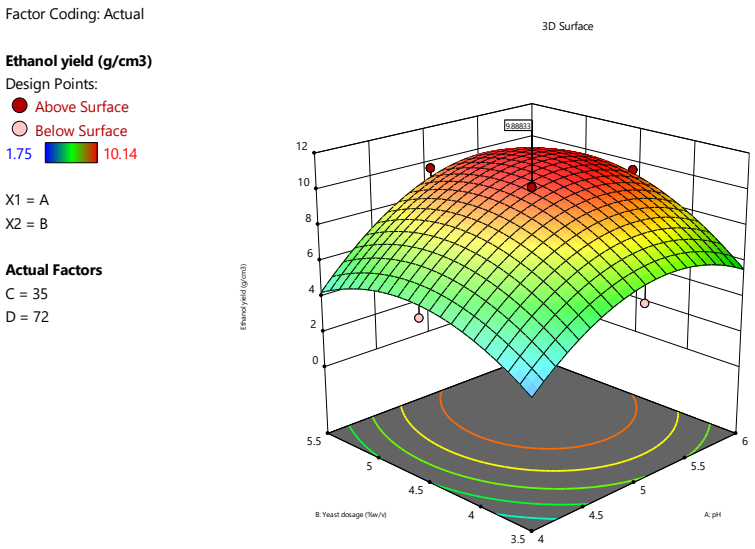

Figure 3: Ethanol yield versus pH and yeast dosage

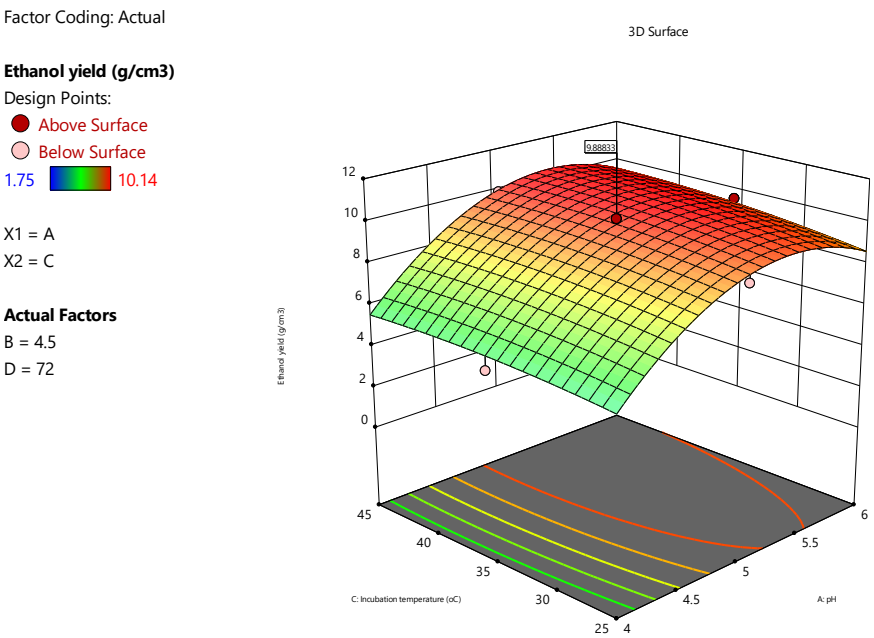

DOI: 10.51975/233801011.som
Journal of the Nigerian Society of Chemical Engineers, 38(1), 2023

Figure 4: Ethanol yield versus pH and incubation temperature

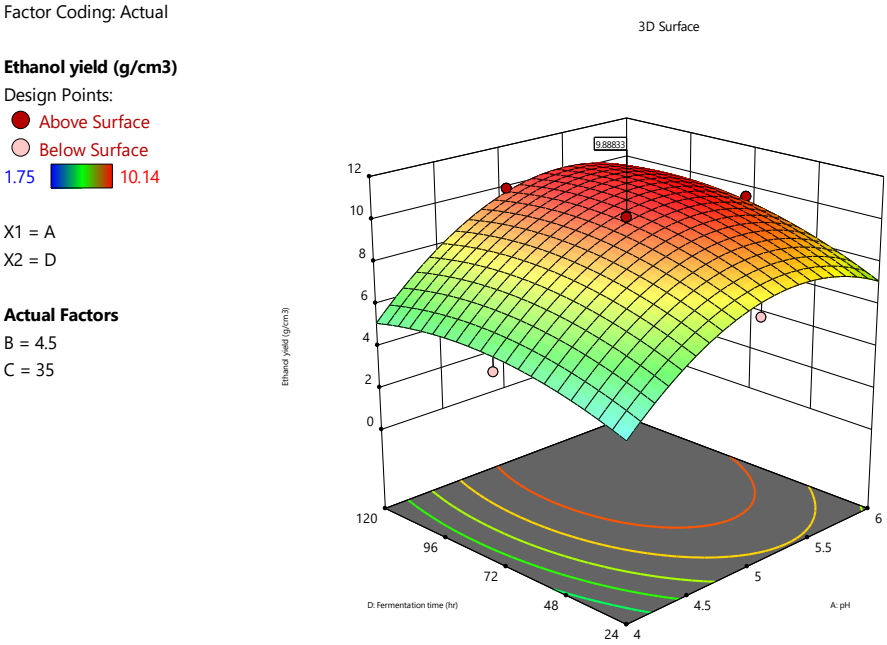

Figure 5: Ethanol yield versus pH and fermentation time

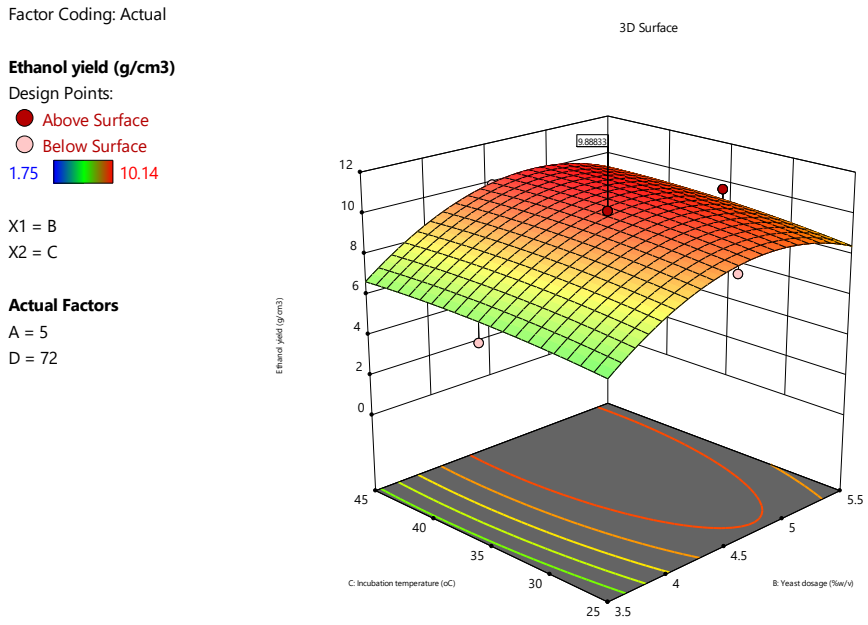

Figure 6: Ethanol yield versus yeast dosage and incubation temperature

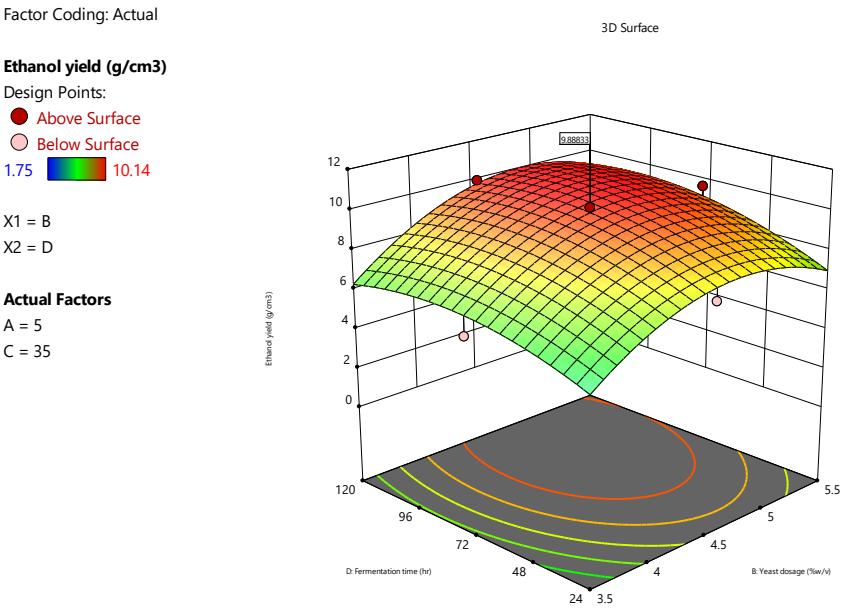

Figure 7: Ethanol yield versus yeast dosage and fermentation time

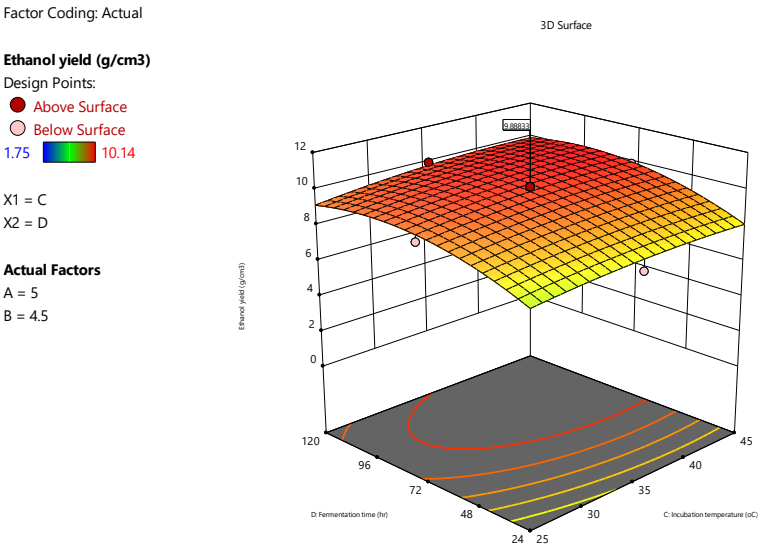

Figure 8: Ethanol yield versus incubation temperature and fermentation time

3.4.5 Validation of the optimum result

Validation result of the optimum ethanol yield is presented in Table 6. Optimum ethanol yield was compared with that of experimental ethanol yield using percentage deviation. The determined percentage deviation of 1.59% is less than 5%, which confirmed that the model adequately predicted the experimental data.

Table 6.

Optimum parameters and the validation.

Optimum pH	Optimum yeast dosage	Optimum incubation temperature (ºC)	Fermentation time (hr)	Optimum ethanol yield% g/cm3	Experimental ethanol yield% g/cm3	Percentage deviation (%)
5	4.5	35	72	9.89	10.05	1.59

4.0 CONCLUSION

Despite the values of the African Star Apple revealed in the literatures, it is yet to find prominence in industrial application due to lack of experimental and statistical

analysis of the sugar content and its application in bioethanol production. From this analysis, it was observed that African star apple contains 54.97% carbohydrate and predominant functional groups of the sample include; N-H stretch, O-H stretch, C≡C stretch, C-H out of plane, C=O stretch, N-H deforming, S=O stretch, N=O stretch and C-F stretch. The presence of the heteroatoms in the structure of African star apple confirms that it is a potential feedstock for bioethanol production. The developed quadratic model adequately described the relationship between ethanol yield and the considered factors of pH, yeast dosage, incubation temperature and fermentation time. The optimum ethanol yield of 9.89 g/cm^3 was obtained at pH of 5, yeast dosage of 4.5 %wt/v, incubation temperature of 35^{o}C and fermentation time of 72 hrs. This study is the first to characterize star apple fruit pulp and to determine its total sugar content for bioethanol production.

REFERENCES

Abdulkareem, A. S., Ayo, S. A., and Ogochukwu, M.U., (2015). Production and Characterization of Bioethanol from Sugarcane Bagasse as Alternative Energy Sources, Proceedings of the World Congress on Engineering 2015 Vol II WCE 2015, July 1 - 3, 2015, London, U.K

Aboaba, O., Smith, S., & Olide, F. O., (2006). Antimicrobial effect of Edible plant Extract on Escherichia.Coli, 0157:H7. *Pakistan. Journal of Nutrition, 5(4)*, 325-327.

Adeboyejo, F. O., Oguntoye, M. A., and Awe, O. E., (2019). Phytochemical components of beverages from African Star Apple (*Chrysophyllum albidum*) tissue fractions under ambient storage. *African Journal of Food Science, 13*(10), 225-234.

Adekanmi, D. G., and Olowofoyeku, A. E., (2020). African Star Apple: Potentials and Application of Some Indigenous Species in Nigeria, *J. Appl. Sci. Environ. Manage*, 24 (8), 1307-1314.

Akubor, P. I., Yusuf, D., and Obiegunam, J. E., (2013). Proximate composition and some functional properties of flour from the kernel of African star apple (Chrysophyllum albidum), *International Journal of Agricultural Policy and Research*, 1(3), 062-066.

Alemayehu G, (2014). Bioethanol Production from Fruit Wastes and Factors Affecting Its Fabrication. International Journal of Chemical and Natural Sciences, 2(5) 132-140

Amusa, N. A., Ashaya, O. E., and Oladapo, M. O., (2005). Biodeterioration of the African star apple (Chrysophyllum albiddum) and the effect on its food value. *African Journal of Biotechnology*, 11(3), 56-59.

Asare, I. K., Abenaa, A. O., Duah-Bissiw, D., Ofosu, D. O., & Darfour, B., (2015). Nutritional and phytochemical constituents of the African Star Apple (*Chrysophyllum albidum* g. Don) Annals. *Food Science and Technology*.

Association Official Analytical Chemists (1990). Official Methods of Analysis 15th Edition American Association of Analytical Chemists, Washington D C, 9999-1001.

Azevedo, A. W. M., (2007). Viability Study of Ethanol Obtention from Kaki (Saccharomyces cereviseae) Fruit Must

Balat M., (2009). Recent trends in global production and utilization of bioethanol fuel. *Appl. Energy*. 86 (11), 2273-2282.

Bello, F. A., and Henry, A. A., (2015). Storage Effects and the Postharvest Quality of African Star Apple Fruits (Chrysophyllum africanum) Under Ambient Conditions. *African Journal of Food Science and Technology*, 6, 35-43.

Cheng, K. K., Ge, J. P., Zhang, J. A., Ling, H. Z., Zhou, Y. J., Yang, M. D., & Xu, J. M. (2007). Fermentation of pre-treated sugarcane bagasse hemicelluloses hydrolysate to ethanol by Pachysolen tannophilus. *Biotechnology letters*, 29(7), 1051-1055.

Demirbas, A., Karslioglu, S., (2007). Biodiesel production facilities from vegetable oils and animal fats. Energy Source. (A) 29, 133–141.

Elemike E. E, Oseghale O. C., & Okoye A. C., (2015) "Utilization of cellulosic cassava waste for bio-ethanol production," Journal of Environmental Chemical Engineering, vol. 3, no. 4, pp. 2797-2800.

Farrell A. E., Plevin R. J., Turner B. T., Jones A. D., & O'Hare M., Kammen D. M. (2006). Ethanol can contribute to energy and environmental goals. *Sci*., 311(5766), 506-508

Hahn-Hagerda, B., Gable l. M., Gorwa-Graslund, M. F., Liden, G., & Zacchi, G., (2006), Bioethanol the fuel of tomorrow from the residues of today. Trends Biotechnology, 24 (12), 549-556.

Hammond, J, B., Egg, R., Diggins, D., & Coble, G.C,. (1996) Alcohol from bananas. *Bioresource Technology*, 56, 125-130.

Ibeto, C. N., Ofoefule, A. U., & Agbo, K. E., (2011) A global overview of biomass potentials for

bioethanol production: A renewable alternative fuel. Trends in Applied Science Research, 6, 410-425.

Ibrahim, H. O., Osilesi, O., Adebawo, O. O., Onajobi, F. D., & Karigidi, K. O., (2017). NutrientsCompositions and Phytochemical Contents of Edible Parts of Chrysophyllum albidum Fruit. *Journal of Nutrition and Food Science*, 7, 579.

Khan, Dwivedi., (2013). Fermentation of Biomass for Production of Ethanol: A Review. *Environmental journal.* 3(1) 1-13.

Kuhad, R.C., Gupta, R., Khasa, Y.P., Singh, A. & Zhang, Y.H.P,. (2011). Bioethanol production from pentose sugars: current status and future prospects. *Renew. Sust. Energ*. Rev. 15, 4950–4962.

Kumar, V., Nanda, M., Joshi, H. C., Singh, A., Sharma, S., & Verma, M., (2018). Production of biodiesel and bioethanol using algal biomass harvested from fresh water river. *Renewable Energy*, 116, 606–612.

Lee, Z., & Park, S., (2020). Particulate and gaseous emissions from a direct injection spark ignition engine fueled with bioethanol and gasoline blends at ultra-high injection pressure. *Renewable Energy*, 149, 80-90.

Lima, E. E. et al., (2015). Production of second-generation ethanol from the bagasse of cashew nuts. Caatinga, Mossoró, 28 (2), 26-35.

Linden, T., & Hahn-Hägerdal, B., (1989). Fermentation of lignocellulosic hydrolysates with yeast and xylose isomerase. *Enzyme, Microbial Technol*ogy, 11, 583-589.

Naik, S. N., Goud, V. V., Rout, P. K., Dalai, A. K., (2010). Production of first and second generation biofuels: A comprehensive review, Renewable and Sustainable Energy Reviews. 14 (2), 578–597.

Odugbemi, T.O., Akinsulire, O.R., Aibinu, I.E., & Fabeku P.O., (2007). Medicinal plants useful for malaria therapy in Okeigbo, Ondo state, southwest Nigeria. *Afr J Tradit Complement Altern Med* 4,191–198.

Okwu, C., Osazuwa, E., and Igberaese, S., (2018). Nutritional and Chemical Composition of three Fruit Tastes of *Chrysophyllum albidum* (African Star Apple) in Nigeria. *Inter. J. Adv. Res. Sci.Eng. Tech. 5*(1)

Omotioma, M., & Onukwuli, O. D., (2019). Phytochemical and Thermodynamic Studies of Pawpaw Leaf (Asimina trilola) Extract as Corrosion Inhibitor of Zinc in KOH Medium. *Journal of the Nigerian Society of Chemical Engineers*, 34(1), 53-61.

Omotioma, M., & Onukwuli, O. D., (2016), Corrosion Inhibition of Mild Steel in 1.0M HCl with Castor Oil Extract as Inhibitor. *Int. J. Chem. Sci.,* 14(1), 103-127.

Omotioma, M., & Onukwuli, O. D., (2015), Inhibitive and Adsorption properties of Leaves Extract of Bitter Leaf (Vernonia amydalina) as Corrosion Inhibitor of Aluminium in 1.0M NaOH, *Der Pharma Chemica*, 7(11), 373-383.

Omotioma, M., Mbah, G.O., Ikegbunam, E.F.W., & Anyankpele, P., (2013). Production of Biodiesel from Seed Oil of Locally Sourced African Star Apple, and its Relative Analysis with Petroleum Diesel. *Journal of Sciences and Technology (JST)*, 19, 53- 59.

Onimawo, I. A., & Akubor, P. I., (2012). Food Chemistry (Integrated Approach with Biochemical background). 2nd edn. Joytal printing press, Agbowo, Ibadan, Nigeria.

Onukwuli, O. D., & Omotioma, M. (2016). Optimization of the inhibition efficiency of mango extract as corrosion inhibitor of mild steel in 1.0M H_2SO_4 using response surface methodology. *Journal of Chemical Technology and Metallurgy*, 51 (3), 302 – 314.

Onukwuli O.D., Chizoo E., Akuzuo U.O., & Eyisi R., (2021), Comparative analysis of the application of artificial neural network-genetic algorithm and response surface methods- desirability function for predicting the optimal conditions for biodiesel synthesis from chrysophyllum albidum seed oil, *Journal of Taiwan Institute of Chemical Engineers*. 125, 153-167

Oiwoh, O., Ayodele, B. V., Amenaghawon, N. A. & Okieimen, C. O. (2018). Optimization of bioethanol production from simultaneous saccharification and fermentation of pineapple peels using Saccharomyces cerevisiae, *J. Appl. Sci. Environ. Manage.*, 22 (1) 54-59.

Randor, R., Robert, E. J., Al, D., Matthew, C. P., (2010). Genetic Engineering of Algae for Enhanced Biofuel Production. *Eukaryotic Cell. 9 (4), 486–501.*

Ruth, C,A, Cristina, R., Andy, D., (2022). Micro-Microalgae Properties and Applications. Encyclopaedia of Smart Materials 2,732-758.

Segui, G. L., Fito, Maupoey P., (2018). An integrated approach for pineapple waste valorisation. Bioethanol production and bromelain extraction from pineapple residues. *Journal of Cleaner Production*, 172, 1224-1231.

Silva, J. O. V. E., Almeida, M. F., da Conceição Alvim Ferraz M., & Dias, J. M., (2017). Integrated production of biodiesel and bioethanol from sweet potato, *Renewable Energy*, 124, 114-120.

Tripathi, S., (2018). Optimization of Fermentation Conditions for Ethanol Production from Renewable Biomass Using Response Surface Methodology. *Journal of Petroleum & Environmental Biotechnology*, 9 (4), 379 - 387.

Ureigho, U. N., (2010). Nutrient Values of *Chrysophyllum albidum* Linn African Star Apple as a Domestic Income Plantation Species. *African Research, 4*, 50-56

Vertes, A.A., Qureshi, N., Blaschek, H.P., & Yukawa, H., (2009). Biomass to biofuels: strategies for global industries. *Wiley publications*.

Ye, F., Li, Y., Lin, Q & Zhan, Q., (2017). Modelling of China's cassava-based bioethanol supply chain operation and coordination. *Energy*, 120, 217-228.

Ylitervo, P., (2008). Production of ethanol and biomass from orange peel waste by mucorindicus. University College of Borås, Borås, 1-61.

Zhang, J., & Smith, K. R., (2007). Household Air Pollution from Coal and Biomass Fuels in China: Measurements, Health Impacts, and Interventions. *Environmental Health Perspectives, 115 (6), 848–855.*

JOURNAL OF THE NIGERIAN SOCIETY OF CHEMICAL ENGINEERS INSTRUCTION TO AUTHORS

1. TYPES OF PUBLICATION

The Journal of the Nigerian Society of Chemical Engineers will publish articles on the original research on the science and technology of Chemical Engineering. Preference will be given to articles on new processes or innovative adaptation of existing processes. Critical reviews on current topics of Chemical Engineering are encouraged and may be solicited by the Editorial Board. The following types of articles will be considered for publication:

a. Full length **articles or review papers**.
b. **Communication** – a preliminary report on research findings.
c. **Note** – a short paper describing a research finding not sufficiently completed to warrant a full article.
d. **Letter to the Editor** – comments or remarks by readers and/or authors on previously published materials.

The authors are entirely responsible for the accuracy of data and statements. It is also the responsibility of authors to seek ethical clearance and written permission from persons or agencies concerned, whenever copyrighted material is used.

For now the journal is published twice in a year, March/April and September/October.

2. MANUSCRIPT REQUIREMENTS

a. The **Manuscript** should be written in clear and concise English and typed (single column) in Microsoft Word using double spacing on A4-size paper, Times New Romans font and 12 point. A full length article or review should not exceed 15 pages. Margin should be Normal (i.e. 2.54cm for Top, Bottom, Left & Right margins).
b. The **Manuscript** should be prepared in the following format: Abstract, Introduction, Materials and Methods, Results, Discussion, Conclusion, Acknowledgements, and References.
c. The **Manuscript** must contain the full names, address and emails of the authors. In the case of multiple authorship, the person to whom correspondence should be addressed must be indicated with functional email address. As an examples, authors' names should be in this format:
Momoh, S. O., Adisa, A. A. and **Abubakar, A. S.**
If the addresses of authors are different, use the following format:
***Momoh, S. O.[1], Adisa, A. A.[2]** and **Abubakar, A. S.[3]**
Use star * to indicate the corresponding author.
d. **Symbols** should conform to America Standard Association. An abridged set of acceptable symbols is available in the fourth edition of Perry's Chemical Engineering Handbook. Greek letters, subscripts and superscripts should be carefully typed. A list of all symbols used in the paper should be included after the main text as **Nomenclature**.
e. All **Units** must be in the SI units (kg, m, s, N, etc).
f. The **Abstract** should be in English and should not be more than 200 words. The Abstract should state briefly the purpose of the research, methodology, results, major findings and major conclusions. Abstracts are not required for Communications, Notes or Letters.
g. **Citation** must be in the Harvard Format i.e. (Author, Date). Examples are (Smith, 1990) or (Jones et al, 2011). (Kemp, 2000) demonstrated that …..; (Mbuk, 1985; Boma, 1999; Sani, 2000) if more than two authors. (Telma, 2001a), (Telma, 2001b); etc if the citation have the same author and year of publication.
For more information on Harvard Referencing:
Guide visit http://www.citethisforme.com/harvard-referencing
h. **References** must also be in the Harvard Format i.e. (Author, Date, Title, Publication Information). References are listed in alphabetical order. Examples are shown below:
Haghi, A. K. and Ghanadzadeh, H. (2005). A Study of Thermal Drying Process. *Indian Journal of Chemical Technology*, Vol. 12, November 2005, pp. 654-663
Kemp, I.C., Fyhr, C. B., Laurent, S., Roques, M. A., Groenewold, C. E., Tsotsas, E., Sereno, A. A., Bonazzi, C. B., Bimbernet, J. J. and Kind M.(2001). Methods for Processing Experimental Drying Kinetic Data. *Drying Technology*, 19: 15-34.
i. **Tables** should contain a minimum of descriptive materials. Tables should be numbered serially throughout the manuscript in Arabic numerals (1, 2, 3, etc), and should be placed at the referenced point with captions (centralised) placed at the top of the table.
j. **Figures**, charts, graphs and all illustrations should be placed at the referenced point, numbered serially throughout the manuscript in Arabic numerals (1, 2, 3, etc) and incorporated in the text. Caption for Figures should be placed at the bottom of the Figure (centralised). Lettering set or symbols should be used for all labels on the figures, graphs, charts,

photographs even when drawn in colours. (Note that figures drawn in colours may be unreadable if printed in black and white).

k. **Equations** should be typed using MS Word Equation Editor and should be centred and numbered serially throughout the manuscript (in Arabic numeral) at the right margin.
l. Wherever possible, **Fractions** should be shown using the oblique slash. E.g. x/y
m. **Footnotes** should not be incorporated in the text.
n. **Acknowledgements** should appear at the end of the paper, before the list of references.

3. SUBMISSION OF MANUSCRIPTS

Manuscripts should be submitted by sending a Microsoft Word document (taking into account the Manuscript Requirements described in section 2 above) to the following email address: nschejournal@yahoo.com and copy stevmomoh@yahoo.com**.**

All correspondences are directed to the Editor-in-Chief using the submission emails addresses: nschejournal@yahoo.com and copy stevmomoh@yahoo.com. Meanwhile the online submission of articles on the journal website will soon be ready.

Authors should note that:

a. All authors listed in the manuscript have significantly contributed to the research.
b. All authors are obliged to provide retractions or corrections of mistakes.
c. All references cited are listed and financial support acknowledged.
d. It is forbidden to publish same research in more than one journal.

The fee charged for paper review and publication will be borne by the authors as follows:

a. Manuscript Review charges = N6,500 payable by both Members and Non-Member. Overseas is $30.00.
b. Publication Charges = N10,000 payable by Non-Members and Members who are not financially up-to-date. Overseas is $40.00.
c. Members would only get one (1) Journal free and buy the other if they so wish.
d. Corresponding Author whose paper is published on a particular edition would get one (1) free copy on behalf of all the co-authors. Other co-authors will buy if they so wish.

All fees are paid after the paper had been accepted for publication. These charges may be reviewed from time to time by the Governing Board of Directors of the Society.

4. ACCEPTED PAPERS

On acceptance, authors will be required to submit a copy of their manuscripts using Microsoft Word by emails to nschejournal@yahoo.com and copy stevmomoh@yahoo.com.

The following additional information should be observed for accepted papers: (i) Typed in Microsoft Word using 1.15 spacing on A4-size paper, Times New Romans font and 10 point; (ii) Margin should be 2.54cm for Top & Bottom; 2.20cm for Left & Right margins; (iii) The abstract should be one column document while the body of the manuscript should be double columns with 0.5cm gutter spacing except some tables and figures that may have to go in for one column document.

5. PUBLICATION

Full NSChE Journal edition in hard copy will be published twice annually – March/April Edition and September/October Edition.

6. REPRINT

Reprints are available on request at a moderate fee per page. Orders must be placed before the paper appears in Print.

7. READER'S INFORMATION

The papers are wholly the view of their author(s) and therefore the publisher and the editors bear no responsibility for such views.

8. SUBSCRIPTION INFORMATION

The subscription price per volume is as follows:

a. Individual Reader - N3,000.00
b. Institutions, Libraries, etc.- N5,000.00
c. Overseas Subscription - $100.00

Request for information or subscription should be sent to the Editor-in-Chief through the following emails addresses: nschejournal@yahoo.com and copy stevmomoh@yahoo.com.

9. COPYRIGHT NOTICE

By submitting your manuscript to the Journal, you have agreed that the copyright of the published material belongs to the journal.

10. PRIVACY STATEMENT

The names and email addresses entered in this journal site will be used exclusively for the stated purposes of this journal and will not be made available for any other purpose or to any other party.